CR-152023

APPLICATION OF SYSTEM IDENTIFICATION TO ANALYTIC ROTOR MODELING FROM SIMULATED AND WIND TUNNEL DYNAMIC TEST DATA

Part II of Final Report under Contract NAS2-7613

Prepared for the Ames Directorate, USAAMRDL

at Ames Research Center, Moffett Field, California

by

K. H. Hohenemser

and

D. Banerjee

Department of Mechanical Engineering

Washington University

School of Engineering and Applied Science

St. Louis, Missouri 63130

June 1977

APPLICATION OF SYSTEM IDENTIFICATION TO ANALYTIC ROTOR MODELING FROM SIMULATED AND WIND TUNNEL DYNAMIC TEST DATA

Part II of Final Report under Contract NAS2-7613

Prepared for the Ames Directorate, USAAMRDL
at Ames Research Center, Moffett Field, California

by

K. H. Hohenemser

and

D. Banerjee

Department of Mechanical Engineering

Washington University
School of Engineering and Applied Science
St. Louis, Missouri 63130

June 1977

APPLICATION OF SYSTEM IDENTIFICATION TO ANALYTIC ROTOR MODELING FROM SIMULATED AND WIND TUNNEL DYNAMIC TEST DATA

Part II of Final Report under Contract NAS2-7613

Abstract

This report begins with an introduction to aircraft state and parameter identification methods. A simplified form of the Maximum Likelihood method is selected to extract analytical aeroelastic rotor models from simulated and dynamic wind tunnel test results for accelerated cyclic pitch stirring excitation. The goal is to determine the dynamic inflow characteristics for forward flight conditions from the blade flapping responses without direct inflow measurements. The rotor blades are essentially rigid for inplane bending and for torsion within the frequency range of study, but flexible in out-of-plane bending. Reverse flow effects are considered for high rotor advance ratios.

Two inflow models are studied; the first is based on an equivalent blade Lock number, the second is based on a time delayed momentum inflow. In addition to the inflow parameters, basic rotor parameters like the blade natural frequency and the actual blade Lock number are identified together with measurement bias values. The effect of the theoretical dynamic inflow on the rotor eigenvalues is studied. A relation between the accuracy of the identified parameters and the length of the input data is established in simulation studies.

It is found that the first inflow model using an optimized equivalent blade Lock number is very accurate for rotor advance ratios of .4 and above, while for lower advance ratios, the second inflow model using a time delayed momentum inflow provides better accuracy. For the first inflow model the identified equivalent Lock number deviates systematically from theoretical values established in the literature. The identified analytical models are verified by predicting the test results not used in the identification process.

Preface to Final Report under Contract NAS2-7613

Work under Contract NAS2-7613 started on July 1, 1973. The contract was originally awarded for a 3 year period.

Due to the slower than anticipated progress of the experimental work, not all research goals had been achieved by 30 June 1976. Since less than the anticipated cost for personnel and equipment had been spent, the research contract was extended by a year without increase in funding.

The research goals as stated in the contract were:

(a) Assess analytically the effects of fuselage motions on stability and random response. The problem is to develop an adequate but not overly complex flight dynamics analytical model and to study the effects of structural and electronic feedback, particularly for hingeless rotors.

(b) Study by computer and hardware experiments the feasibility of adequate perturbation models from non-linear trim conditions. The problem is to extract an adequate linear perturbation model for the purpose of stability and random motion studies. The extraction is to be performed on the basis of transient responses obtained either by computed time histories or by model tests.

(c) Extend the experimental methods to assess rotor wake-blade interactions by using a 4-bladed rotor model with the capability of progressing and regressing blade pitch excitation (cyclic pitch stirring), by using a 4-bladed rotor model with hub tilt stirring, and by testing rotor models in sinusoidal up or side flow.

Including the final report, 10 reports under Contract NAS2-7613 have been submitted. They are listed as P. 1 to P. 10 at the end of the Preface. P. 1 and P. 10 pertain to research goal (a). P. 2, P. 4, P. 6, P. 7, P. 8, P. 9, pertain to research goal (b). P. 3 and P. 5 pertain to research goal (c). The latter is not as yet complete since neither hub tilt stirring nor testing is sinusoidal up or side flow has been performed. While P. 10 describes only work done during FY 1977, P. 8 and P. 9 combine both FY 1977 work results and summaries of earlier results, so that the three parts of the Final Report can be read without recourse to the earlier reports. P. 8 includes much new material not available when the preceding Yearly Report P. 7 was written. The experimental data of P. 9 have all been obtained in FY 77.

So far 3 publications came out of the research under Contract NAS2-7613. They are listed as P. 11, P. 12, P. 13.

List of Reports and Papers under Contract NAS2-7613

P 1. Hohenemser, K. H. and Yin, S. K., "Methods Studies Toward Simplified Rotor-Body Dynamics", Part I of First Yearly Report under Contract NAS2-7613, June 1974.

P 2. Hohenemser, K. H. and Yin, S. K., "Computer Experiments in Preparation of System Identification from Transient Rotor Model Tests", Part II of First Yearly Report under Contract NAS2-7613, June 1974.

P 3. Hohenemser, K. H. and Crews, S. T., "Experiments with a Four-Bladed Cyclic Pitch Stirring Model Rotor", Part III of First Yearly Report under Contract NAS2-7613.

P 4. Hohenemser, K. H., Banerjee, D. and Yin, S. K., "Methods Studies on System Identification from Transient Rotor Tests", Part I of Second Yearly Report under Contract NAS2-7613, June 1975.

P 5. Hohenemser, K. H. and Crews, S. T., "Additional Experiments with a Four-Bladed Cyclic Pitch Stirring Model Rotor". Part II of Second Yearly Report under Contract NAS2-7613, June 1975.

P 6. Hohenemser, K. H., Banerjee, D. and Yin, S. K., "Rotor Dynamic State and Parameter Identification from Simulated Forward Flight Transients", Part I of Third Yearly Report under Contract NAS2-7613, June 1976.

P 7. Hohenemser, K. H. and Crews, S. T., "Rotor Dynamic State and Parameter Identification from Hovering Transients", Part II of Third Yearly Report under Contract NAS2-7613, June 1976.

P 8. Hohenemser, K. H. and Crews, S. T., "Unsteady Hovering Rotor Wake Parameters Identified from Dynamic Model Tests", Part I of Final Report under Contract NAS2-7613, June 1977.

P 9. Hohenemser, K. H. and Banerjee, D., "Application of System Identification to Analytic Rotor Modeling from Simulated and Wind Tunnel Dynamic Test Data", Part II of Final Report under Contract NAS2-7613, June 1977.

P 10. Hohenemser, K. H. and Yin, S. K., "Finite Element Stability Analysis for Coupled Rotor and Support Systems", Part III of Final Report under Contract NAS2-7613, June 1977.

P 11. Hohenemser, K. H. and Yin, S. K., "On the Use of First Order Rotor Dynamics in Multiblade Coordinates", 30th Annual National Forum of the American Helicopter Society, May 1974, Preprint 831.

P 12. Banerjee, D. and Hohenemser, K., "Optimum Data Utilization for Parameter Identification with Application to Lifting Rotors", Journal of Aircraft, Vol. 13, No. 12, December 1976, pp. 1014-1016.

P 13. Banerjee, D., Crews, S. T., Hohenemser, K. H. and Yin, S. K., Identification of State Variables and Dynamic Inflow from Rotor Model Dynamic Tests", Journal American Helicopter Society, Vol. 22, No. 2, April 1977.

TABLE OF CONTENTS

TABLE OF CONTENTS
(continued)

TABLE OF CONTENTS
(continued)

LIST OF FIGURES

LIST OF FIGURES
(continued)

LIST OF FIGURES
(continued)

LIST OF FIGURES
(continued)

LIST OF TABLES

LIST OF TABLES
(continued)

APPLICATION OF SYSTEM IDENTIFICATION TO ANALYTIC ROTOR MODELING FROM SIMULATED AND WIND TUNNEL DYNAMIC TEST DATA

1. INTRODUCTION

System Identification is a method of correlating a mathematical model of a system with transient responses obtained either experimentally or from the time history of a more complete analytical model of the system. It is particularly useful if a linear perturbation model of a basically non-linear system is to be identified.

Methods for state and parameter estimation from transients are widely used in aircraft testing (1)*, (2), (3) and (4). The problem is to obtain optimum estimates (based on certain performance criteria) of initial states and of unknown parameters (derivatives) from noisy measurements of some inputs and response variables. In most cases of airplane parameter identification a constant coefficient system is used as an analytical model. For lifting rotor applications, a periodic coefficient system model may be required (5).

*The numbers in parantheses in the text indicate references in the Bibliography.

While the identification of stability and control derivatives for fixed wing and rotary wing aircraft from transients is by now a well established method, the question arises whether or not similar methods can also be used to obtain some insight with respect to aeroelastic rotor characteristics. When using linear perturbation equations from a non-linear trim condition, frequency response testing is one way to correlate a mathematical model with experimental dynamic data. This method has been occasionally used for wind tunnel rotor model tests (6) and (7). A less laborious and less time consuming method of rotor dynamic testing is to extract analytical perturbation models from transient rotor responses. The study described herein is the first attempt of accomplishing this objective for an aeroelastic rotor model in forward flight conditions. Since new ground is covered by extending aircraft identification methods to aeroelastic rotor problems, extended simulation studies have to be performed to assure the feasibility of the identification process.

A lifting rotor is both structurally and aerodynamically a highly complex system that has not as yet been fully explored. Each blade has natural modes with predominantly out-of-plane (flapping), inplane (lead-lag) and torsional motions that are structurally and aerodynamically coupled. Furthermore the various blades of a rotor are also coupled by hub angular or linear motions, by control element motions and by the rotor inflow. In the following studies a drastically simplified analytical rotor

model will be used, where the blades are essentially rigid in inplane and torsional motion and where the rotor hub is also rigidly supported. Thus only out-of-plane (flapping) blade motions are considered and the only inter-blade coupling is from the rotor inflow. While there is considerable literature on blade flap-bending, for example (8), (9) and (10), and while the steady rotor inflow has been frequently studied, for example in (9), the only dynamic inflow theory applicable to forward flight conditions is given in (11). The present study uses for moderate rotor advance ratio an analytic inflow model that is an extension of that given in (11). It correlates this model with transient wind tunnel test data with the help of state and parameter identification. The corresponding study for hovering conditions is presented in (12).

In addition to the inflow model of (11) a substantially simpler inflow model will also be studied, based on the replacement of the blade Lock number by an optimized equivalent value. This concept was originally suggested for steady rotor conditions in (8) and for dynamic rotor conditions in (13). Theoretically the equivalent Lock number should be a complex number but will be assumed here as a real number, corresponding to a quasi-steady analysis. The results with the two selected inflow models will be compared to the rotor responses when the dynamic inflow is entirely neglected as is done in most current aeroelastic rotor analyses.

It is seen in (14) that in hovering conditions and using the theoretical inflow model of (11), the damping of the regressing rotor flapping mode can be substantially reduced, particularly at low collective pitch setting. The effect on rotor eigenvalues, of the inflow models studied herein for forward flight conditions, will be determined to find out the applicability of the various inflow models and the frequency ranges in which they are suitable. The sensitivity of the rotor eigenvalues to variations in the parameters will also be considered.

2. AIRCRAFT STATE AND PARAMETER IDENTIFICATION METHODS

The review of identification methods to be given in the following is by no means complete. Only the most important methods are discussed. Only rough outlines are given for the various methods. Details of the derivations and of the application algorithms are found in the cited literature.

2.1 ELEMENTS OF SYSTEM IDENTIFICATION FROM TRANSIENTS

System identification is the process of extracting numerical values for system parameters and other subsidiary parameters (process and measurement noise covariances, bias, initial states, etc.) from the time history of control or other inputs and of the resulting system responses. A schematic for the measurements is shown in Figure 1. The process of system identification involves five steps:

1. Selection of a suitable input that insures participation of all important modes of the system in the transient response.
2. Selection of sufficiently complete and accurate instrumentation to measure the key input and output variables.
3. Selection of a mathematical model that adequately represents the actual system characteristics.
4. Selection of an efficient criterion function and estimation algorithm for the identification of the unknown system parameters.

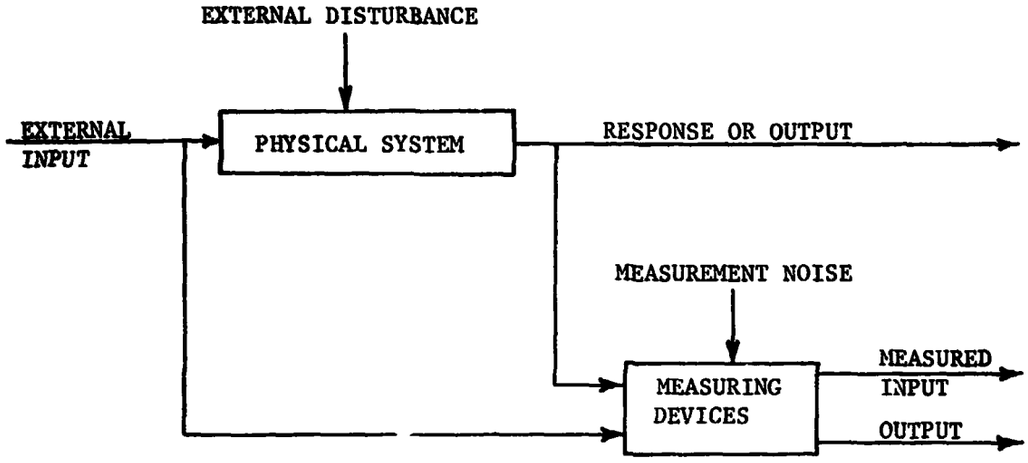

Figure 1. Schematic of Measurements for System Identification.

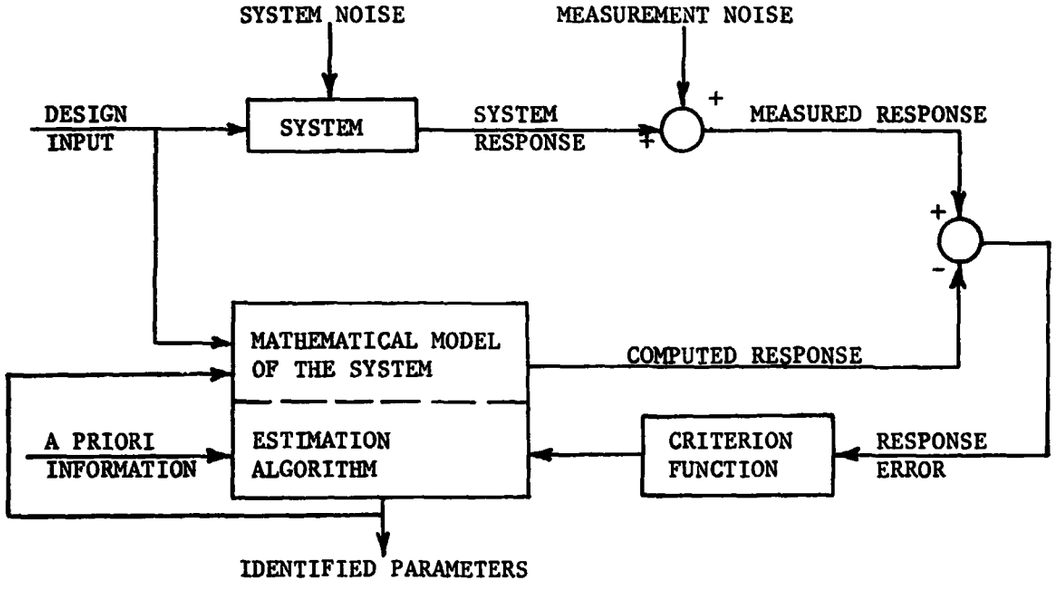

Figure 2. Illustration of System Identification.

5. Validation of the identified mathematical model by comparing its results to test results not used for the system identification.

The concept of system identification is illustrated in Figure 2. The design input is fed both to the actual system and to its mathematical model that contains the unknown parameters. The measured response, polluted by measurement noise, is compared with the computed response from the mathematical model. The difference between these two responses, the response error, is used in the parameter estimation technique based on the criterion function and optimizing technique. The estimation algorithm may also use apriori information, e.g., initial statistics of the parameters. Here we will be mainly concerned with the fourth of the previously listed steps, that is with the various estimation algorithms.

The mathematical representation of the system will be given in the non-linear case by:

System equation $\dot{x}(t) = f(x,u,t) + \Gamma(t)w(t)$ (1)

Initial condition $x(t = 0) = x_0$

Measurement Equation $y(t) = h(x,u,t) + v(t)$ (2)

If the system is linear, equations 1 and 2 reduce to

$$\dot{x}(t) = F(t)\, x\,(t) + G(t)\, u(t) + \Gamma(t)\, w(t) \quad (3)$$

$$y(t) = H(t)\, x\,(t) + D(t)\, u(t) + g + v(t) \quad (4)$$

2.2 CLASSIFICATION OF IDENTIFICATION ALGORITHMS

The various estimation algorithms can be classified into two groups presented in Table 1. The first group listed in Table 1 above the double line is based on statistical regression and does not admit a probabilistic interpretation. The algorithms listed in Table 1 below the double line are based on probabilistic interpretation. In the equation error estimate no measurement noise is modeled; the following 4 methods include both measurement and system noise, while in the output error estimate no system noise is modeled. The various algorithms listed in Table 1 will be discussed in the following sections.

2.3 EQUATION ERROR ESTIMATES

Equation error methods assume a performance criterion that minimizes the square of the equation error (process noise). They are least squares techniques and they require the knowledge of all response variables (states) and their derivatives. In the so called <u>least squares method</u> the unknown parameters are selected such that the integral over the square of the state equation error is minimized, see for example (2). With equation 1 we have the error function (the upper integration limit T is the time over which the measurements are taken)

$$J = \int_0^T [\dot{x} - f(x,u,\theta,t)]^T \, W[\dot{x}-f(x,u,\theta,t)]dt \qquad (5)$$

Table 1. Classification of Estimation Algorithms.

Classification of Estimate	Criterion for Estimate	Solution for Estimate
Equation Error Estimate (no measurement noise is modeled)	$\hat{\theta}$ Minimizes equation error squares and/or integrated equation error squares	Closed form global or sequential optimization by optimum filter (Method function $\delta(t-t_i)$ or e^{-st}).
Bayesian Estimate	$\hat{\theta} = E(\theta/Z)$	—
Quasi-Bayesian Estimate with augmented state	$\hat{\theta}, \hat{x}$ such that $\underset{\theta,x}{\text{MAX}}\ p(\theta,x/Z) = p(\hat{\theta},\hat{x}/Z)$	Sequential optimization by optimum non-linear filter (extended Kalman filter with or without local iteration and/or smoothing).
Quasi-Bayesian Estimate	$\hat{\theta}$ such that $\underset{\theta}{\text{MAX}}\ p(\theta/Z) = p(\hat{\theta}/Z)$	Iterative global optimization with state Kalman filter equations as constraints.
Maximum Likelihood Estimate	$\hat{\theta}$ such that $\underset{\theta}{\text{MAX}}\ p(Z/\theta) = p(Z/\hat{\theta})$	
Output Error Estimate (no system noise is modeled)	$\hat{\theta}$ minimizes output error squares	Iterative global optimization with system equations as constraints.

W is a positive definite weighting matrix. An appropriate choice for W would be Q^{-1} where Q is the covariance of the process noise. For the usual digital data processing, the variables $\dot{x}$, x, u are sampled, and only available at discrete time points t_i. Mathematically the sampling process can be expressed by multiplying the system equation with the delta function $\delta(t - t_i)$. The integral of equation 5 then becomes a sum. One can use instead of the delta function also a different "method function", for example e^{-st}, that would allow taking the Laplace transforms.

If the system is linear in the unknown parameters θ, the system equation can be written in the form

$$\dot{x}(t) = F(x,u,t)\theta + \Gamma(t)\, w(t) \tag{6}$$

and the performance criterion (5) becomes

$$J = \int_0^T [\dot{x} - F(x,u,t)\theta]^T\, W[\dot{x} - F(x,u,t)\theta]dt \tag{7}$$

Since the function inside the integral has continuous derivatives with respect to θ we set

$$\partial J/\partial\theta = 0 \tag{8}$$

thus resulting in the closed form sclution

$$\hat{\theta} = \left[\int_0^T F^T(x,u,t)W\, F(x,u,t)dt\right]^{-1} \int_0^T F^T(x,u,t)W\, \dot{x}(t)dt \tag{9}$$

The first factor is the covariance matrix of the estimate. If the system is non-linear in the unknown parameters, the solution equation 9 can be replaced by an iterative solution where $F(x,u,t)$ is substituted by $\partial f(x,u,\theta_k,t)/\partial\theta$ and $\hat{\theta}$ on the left hand side is replaced by $\hat{\theta}_{k+1}$. It can be shown (for example (1)) that the parameters in the n^{th} row of $f(x,u,\theta,t)$ are independent of all the elements of $\dot{x}(t)$ except $\dot{x}_n(t)$. This independence is one of the drawbacks of the least squares method, in that only one of the measured state derivatives is used in determining a given row of the $f(x,u,\theta,t)$ matrix. If one of the signals has not been measured, the least squares method does not provide an estimate of the parameters related to that signal. This independence also illustrates the fact that the estimate of one row of the $f(x,u,\theta,t)$ matrix is obtained independent of the other rows, and no "trade-off" can be made between elements in different rows to improve the estimate.

For some applications it is practical to include the state vectors in the error minimization. In the modified least squares method a combination of the standard least squares with the integrated least squares is used. The parameters obtained by this method not only trace the derivative of the state but also the state itself over the selected time interval. The performance criterion now includes in addition to the equation error also the integrated equation error:

$$J = \int_0^T \left|\left|\dot{x}(t) - F(x,u,t)\theta + \int_0^t \dot{x}(\tau)d\tau - \int_0^t F(x,u,\tau)\theta\, d\tau\right|\right|_W dt \qquad (10)$$

where W is a positive definite weighting matrix and where

$$||A||_W \triangleq A^T W A \qquad (11)$$

Minimizing the expression, equation 10 results in the estimate

$$\hat{\theta} = \left[\int_0^T \{F(x,u,t) + \int_0^t F(x,u,\tau)\, d\tau\}^T W\{F(x,u,\tau) + \int_0^t F(x,u,\tau)\, d\tau\}\, dt\right]^{-1} \left[\int_0^T \{F(x,u,t) + \int_0^t F(x,u,\tau)d\tau\}^T W\{\dot{x}(t) + \int_0^t \dot{x}(\tau)\, d\tau\}dt\right] \qquad (12)$$

This method has the same row independence of $f(x,u,\theta,t)$ as the standard least squares method.

Since these methods do not allow for measurement errors, they result in biased estimates when this type of error does exist. When measurement errors are small, as is increasingly the case in modern instrumentation, the equation error method is preferable over other methods because of its simplicity. It is widely used

also when measurement errors are substantial and then serves as start-up technique for the output error and other iterative methods.

In many applications, measurements of some of the responses or their derivatives are not available. If the response but not the rate of response is measured, it is tempting to differentiate the measured response. However, the differentiation of measured data introduces additional uncertainty so that this technique is usually inaccurate. If e^{-st} is used as a methods function, Laplace transforms can be used. The estimation then reduces to an algebraic manipulation of the data that avoids their differentation. The Laplace transform technique as a substitute of differentiating measurement data is discussed in (16).

2.4 BAYESIAN AND QUASI-BAYESIAN PARAMETER ESTIMATES

In the preceding methods we specified a cost criterion J that represented the "loss" resulting from an incorrect estimation of the unknown system parameters. The parameters were then selected in such a way as to minimize the loss. If a priori probabilities exist not only for the measurement errors but also for the unknown parameter vector θ then one can define an expected loss and select the parameter vector in such a way as to minimize this expected loss. Such an estimate is called a Bayesian estimate, see for example (17).

The form of a Bayesian estimate depends on the form of both the loss function and of the a priori probability distribution of the measurement and the parameter vector.

For the particular case of positive semi-definite quadratic loss functions, the Bayesian estimate is the mean of θ conditioned on the observations. This is true regardless of the distribution of measurement and parameter vector (18) and (19). It has also been shown that for the case of unimodal symmetric a posteriori distribution of the parameters given the observations, the Bayesian estimate is the conditional mean for all loss functions which are symmetric and convex upwards. For these reasons the Bayesian estimate can be defined generally as the conditional mean of the parameter distribution.

In order to compute the conditional mean, it is first necessary to determine the conditional probability density for θ. This density can be written from Bayes rule as (Z is the set of all observations)

$$p(\theta/Z) = p(Z/\theta)\, p(\theta)/p(Z) \tag{13}$$

The denominator is a normalizing factor determined from

$$p(Z) = \int_{\text{all } \theta} p(Z/\theta)\, p(\theta)\, d\theta \tag{14}$$

The optimal Bayesian estimate is now given by

$$\hat{\theta} = (1/p(Z)) \int_{\text{all } \theta} \theta\, p(Z/\theta)\, p(\theta)\, d\theta \tag{15}$$

In general, the evaluation of equations 14 and 15 would require the solution of the system equations for all possible values of the parameter vector θ.

This is a large effort, especially if the dimension of θ is large. If $p(\theta/Z)$ is unimodal and symmetric about its mean value, the conditional mean corresponds to the mode. Since $p(Z)$ is merely a scale factor the finding of the mode requires neither the evaluation of the integral in equation 14 nor that in equation 15. The mode $\tilde{\theta}$ of θ has the property

$$\max_{\theta} p(\theta/Z) \sim \max_{\theta} p(Z/\theta)\, p(\theta) = p(Z/\tilde{\theta})\, p(\tilde{\theta}) \qquad (16)$$

Even if the a priori density $p(\theta)$ is symmetric it does not follow that the conditional density $p(\theta/Z)$ is also symmetric since in general the observations depend non-linearly on the parameters. Estimation according to equation 16 is, therefore, called "quasi-Bayesian" estimation. Another designation used for example in (3) is maximum a posteriori probability (MAP) parameter estimate. Since the logarithm is a monotonic function of its argument, we can replace equation 16 by maximizing the expression

$$J = \log p(Z/\theta) + \log p(\theta) \qquad (17)$$

If no a priori information about the parameters θ is available, that is, if the a priori density is uniform, $p(\theta)$ = constant, the quasi-Bayesian estimate reduces to the "Maximum Likelihood" estimate which involves finding the maximum of $p(Z/\theta)$.

2.5 ESTIMATES ASSUMING GAUSSIAN DISTRIBUTIONS

The evaluation of equation 17 becomes particularly convenient if we assume Gaussian densities for the parameters, for the observations and for the system states. In linear systems and linear measurement

equations (equations 3 and 4) one needs only to assume that the system noise $w(t)$ and the measurement noise $v(t)$ is Gaussian. It then follows that states $x(t)$ and observations $y(t)$ are also Gaussian. For non-linear systems with Gaussian noise, $p(Z/\theta)$ tends to a Gaussian density as the sampling rate is increased (see for example (1), p.29). The assumption of Gaussian densities for all variables is, therefore, a reasonable one. Since θ is a m x 1 vector we now have the a priori density

$$p(\theta) = \left|P_\theta\right|^{-1/2} (2\pi)^{-m/2} \exp - (1/2)(\theta-\bar{\theta})^T P_\theta^{-1} (\theta-\bar{\theta}) \quad (18)$$

Except for a constant additive term, log $p(\theta)$ is now given by

$$\log p(\theta) = (-1/2) (\theta-\bar{\theta})^T P_\theta^{-1} (\theta-\bar{\theta}) \quad (19)$$

In order to obtain an expression for log $p(Z/\theta)$ in equation 17, we assume that Z consists of N consecutive observations $y(1) .. y(N)$.

$$Z = Y_N = \{y(1), \ldots y(N)\} \quad (20)$$

With successive application of Bayes rule we obtain

$$p(Y_N/\theta) = p(y(1), \ldots, y(N)/\theta) = p(y(N)/Y_{N-1},\theta)\, p(Y_{N-1}/\theta)$$

$$\ldots\ldots\ldots\ldots$$

$$= \prod_{j=1}^{N} p(y(j)/Y_{j-1},\theta) \quad (21)$$

Taking the logarithm we have

$$\log p(Y_N/\theta) = \sum_{j=1}^{N} \log p(y(j)/Y_{j-1}, \theta) \quad (22)$$

$(y(j)/Y_{j-1},\theta)$ is the observation estimate at time j given all preceding observations and given the parameters. We denote the

observations by $y(j)$ and its expected value and covariance respectively by $\hat{y}(j/j-1)$ and $B(j/j-1)$. We further denote the "innovation" by

$$y(j) - \hat{y}(j/j-1) = \nu(j) \tag{23}$$

Since $y(j)$ is a r x 1 observation vector, its Gaussian density is

$$p(y(j)) = |B(j/j-1)|^{-1/2} (2\pi)^{-r/2} \exp\left\{-(1/2)\nu^T(j) B^{-1}(j/j-1)\nu(j)\right\} \tag{24}$$

Taking the logarithm of equation 24, summing according to equation 22, inserting in equation 17 and inverting the sign we have now to minimize the expression (see also equation 19)

$$\sum_{j=1}^{N} \{\nu^T(j)B^{-1}(j/j-1)\nu(j) + \log|B(j/j-1)|\} + (\theta-\bar{\theta})^T P_\theta^{-1} (\theta-\bar{\theta}) \tag{25}$$

If no a priori information is available before taking observations, the last term in the expression 25 is constant and we then have the criterion for the Maximum Likelihood estimation. Bayesian or quasi-Bayesian estimation is rarely used since a priori densities for the parameters are in most applications not available.

2.6 MAXIMUM LIKELIHOOD PARAMETER ESTIMATION

According to expression 25, Maximum Likelihood estimation is equivalent to minimizing the so-called likelihood function

$$J(\theta) = \sum_{j=1}^{N} [\nu^T(j)B^{-1}(j/j-1)\nu(j) + \log |B(j/j-1)|] \tag{26}$$

In the presence of system noise the minimization of the expression 26 is very difficult. When going from time j-1 to time j one first has to solve the prediction equations for the estimate of the state and for its covariance. Assuming the linear system equation 3 with zero mean Gaussian system noise w(t) the prediction is given by

$$\dot{\hat{x}}(j/j-1) = F\,\hat{x}(j/j-1) + G\,u(t)\ ,\ (j-1) \leq t \leq j \qquad (27)$$

$$\dot{P}(j/j-1) = F\,P(j/j-1) + P(j/j-1)F^T + \Gamma\,Q\,\Gamma^T \qquad (28)$$

where Q is the system noise covariance and P the state covariance. These equations use the estimated state and its covariance at time j-1: $\hat{x}(j-1/j-1)$ and $P(j-1/j-1)$, to predict the state and its covariance at time j: $\hat{x}(j/j-1)$ and $P(j/j-1)$. This is the prediction before we know the result of the observations at time j. After the observations y(j) have been made the optimum estimate is given by the Kalman filter equations for the state and for its covariance:

$$\hat{x}(j/j) = \hat{x}(j/j-1) + K(j)\,(y(j) - H\,\hat{x}(j/j-1)) \qquad (29)$$

$$P(j/j) = (I - K(j)\,H)\,P(j/j-1) \qquad (30)$$

with the filter gain

$$K(j) = P(j/j-1)\,H^T\,(H\,P(j/j-1)\,H^T + R)^{-1} \qquad (31)$$

The covariance of the observations $B(j/j-1)$ that occurs in the cost function 26 is given in terms of the state covariance before observations by

$$B(j/j-1) = H\ P(j/j-1)\ H^T + R \qquad (32)$$

Thus the terms in the expression 26 that is to be minimized require the solution of the prediction equations 27 and 28 for each time interval and of the up-date equations 29 and 30 at each sampling time together with the solution of the measurement equation 4. (1) gives an algorithm for the solution of the problem. However, due to its complexity this algorithm has not as yet been applied to a practical problem of aircraft parameter estimation, see for example (20).

The problem of minimizing the expression 26 is greatly simplified if the observation covariance $B(j/j-1)$ can be assumed constant. This is for example true for zero system noise, when according to equation 32, $B(j/j-1) = R$. The problem then reduces to minimizing the cost function

$$J(\theta) = \sum_{j=1}^{N} \nu^T(j)\ R^{-1}\ \nu(j) \qquad (33)$$

where $\nu(j)$ is given by the innovation term 23. Since equation 33 represents (according to equations 2 and 4) the sum of the measurement error squares, the estimation with equation 33 is also called output error method of estimation. There are several algorithms

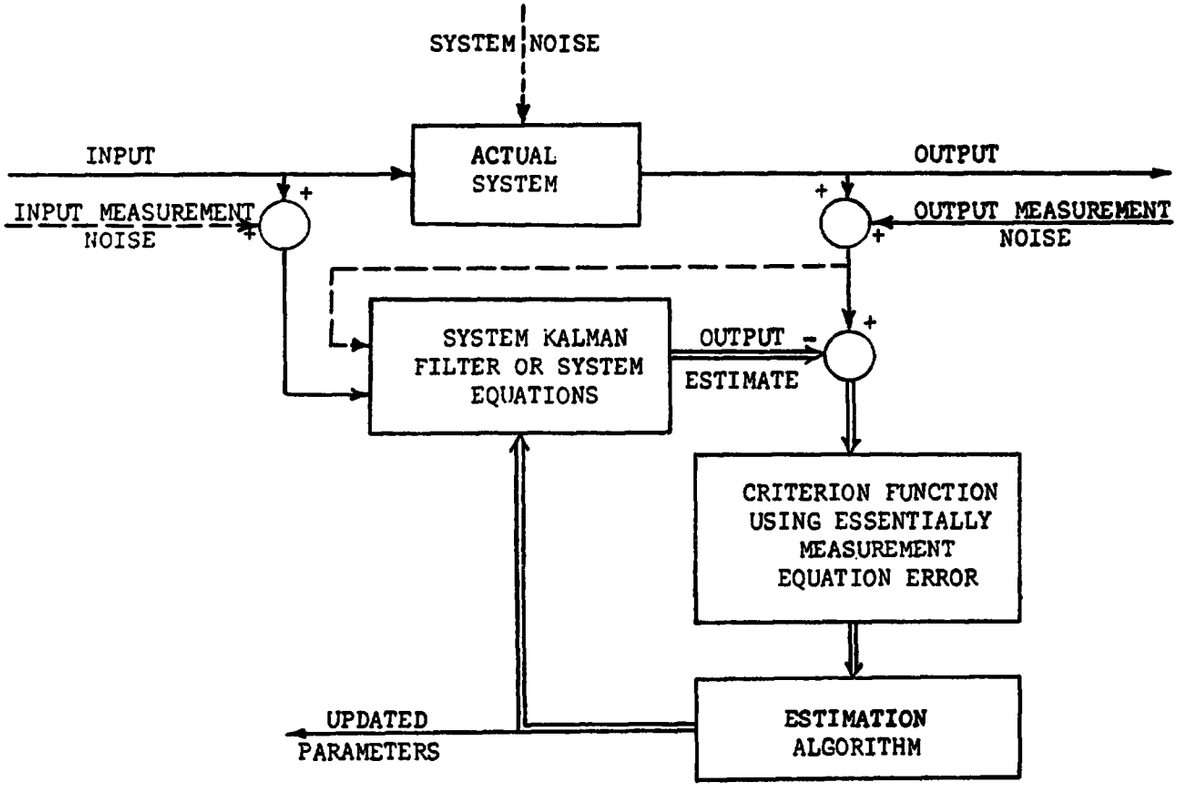

Figure 3. Block Diagram of Maximum Likelihood Identification Procedure.

available to perform the optimization of $J(\theta)$ from equation 33. The most widely used is the modified Newton-Raphson or quasilinearization method. It has the advantage that the sensitivity or information matrix is obtained as a byproduct. The inverted information matrix gives the Cramer-Rao lower bound for the parameter covariance. This lower bound is found in many applications to be a more meaningful measure of the accuracy of the parameter estimate than the parameter covariance obtained from the equation error method (first factor in equation 9).

A block diagram of the complete and the simplified Maximum Likelihood identification procedure is shown in Figure 3. The iteration loop is indicated by double lines. Neglecting the three signals shown by dashed lines, the Kalman filter reverts to the deterministic solution of the system equations.

2.7 SOME PROPERTIES OF THE MAXIMUM LIKELIHOOD ESTIMATE

The Maximum Likelihood estimation technique has several theoretically justifiable properties which makes it the best accepted estimation technique to date. Some of the proven properties of the Maximum Likelihood method are:

1. The Maximum Likelihood estimate is consistent, i.e., the parameter estimates converge (in probability) to its true values as the number of observations N approaches infinity.
2. The Maximum Likelihood estimate is asymptotically Gaussian.
3. The Maximum Likelihood is invariant, i.e., if $\hat{\theta}$ is the Maximum Likelihood estimate of the parameter vector θ, and if $u(\theta)$ is a

function of θ with a single valued inverse, then $u(\hat{\theta})$ is the Maximum Likelihood estimate of $u(\theta)$.

4. The Maximum Likelihood estimate has a variance that approaches the Cramer-Rao lower bound asymptotically, i.e., it is asymptotically efficient.

It can be easily shown that ((17) and (19)), from a Bayesian point of view, the Maximum Likelihood parameter estimates for our model are unbiased.

The next question of interest would be a comparison of the covariance of the parameter estimates obtained from different estimation techniques. It can be seen that an efficient estimator (i.e., that estimation scheme which gives the parameter covariance equal to the Cramer-Rao lower bound) can only be the Maximum Likelihood estimator. An efficient estimator also has to satisfy

$$\frac{\partial J}{\partial \theta} = \left[\hat{\theta}(Z) - \theta\right] k(\theta) \tag{34}$$

where $\hat{\theta}(Z)$ is an unbiased estimate of θ (i.e., $E(\hat{\theta}(Z)) = \theta$), J is the likelihood function and $k(\theta)$ is any function of θ. Hence, if the likelihood function J does not satisfy equation 34, then nothing is known about the covariance of the parameter estimates obtained by the Maximum Likelihood method. In the above condition, unbiased estimators which give lower covariance than the Maximum Likelihood estimator may exist, though there does not exist any general rule for finding them.

2.8 OUTPUT ERROR METHOD USING QUASILINEARIZATION

We use an iterative method beginning with an initial parameter estimate $\hat{\theta} = \theta_0$. The problem is to find a zero of the gradient of the cost function 33, $\partial J/\partial\theta = 0$. Consider a two-term Taylor series expansion of $\partial J/\partial\theta$ about the kth iteration value of θ

$$(\partial J/\partial\theta)_{k+1} \simeq (\partial J/\partial\theta)_k + (\partial^2 J/\partial\theta^2)_k \Delta\theta_{k+1} \tag{35}$$

where

$$\Delta\theta_{k+1} \overset{\Delta}{=} \theta_{k+1} - \theta_k$$

$(\partial^2 J/\partial\theta^2)_k$ is the second gradient of the cost function with respect to θ at the kth iteration. If equation 35 is a sufficiently close approximation, the change in θ for the (k+1)th iteration to make $(\partial J/\partial\theta)_{k+1}$ approximately zero is

$$\Delta\theta_{k+1} = -[(\partial^2 J/\partial\theta^2)_k]^{-1} (\partial J/\partial\theta)_k \tag{36}$$

Using now for $\nu(j)$ the two term expansion

$$\nu(j)_k \simeq \nu(j)_{k-1} + \frac{\partial}{\partial\theta} (\nu(j))_k \Delta\theta_k \tag{37}$$

one obtains for the first and second gradients of the cost function

$$(\partial J/\partial\theta)_k = 2 \sum_{j=1}^{N} \frac{\partial}{\partial\theta} [(\nu(j)]_k^T R^{-1} [\nu(j)]_k \tag{38}$$

$$M = (\partial^2 J/\partial\theta^2)_k = 2 \sum_{j=1}^{N} \frac{\partial}{\partial\theta} [\nu(j)]_k^T R^{-1} \frac{\partial}{\partial\theta} [\nu(j)]_k \tag{39}$$

We thus need solutions for $\nu(j)_k$ and $\frac{\partial}{\partial\theta}\ \nu(j)_k$. For this purpose we first solve the system and measurement equations

$$\begin{aligned}\dot{\hat{x}} &= f(\hat{x}, u, t)\\ \hat{y} &= h(\hat{x}, u, t)\end{aligned} \tag{40}$$

for each iteration whereby the initial conditions are either obtained from the measurements or are included in the unknown parameters θ. The innovation is now obtained from equation 23. Next we solve the "sensitivity equations" for each iteration

$$\begin{aligned}\partial\dot{\hat{x}}/\partial\theta_i &= \partial f/\partial\theta_i + \partial f/\partial x\Big|_{x=\hat{x}}\ \partial\hat{x}/\partial\theta_i\\ \partial\hat{y}/\partial\theta_i &= \partial h/\partial x\Big|_{x=\hat{x}}\ \partial\hat{x}/\partial\theta_i\end{aligned} \tag{41}$$

The initial conditions of $\partial\hat{x}/\partial\theta_i$ are zero except when $x(0)$ is identified as part of the parameters θ. In this case the initial partials have the value one. With equation 23 we can now compute the first and second gradient of the cost function, equations 38 39, and then obtain the change in parameters for the next iteration from equation 36. This involves the inversion of the sensitivity matrix M (equation 39), whereby M^{-1} is the Cramer-Rao lower bound for the covariance of the parameters.

The method is easily extended to the case with a priori information on the parameters, equation 25. The sensitivity matrix 39 is then augmented by the term $2P_\theta^{-1}$, and the gradient 38 is augmented by the term $2P_\theta^{-1}(\theta_0 - \theta_{k-1})$, see (16).

2.9 PARAMETER ESTIMATION BY FILTERING

The parameter estimation methods discussed so far can be denoted as "global" methods. The performance criterion includes the test data for the entire duration of the transient. Filtering is an important tool in state and parameter estimation. It can be used either in conjunction with global estimates, or it can be used as a direct approach to state and parameter estimation. An example of the first type of filter applications is the prefiltering of test data before using them in a least squares regression estimate, see for example (3). The Graham digital filter can remove high frequency noise. A Kalman filter can be used to estimate state variables and their rates not directly measured. It also removes the noise in the measurements. The role of the Kalman filter in Maximum Likelihood estimation has been shown in equations 27 to 31, where it is used to establish the innovation sequence.

In addition to applications in global estimation methods, filters can also be used as substitutes for global methods. The advantage of such direct filter methods is a reduction in computer effort particularly in cases with a large number of parameters. The disadvantage is that unlike the inverted information matrix of the Maximum Likelihood method that provides a lower bound on the parameter covariances, no physically meaningful parameter covariances are obtained with the direct filter methods. The covariance propagation equations require initial values that are usually impossible to obtain in any rational way. Though improvements of the filter solution (forward time integration) can be achieved by smoothing (backward

time integration), the final parameter covariances remain arbitrary, since they evolve from arbitrary initial covariance estimates.

Assuming that all state variables and their rates have been either measured or are otherwise known from manipulating the measurement data, the unknown parameters, if they occur in linear form in the state equation, can be found by application of a linear filter, see for example (5). The classical regression method is a special case of this direct filtering method, namely for infinite initial parameter covariances. In classical regression one obtains a single value of the error covariance matrix. The direct filter application allows the use of a finite initial error covariance matrix and it gives the evolution of this matrix as a function of time. One thus obtains an indication when to stop processing the test data after their information contents has been exhausted. As mentioned before, the absolute values of the error covariances are meaningless, since one usually does not have a rational way of establishing initial values for the parameter covariances.

A method that appears to be economic of computer time for large numbers of unknown parameters was used in (3) for application to helicopters. The method consists of a simultaneous identification of states and parameters with the help of a non-linear filter. In other words, the unknown parameters are treated as additional state variables. Since there occur products of state variables and parameters, the system equation is a non-linear one. The so called extended Kalman filter appears to be particularly useful for this purpose.

Either non-linear filtering alone or linear filtering in combination with smoothing is performed. The absolute values of the parameter covariances are again of no physical significance since they depend on the arbitrary initial values. In the following, a brief discussion of the direct use of filters in parameter estimation is given.

2.10 LINEAR FILTER METHOD OF PARAMETER ESTIMATION

2.10.1 Linear Sequential and Global Estimators

In (5) the parameter identification is performed from a "system equation"

$$\dot{\theta} = 0 \tag{42}$$

and a "measurement equation"

$$\zeta = h(x,\theta)+v \tag{43}$$

Equation 43 is actually the system equation arranged in a form where the left hand side contains all terms that are free of the unknown parameters θ. If the system equation is linear in the state variables x and in the unknown parameters θ, $h(x,\theta)$ is a linear function of the parameters. The noise vector v refers only to the terms on the left hand side of equation 43. The state variables that are multiplied by the unknown parameters in $h(x,\theta)$ must be noise free. To obtain the parameter θ, both ζ and x must be known. If only part of the variables in ζ and x have been measured, Kalman filtering is required in order to reconstitute the missing terms.

Optimal parameter estimates θ can be obtained, under the assumption that v is zero mean Gaussian white noise, by minimizing the cost function

$$J=(1/2)\{(\theta(0)-\hat{\theta}(0))^T P_\theta^{-1}(0)(\theta(0)-\hat{\theta}(0))+\int_0^T (\zeta-h(x,\theta))^T R^{-1} (\zeta-h(x,\theta))dt\} \tag{44}$$

where the a priori estimates $\theta(0)$, $P_\theta(0)$ are assumed to be given together with the noise covariance matrix R. The differential equations associated with this optimal problem are (see for example (21))

$$\dot{\hat{\theta}} = P_\theta(\partial h/\partial\theta)^T R^{-1}(\zeta - h(x,\hat{\theta})) \tag{45}$$

$$\dot{P}_\theta = - P_\theta(\partial h/\partial\theta)^T R^{-1}(\partial h/\partial\theta)P_\theta \tag{46}$$

These equations can be integrated with the aid of the initial a priori estimate for the parameters $\theta(0)$ and their covariance matrix $P_\theta(0)$, which results in the optimal parameter estimate at each time t given the preceding measurements. Since the initial parameter covariance is usually not known and the assumed values are rather arbitrary, the matrix P_θ from the integration of equation 46 is not a useful measure of the actual parameter covariance. However, once P_θ has approached zero, the effect of any further measurements on the estimate θ also approaches zero as is

evident from equation 45. P_θ, therefore, is valuable in judging for what length of time the data should be processed. Equations 45 and 46 represent the "linear estimator" used in (22) and (5).

Instead of the sequential estimation by integrating equations 45 and 46 with some initial estimates $\theta(0)$ and $P_\theta(0)$, one can also obtain a "global" estimate directly from equation 44. If one assumes that one and the same parameter estimate $\hat{\theta}$ is valid throughout the time range from 0 to T, one obtains by setting $\partial J/\partial\theta = 0$

$$\hat{\theta} = \left[P_\theta^{-1}(0) + \int_0^T (\partial h/\partial\theta)^T R^{-1} (\partial h/\partial\theta) dt\right]^{-1} \left[P_\theta^{-1}(0)\theta(0) + \int_0^T (\partial h/\partial\theta)^T R^{-1} (\zeta - h(x,\theta))\, dt\right] \tag{47}$$

(See for example the appendix of (5).) A convenient assumption is $P_\theta^{-1}(0) = 0$, which means an infinite initial parameter covariance matrix. Then the above estimate, equation 47, reduces to the equation error estimate, equation 9. The initial estimate $\theta(0)$ is then not required and the evaluation of equation 47 is reduced to the determination of fixed boundary integrals, a matrix inversion and a matrix multiplication. The parameter covariance matrix at the time T is given by the first factor of equation 47:

$$P_\theta(T) = \left[P_\theta^{-1}(0) + \int_0^T (\partial h/\partial\theta)^T R^{-1} (\partial h/\partial\theta) dt\right]^{-1} \tag{48}$$

which follows from the integration of equation 46, (see for example the appendix of (5)). $P_\theta(T)$ from equation 48 can again be used to judge whether or not all the significant information contents has been extracted from the data.

2.10.2 Iterative Equation Error Estimation with Updated Kalman Filter

When using the parameter estimation methods of the preceding section, it is necessary to first determine, from the noisy deflection measurements, estimates for the deflections, for their rates, and for the accelerations. In (22) this was done by passing the noisy deflection data through a digital filter that takes out the noise above a certain frequency without distorting the signal in the low frequency range. The filtered deflections were then either differentiated twice, or a Kalman filter was applied in order to obtain the derivatives. Later studies in (22) showed large errors in the parameters for too low cut-off frequency of the digital filter. It was then decided in (22) to omit the digital filter and instead use the Kalman filter in an iterative way. In typical examples, it was found in (22) that the second iteration was as accurate as the result with the combined digital and Kalman filter. A block diagram of the method is shown in Figure 4. The iteration loop is indicated by the double lines. The system Kalman filter gives optimal state estimates from incomplete and noisy input and output measurements. The filter needs estimates of the system parameters that are updated after each iteration.

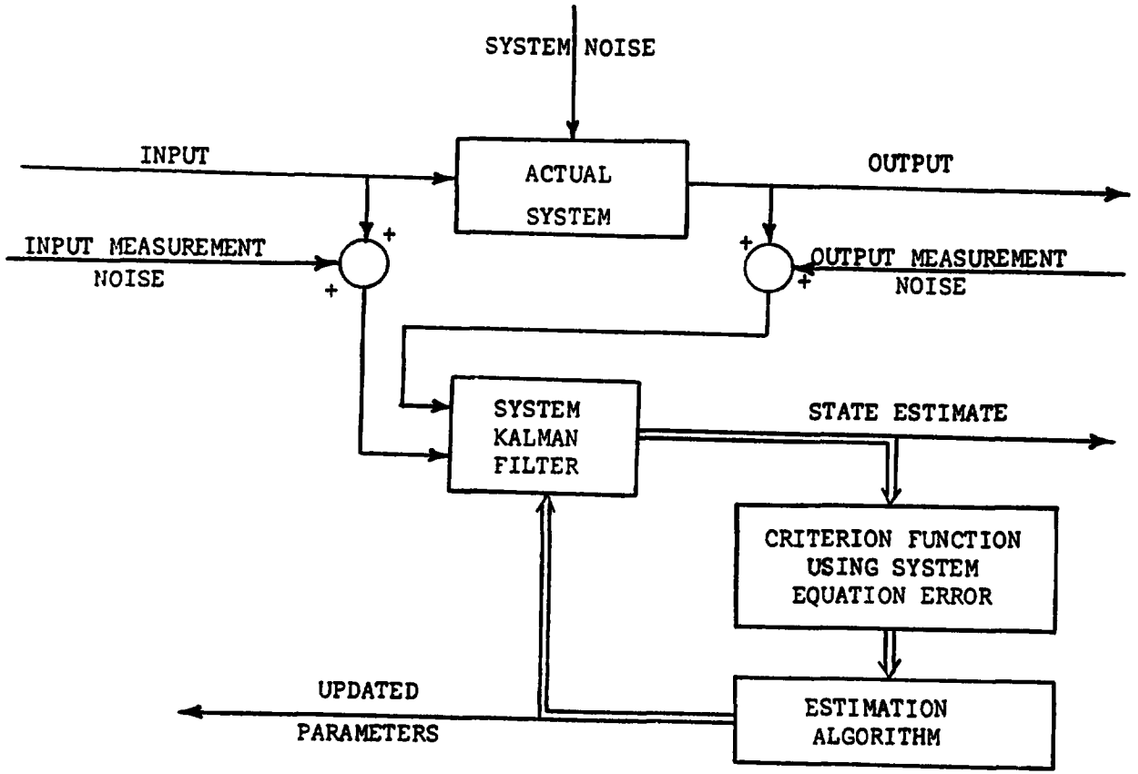

Figure 4. Block Diagram of Iterated Equation Error Estimation with Updated Kalman Filter.

Only simulated noisy blade flapping measurements were used in the Kalman filter. The filter provided the deflection rates and accelerations needed for the "global" parameter estimate, but not the deflections themselves. In other words, the parameter estimate was performed with the simulated noisy deflection measurements and with the rates and accelerations from the Kalman filter. In the first iteration, a Kalman filter with estimated parameter values was used (typically 20% error). After updated parameter values had been obtained, a second pass with an updated Kalman filter was performed, etc. The deflection data remained the same for each iteration, but the rates of deflection and the accelerations were updated. This method worked well for the single blade identification.

2.11 BAYESIAN ESTIMATION AS A FILTERING PROBLEM

If we extend the quasi-Bayesian or maximum a posteriori probability (MAP) criterion 16 to include both the parameters θ and the states $x(t)$, we have

$$\max_{x(t),\theta} p(x(t),\theta/Z) \sim \max_{x(t),\theta} p(Z/x(t),\theta)p(x(t),\theta) \tag{49}$$

Assuming now the non-linear system and measurement equations 1 and 2, and assuming further that states and parameters have Gaussian distributions of the form of equation 18, the criterion 49 becomes (see (3) and (23)) one of minimizing the quadratic function

$$J = (1/2)\left[\left|\left|\theta(0)-\hat{\theta}(0)\right|\right|^2_{P^{-1}_{\theta}(0)} + \left|\left|x(0)-\hat{x}(0)\right|\right|^2_{P^{-1}(0)}\right. \tag{50}$$

$$\left. + \int_0^T \left\{\left|\left|y(t)-h(x,u,t)\right|\right|^2_{R^{-1}} + \left|\left|w(t)\right|\right|^2_{\Gamma Q^{-1}\Gamma^T}\right\}dt\right]$$

subject to the constraint equation 1. If the system and measurement equations 1 and 2 are linearized about the current estimates x and θ the recursive solution of the minimization problem 50 results in the extended Kalman filter equations given for the continuous case by (see (3))

$$\dot{\hat{x}} = (\partial f/\partial x)\hat{x} + (\partial f/\partial u)u + P(\partial h/\partial x)^T R^{-1}(y-(\partial h/\partial x)\hat{x})$$

$$\dot{\hat{\theta}} = P_{\theta x}(\partial h/\partial x)^T R^{-1}\,(y - (\partial h/\partial x)\hat{x})$$

$$\dot{P} = (\partial f/\partial x)P + P(\partial f/\partial x)^T - P(\partial h/\partial x)^T R^{-1}(\partial h/\partial x)P + Q \qquad (51)$$

$$+ (\partial f/\partial \theta)P_{\theta x} + [(\partial f/\partial \theta)P_{\theta x}]^T$$

$$\dot{P}_{\theta x} = P_{\theta x}(\partial f/\partial x)^T + P'(\partial f/\partial \theta)^T - P_{\theta x}(\partial h/\partial x)^T R^{-1}(\partial h/\partial x)P$$

with $P' = - P_{\theta x}(\partial h/\partial x)^T R^{-1}(\partial h/\partial x)P_{\theta x}^T$

Even if the original system is linear, the augmented system is non-linear and hence the filtering problem must be solved by a non-linear filtering technique. In (3) the raw data are pre-processed by a digital filter and by a Kalman filter that does not use the unknown parameters but merely makes use of the transformation equations from a space-fixed to a body-fixed reference system (Euler equations).

Lebacqz in (24) applies basically the same method except for a discrete instead of the continuous filter formulation. He further uses a one stage filtering-smoothing algorithm which has the advantages of reducing the bias due to non-linearities and of making the algorithm less sensitive to initial conditions. Mehra, in (1), is critical of using an extended Kalman filter for the augmented state including the unknown parameters. His arguments are that the uncertainties

in the states are usually much smaller than the uncertainties in the parameters. Therefore the assumption of local linearization about the latest estimate which are acceptable for state estimation with an extended Kalman filter are generally less valid for parameter estimation. Moreover, the filter for the augmented state assumes knowledge of the a priori parameter covariances which are unknown. As mentioned before, the arbitrary a priori parameter covariance used as initial conditions for a filter that includes parameters as state variables gives unreliable confidence limits on the parameter estimates. An added difficulty of applying a filter to the augmented state is that poor a priori estimates of the parameters make the convergence rate slow or may even cause divergence of the filter solution. Though improvements can be applied to the extended Kalman filter like local smoothing and local iteration and smoothing, the basic shortcomings of this method appear to have been correctly described in (1). Unfortunately, the application of the complete algorithm of Maximum Likelihood identification given in (1) is for a large system much more demanding of computer size and time than the filter solution with the augmented state. While aircraft parameter identification with the complete Maximum Likelihood algorithm of (1) has not as yet been accomplished, the method of filtering the augmented state has been applied to several aircraft parameter identification cases, for example in (3) and (24).

2.12 IDENTIFIABILITY PROBLEMS

Identifiability problems can occur no matter what identification algorithm is used. They are related to the initial 3 steps involved in system identification as listed at the beginning of this chapter:

the selection of a suitable input, the selection of the instrumentation, and the selection of the mathematical model. A few comments are added here to point out some difficulties that have been encountered due to these three initial steps.

If the input does not adequately excite some of the system modes, the associated parameters cannot be adequately identified. Sometimes it is practical to combine the responses to various types of inputs into a single identification run, see (3). While each of the single inputs excites only a limited number of modes, the combination of inputs provides an adequate excitation of all modes required for the estimation of the parameters. Efforts have also been made to design inputs on the basis of certain optimization criteria. More details on this problem are given in (25).

If there are large unaccounted for instrumentation errors, non-physical parameter values may result. In (26), instrumentation lags and control measurement errors were found to be most significant. Static measurement errors and instrumentation lags can be a much greater source of parameter inaccuracies than white noise. A detailed analysis of the relationship between static and dynamic measurement errors in states and control inputs and the accuracy of the parameter estimates is required.

If the selected mathematical model for the system is inadequate the parameters are forced to account for some unmodeled effects. The estimated parameters may, therefore, be quite different from those determined by aerodynamic theory or wind tunnel tests would indicate. A good example is given in (27) where a six degree of

freedom mathematical model for a helicopter gave unrealistic derivatives, since it had to account for effects of some neglected modes. A unique six degree of freedom linear model for the helicopter flight dynamics does not actually exist. When a nine degree of freedom mathematical model is used, these difficulties disappear. Modeling errors are also a major cause for the lack of convergence of iteration procedures or of parameter identification by filtering methods. The best remedy against difficulties from modeling errors is the adoption of a more suitable mathematical model. Some other measures to improve the convergence of iteration procedures or of filtering methods will be briefly discussed. In the cases where a priori values of parameters, for example from theory or from wind tunnel tests, are available, one can use an a priori weighting matrix that expresses the confidence in these values and prevents the algorithm from deviating too much from the a priori values. Sometimes there exist some relationships between the parameters. These should then be used as constraints in the optimization problem to avoid non-physical parameter estimates. If parameter dependencies exist, difficulties are encountered in inverting the information matrix. An exact dependency between parameters should result in a zero eigenvalue of the information matrix. A rank deficient solution makes use of the fact that in case of near parameter dependencies there is a large spread between a set of small eigenvalues and another set of much larger eigenvalues of the information matrix.

In filter solutions, divergence because of modeling errors can occur when the covariance matrix becomes prematurely too small, thus

preventing further test data to be of influence. There are several ways to prevent premature small covariances. One can provide fictitious noise input to the system or one can directly increase the parameter covariance in each time step according to some rule. One can also overweigh the most recent data thus causing the filter to reduce its memory of the data of the more distant past. This indirectly increases the parameter covariance matrix. Since too short data length and too large errors in the initial parameter estimates may also result in non-physical parameter values or in divergence of the identification algorithm, longer transients and better a priori parameter estimates can lead to the avoidance of these difficulties.

2.13 VALIDATION OF ESTIMATES

Once a set of parameter estimates has been obtained the question arises: what confidence can be associated with this set? As mentioned before, the parameter covariance matrix obtained by filtering the augmented state is not a good measure of this confidence. The inverted information matrix obtained with the Maximum Likelihood method represents the Cramer-Rao lower bound for the parameter covariances and is a better measure of this confidence. Using the parameter estimates to predict the transients from which the estimates have been obtained, and computing the rms error with respect to the measured transients, gives another confidence measure. However, if the system is inadequately modeled, one may obtain a small rms error despite the fact that the parameter values are wrong in comparison to theoretical or wind tunnel results, (27).

A better way of validation is to compare the prediction with the results of test data not used in the identification process. In fact, it is good practice not to use all of the available test data for the parameter identification but to reserve some of the runs for such a comparison. Sometimes it is desirable to perform the parameter identification not just with one mathematical model but with a variety of models. In the case described in (27), a mathematical model with more parameters gave a much better identification result than a model with fewer parameters, better in the sense of an improved correlation with theoretically and wind tunnel generated parameters. However, there are also cases where mathematical models with a larger number of parameters gave worse identification results than a model with fewer parameters, see (28). Adequate parameter estimation from transients requires careful attention to the many contributing factors in the input, instrumentation, mathematical modeling, and the estimation algorithm, and the validation of this process can only be considered complete after the rms errors of the prediction with the estimated parameters as compared to test data have been found acceptably small for all types of possible transient excitations of the system.

2.14 APPLICATIONS TO LIFTING ROTORS

Lifting rotor characteristics are not well approximated by the usual set of aerodynamic derivatives. One reason is blade modes that must be considered particularly in rapid transients. Another reason is the dynamic rotor wake that is produced by the time varying rotor thrust and rotor pitching and rolling moments and that

has a feedback effect on the rotor forces and moments. The omission of the blade modes, as shown in (27), results in non-unique and non-physical rotorcraft derivatives. The identification is better if separate rotor degrees of freedom are introduced even in the crude form of a first order lag as was done in (4).

A variety of identification methods has been used with respect to lifting rotors. After preprocessing the test data with a digital filter followed by a Kalman filter that does not contain the aerodynamic derivatives (transformation or Euler equations), least squares identification is applied to rotorcraft transient flight test data in (3) and (27). Each identification run is made with several transients simultaneously. The least squares results are then used as start-up values for an extended Kalman filter for the augmented state. It is not obvious that the extended Kalman filter actually improves on the least squares results, though filter convergence is achieved. In (4) the output error method with quasi-linearization is applied without preprocessing the flight test data. The flight data of both (3) and (4) were obtained in calm air. The equation error method in its filter form was applied in (5) to simulated noisy blade flapping and torsion measurements at high rotor advance ratio. The simulated data were preprocessed by a Graham digital filter, but not by a Kalman filter. (5) assumed that all states and their derivatives had been measured. In contrast (22) assumed that only flapping deflections are measured but not flapping rates or flapping accelerations. For the dynamic wind tunnel tests simulated in (22) there is no way of applying a Kalman filter that does not contain the unknown parameters. However, it was found in

(22) that for the cases studied, a Kalman filter with considerable errors in the unknown parameters was useful in obtaining the non-measured flapping rates and accelerations. The parameter identification was then performed by the equation error method in its filter form.

In (29) the same method (except for using global estimates) is used in an iterative form. In addition, the output error method with quasilinearization is applied to the same and to more complex rotor identification problems.

3. MATHEMATICAL MODELS OF THE FLAPPING RESPONSE OF A HINGELESS ROTOR

3.1 SINGLE BLADE MODEL

Using the simplest analytical model of a lifting rotor, a straight blade flapping about the rotor center, one has in a rotating frame of reference for the flapping angle β the following equation (15).

$$\ddot{\beta} + (\gamma/2)C(t)\dot{\beta} + \omega_1^2\beta + (\gamma/2)K(t)\beta = (\gamma/2)(m_\theta \theta_b + m_\lambda \lambda) \qquad (52)$$

One rotor revolution corresponds to $t = 2\pi$. For neglected reversed flow effects, zero root cut-out and with tip loss factor B, the functions $C(t)$, $K(t)$, $m_\theta(t)$, $m_\lambda(t)$ in terms of rotor advance ratio μ are (15):

$$C(t) = (1/4)B^4 + (1/3)B^3 \mu \sin(t) \qquad (53)$$

$$K(t) = (1/3)B^3 \mu \cos(t) + (1/4)B^2 \mu^2 \sin(2t) \qquad (54)$$

$$m_\theta(t) = (1/4)(B^4 + B^2\mu^2) + (2/3)B^3\mu \sin(t) - (1/4)B^2\mu^2 \cos(2t) \qquad (55)$$

$$m_\lambda(t) = (1/3)B^3 + (1/2)B^2 \mu \sin(t) \qquad (56)$$

In the numerical analysis, we use $B = 0.97$. A simple improvement of this analytical model that takes into account blade bending flexibility is possible (30). In transient conditions, the inflow λ includes the dynamic rotor wake in a complicated form.

As a first approximation of dynamic rotor wake effects one can use in equation 52, instead of the actual blade Lock number, an

equivalent smaller value of γ as suggested in (8) and (13). Such an approximation can be expected to be satisfactory if the transient is relatively slow. For transients with high frequency contents, this approximation is invalid (11). In (11) it is seen that γ^*/γ can be expressed by

$$\gamma^*/\gamma = 1 - 1/(1 + 8\nu/\sigma a + 16K_I i\omega/\sigma a) \tag{57}$$

The parameter ν is defined in equation 70.

The above formulation is based on single harmonic balance of the rotor root moment equation. The γ^* formulation reduces to the one obtained by momentum theory (9) (equation 58), when the phase variation is neglected and $\nu = \mu$ (i.e., when $\bar{\lambda} = \bar{\nu} = 0$).

$$\gamma^*/\gamma = 1/(1 + a\sigma/8\mu) \tag{58}$$

Due to rotor induced cross flow in a wind tunnel, the inflow parameter λ will usually not be well known. In addition, the aerodynamic pitch angle θ_0 is also not well known due to airfoil inaccuracies and pitch setting errors. For the wind tunnel tests considered here, we assume $\lambda = 0$ and use the equivalent Lock number γ^* as an unknown parameter to be determined from the blade flapping measurements. In addition we have a transient blade pitch input θ_b assumed to be known. The problem then is to determine from blade flapping transients caused by blade pitch inputs, the equivalent Lock number γ^* and the equivalent collective pitch setting θ_0.

In order to obtain a more realistic description of the rotor dynamic inflow, it is necessary to formulate the rotor theory in

multiblade coordinates, as is done in the following section. The identification of γ^* is also possible with multiblade coordinates and has, for experimental data, the advantage that the measurements of all the blades are used, and hence, an averaging effect results. In fact, after it was found out that the blade pitch angles differed for individual blades by fractions of a degree, only multiblade measurements were used for the γ^* identification.

3.2 MULTIBLADE FLAPPING EQUATIONS WITH DYNAMIC ROTOR WAKE

It has been noted (10), that for most purposes it would appear adequate to consider the first rotating mode elastic bending effects. The moment balance of all the flapping forces on a rotor blade about the hub is given by (see (10)):

$$(1/\gamma)\ddot{\beta} + (1/2)C(t)\dot{\beta} + (1/\gamma)\omega_1^2\beta + (1/2)K(t)\beta = (1/2)(\lambda m_\lambda + \theta m_\theta) \qquad (59)$$

$$m_\lambda = \int U_T x \, dx \qquad K = \mu \int (\cos t)\, U_T \, x \, \eta' \, dx$$

$$m_\theta = \int U_T^2 \, x \, dx \qquad C = \int U_T \, x \, \eta \, dx \qquad (60)$$

Here the actual first rotating mode $\eta(x)$ is replaced by the closed form expression (see (10)):

$$\eta = x + \kappa[\sinh(3.93x)/2 \sinh 3.93 + \sin(3.93x)/2 \sin 3.93] \qquad (61)$$

$\kappa = 0$ will correspond to a rigid blade mode.

Since the dynamic rotor inflow that couples the motions of the various blades is included, a multiblade representation is necessary. The relation between single blade and multiblade variables for a 4-bladed rotor is:

Blade flapping angle:

$$\begin{bmatrix} \beta_o \\ \beta_I \\ \beta_{II} \\ \beta_d \end{bmatrix} = (1/4) \begin{bmatrix} 1 & 1 & 1 & 1 \\ 2\cos t & -2\sin t & -2\cos t & 2\sin t \\ 2\sin t & 2\cos t & -2\sin t & -2\cos t \\ 1 & -1 & 1 & -1 \end{bmatrix} \begin{bmatrix} \beta_1 \\ \beta_2 \\ \beta_3 \\ \beta_4 \end{bmatrix} \qquad (62)$$

Blade pitch angle: $\theta_k = \theta_o - \theta_I \sin \psi_k + \theta_{II} \cos \psi_k \qquad (63)$

Induced flow: $\nu_k = \nu_o + \nu_I (r/R)\cos \psi_k + \nu_{II}(r/R)\sin \psi_k$

The variable β_d represents differential coning for the 4-bladed rotor, whereby one pair of opposing blades cones up, the other pair cones down. Though a linear distribution of the induced flow over the radius is defined in equation 63, this assumption is not required for the parameter identification process. Different inflow distributions merely produce different values in the identified parameters but do not change the form of the equations.

3.2.1 Flapping Equations without Reverse Flow

For low advance ratios the region of reverse flow is small. Since this region is concentrated near the hub of the rotor, the reverse flow affects the moment balance, and hence the flapping response, very slightly. Hence, for low advance ratios (generally acceptable for $\mu \leq .4$) the flapping equations are greatly simplified by neglecting the reverse flow effects without an appreciable error in the flapping response.

Substituting the transformation equations 62 and 63 in the flapping equation 59, the multiblade representation of the flapping response is obtained. The limits of the integrals in equation 60 are from zero to B to take into account the tip loss factor.

The closed form first mode expression 61 is substituted in equations 60 which, in turn are introduced into the multiblade flapping equations. After some algebraic manipulation, the flapping equations are obtained as follows:

$$\ddot{\beta}_o + (B^4\gamma/8)\dot{\beta}_o + \omega_1^2 \beta_o + (B^3\gamma\mu/12)(\dot{\beta}_{II} + \lambda_{II})$$

$$+ (B^3\gamma/6)\lambda_o - (B^2\gamma\mu^2/8) \sin 2t\ \beta_d - (\gamma/2)\kappa\ (-.028\ \dot{\beta}_o$$

$$+ .014\ \mu\ \dot{\beta}_{II} - .457\mu\ \beta_I + .535\mu^2\ \beta_d)$$

$$= (B^4\gamma/8 + B^2\gamma\mu^2/8)\theta_o - (B^3\gamma\mu/6)\theta_I \qquad (64)$$

$$\ddot{\beta}_I + (B^4\gamma/8)\dot{\beta}_I + (\omega_1^2 - 1)\beta_I + (B^4\gamma/8)(\beta_{II} + \lambda_I)$$

$$+ 2\ \dot{\beta}_{II} + (B^3\gamma\mu/6)\beta_o + (B^2\gamma\mu^2/16)\beta_{II} + (B^2\gamma\mu^2/16)(\sin 4t\ \beta_I - \cos 4t\ \beta_{II})$$

$$- (B^3\gamma\mu/6)(\sin 2t\ \ \dot{\beta}_d + \cos 2t\ \beta_d)$$

$$+ (\gamma/2)\ \kappa(.028(\dot{\beta}_I + \beta_{II}) + (.886)\mu\ \beta_o$$

$$+ (.268)\mu^2 \sin 4t\ \ \beta_I + (.268)\mu^2\ (1 - \cos 4t)\beta_{II}$$

$$+ (.028)\mu \sin 2t\ \dot{\beta}_d - (.886)\mu \cos 2t\ \ \beta_d)$$

$$= (B^4\gamma/8 + B^2\gamma\mu^2/16)\theta_{II} + (B^2\gamma\mu^2/16)(\sin 4t\ \ \theta_I - \cos 4t\ \theta_{II}) \qquad (65)$$

$$\ddot{\beta}_{II} + (B^4\gamma/8)\dot{\beta}_{II} + (\omega_1^2 - 1)\beta_{II} + (B^4\gamma/8)(-\beta_I + \lambda_{II})$$

$$- 2\ \dot{\beta}_I + (B^3\gamma\mu/6)\dot{\beta}_o + (B^2\gamma\mu^2/16)\beta_I + (B^2\gamma\mu/4)\lambda_o$$

$$- (B^2\gamma\mu^2/16)(\cos 4t\ \beta_I + \sin 4t\ \beta_{II}) - (B^3\gamma\mu/6)(\sin 2t\ \beta_d - \cos 2t\ \dot{\beta}_d)$$

$$+ (\gamma/2)\ \kappa((-.028)\mu\ \dot{\beta}_o + (.028)(\dot{\beta}_{II} - \beta_I)$$

$$+ (.268)\mu^2\ (1 - \cos 4t)\beta_I - (.268)\mu^2 \sin 4t\ \beta_{II}$$

$$- (.028)\mu \cos 2t\ \dot{\beta}_d - (.886)\mu \sin 2t\ \beta_d)$$

$$= (B^3\gamma\mu/3)\theta_o - (B^4\gamma/8 + 3\ B^2\gamma\mu^2/16)\theta_I$$

$$- (B^2\gamma\mu^2/16)(\cos 4t\ \theta_I + \sin 4t\ \theta_{II}) \qquad (66)$$

$$\ddot{\beta}_d + (B^2\gamma/8)\dot{\beta}_d + \omega_1^2\ \beta_d - (B^3\gamma\mu/12)\sin 2t\ (\dot{\beta}_I + 2\ \beta_{II} + \lambda_I)$$

$$+ (B^3\gamma\mu/12)\cos 2t\ (\dot{\beta}_{II} - 2\ \beta_I + \lambda_{II})$$

$$- (B^2\gamma\mu^2/8)\sin 2t\ \beta_o - (\gamma/2)\kappa\ (-(.014)\mu \sin 2t\ (\dot{\beta}_I + \beta_{II})$$

$$+ (.014)\mu \cos 2t\ (\dot{\beta}_{II} - \beta_I) + (.535)\mu^2 \sin 2t\ \beta_o$$

$$+ (.443)\mu \cos 2t\ \beta_I + (.443)\mu \sin 2t\ \beta_{II} - (.028)\dot{\beta}_d)$$

$$= (B^2\gamma\mu^2/8)\cos 2t\ \theta_o - (B^3\gamma\mu/6)(\cos 2t\ \theta_I + \sin 2t\ \theta_{II}) \qquad (67)$$

3.2.2 Inflow Model

We adopt here the rotor inflow perturbation model of (9) and (11). The inflow model is based on the relation between the aerodynamic rotor thrust and moment coefficients and the perturbation inflow state variables. Equation 33 of (11), written in our notation, reads

$$\frac{1}{\sigma a}\begin{bmatrix} k_M & 0 & 0 \\ 0 & -k_{I_1} & 0 \\ 0 & 0 & -k_{I_2} \end{bmatrix}\begin{bmatrix} \dot{\nu}_o \\ \dot{\nu}_I \\ \dot{\nu}_{II} \end{bmatrix} + [L_E]^{-1}\begin{bmatrix} \nu_o \\ \nu_I \\ \nu_{II} \end{bmatrix} = \frac{1}{\sigma a}\begin{bmatrix} C_T \\ C_M \\ C_L \end{bmatrix} \tag{68}$$

Rotor thrust and moment coefficients C_T, C_M, C_L are from aerodynamic contributions only. L_E is the empirical L-matrix defined in (9). The theoretical values of k_M, k_{I_1} and k_{I_2}, using potential flow around a solid disk are given in (9) as $k_M = .849$, $k_{I_1} = k_{I_2} = .113$. The components of the L-matrix as well as k_M, k_{I_1} and k_{I_2} will be identified from rotor transient tests. From momentum theory, one obtains according to (11):

$$[L]^{-1} = \frac{1}{\sigma a}\begin{bmatrix} 2v & 0 & 0 \\ 0 & -v/2 & 0 \\ 0 & 0 & -v/2 \end{bmatrix} \tag{69}$$

with

$$v = \frac{\mu^2 + \bar{\lambda}(\bar{\lambda} + \bar{\nu})}{(\mu^2 + \bar{\lambda}^2)^{1/2}} \tag{70}$$

where $\bar{\lambda}$ and $\bar{\nu}$ are the trim values, about which the rotor inflow perturbations ν_o, ν_I, ν_{II} are taken.

The complete L_E^{-1} matrix can be defined as a matrix consisting of 9 parameters as follows:

$$L_E^{-1} = \frac{\mu}{a\sigma}\begin{bmatrix} L_{11} & L_{12} & L_{13} \\ L_{21} & L_{22} & L_{23} \\ L_{31} & L_{32} & L_{33} \end{bmatrix} \tag{71}$$

Substituting equation 71 in equation 68, we get, on expanding

$$\dot{\nu}_o + \mu(1/K_M)\ (L_{11})\nu_o + (L_{12})\nu_I + (L_{13})\nu_{II} = (1/K_M)C_T \tag{72}$$

$$\dot{\nu}_I - \mu(1/K_{I_1})\ (L_{21})\nu_o + (L_{22})\nu_I + (L_{23})\nu_{II} = -(1/K_{I_1})C_M \tag{73}$$

$$\dot{\nu}_{II} - \mu(1/K_{I_2})\ (L_{31})\nu_o + (L_{32})\nu_I + (L_{33})\nu_{II} = -(1/K_{I_2})C_L \tag{74}$$

The parameters τ_o, τ_I and τ_{II} are now defined as follows:

$$\tau_o \triangleq 1/K_M;\quad \tau_I \triangleq 1/K_{I_1};\quad \tau_{II} \triangleq 1/K_{I_2}$$

The thrust and moment coefficients C_T, C_M and C_L are obtained as a function of the state variables, the details of which is given in 8.2.

To match the perturbation inflow model (equation 68), where the inflow variables ν_o, ν_I, and ν_{II} are considered as perturbations about its trim values $\bar{\nu}_o$, $\bar{\nu}_I$ and $\bar{\nu}_{II}$, the flapping equations have to be perturbations about certain trim inputs. Since the flapping equations 64, 65, 66 and 67 are linear equations and since C_T, C_M, C_L in equations 72 to 74 are linearly related to the state variables (see section 8.2), the state variables in equations 64 to 67 and in equations 72 to 74 can be considered as perturbation variables.

λ_o, λ_I, λ_{II} now are identical with the induced downwash variables ν_o, ν_I, ν_{II}. Hence, $\lambda_o = \nu_o$; $\lambda_I = \nu_I$ and $\lambda_{II} = \nu_{II}$.

3.2.3 Flapping Equations with Reverse Flow

With increasing advance ratio, the region of reverse flow becomes larger and its effects can no longer be neglected. The limits of the integrals in equation 60 are no longer simply from 0 to B, but are split up depending on whether the flow in the region is normal, mixed or reversed.

Region 1: $\int \triangleq + \int_0^B$

Region 2: $\int \triangleq \int_{-\mu \sin\psi}^B - \int_0^{-\mu \sin\psi}$

Region 3: $\int \triangleq - \int_0^B$

The three regions are clearly explained in (15). To obtain a closed form analytical solution for the coefficients of all the states in the flapping equations (and in the thrust and moment coefficients), a fourier expansion is obtained for all the coefficients around the azimuth. This gives rise to different sets of coefficients for different advance ratios. The flapping perturbation equations as well as the thrust and moment coefficients are obtained in a manner similar to those obtained by neglecting reverse flow. The blade is assumed to be rigid (i.e. κ is assumed to be zero). The coefficients are provided in 8.4. The flapping equations are listed in 8.3.

3.3 EXCITATION OF PITCH STIRRING TRANSIENTS

For wind tunnel experiments with pitch stirring transients the initial state of the rotor will be given by prescribing the advance

ratio, the collective pitch angle, the rotor angle of attack and the cyclic control setting that will be zero longitudinal cyclic and 1.5^{o} lateral cyclic.

The lifting rotor wind tunnel model described in (31) allows excitation of progressing and regressing flapping modes at various frequencies. By a minor modification of this model, progressing or regressing transients can be excited. One can describe such inputs as pitch stirring transients. In a helicopter, this would amount to cyclic stick stirring, whereby the amplitude of the cyclic pitch would remain constant while the frequency of the stirring motion changes. At the time t_o, pitch stirring is initiated. If we denote the angular pitch stirring speed as ω, positive in the direction of rotor rotation, and the pitch stirring angular acceleration as $\dot{\omega}$, assumed to be constant, we have

$$\omega = \dot{\omega}(t - t_o) \tag{75}$$

For a progressing mode ω is negative and for a regressing mode ω is positive. In a rotating reference system the blade pitch angle is given by

$$\theta = \theta_o + 1.5 \cos [\omega(t-t_o) + t]$$

$$\omega = \begin{cases} 0 & \text{for } t \leq t_o \\ \dot{\omega}(t - t_o) & \text{for } t > t_o \end{cases} \tag{76}$$

In a multiblade representation the blade pitch angle of the kth blade is

$$\theta_k = \theta_o - \theta_I \sin \psi_k + \theta_{II} \cos \psi_k \tag{77}$$

where

$$\theta_I = \begin{cases} 0 & \text{for } t \leq t_o \\ 1.5 \sin \omega(t-t_o) & \text{for } t > t_o \end{cases} \tag{78}$$

$$\theta_{II} = \begin{cases} 1.5 & \text{for } t \leq t_o \\ 1.5 \cos \omega(t-t_o) & \text{for } t > t_o \end{cases} \tag{79}$$

The meaning of these input equations is the following. At the time $t = 0$, a step lateral cyclic pitch input of 1.5 degrees is imposed. At time $t = t_o$, the response to this input is approximately stabilized. At this time the pitch stirring acceleration of $\dot{\omega}$ is introduced which leads to a progressing flapping excitation. The identification starts at $t = t_o$ with the pitch stirring transient. θ_I represents forward cyclic pitch, θ_{II} represents left cyclic pitch. If perturbation equations are considered, the perturbation at time t_o is zero, θ_I excitation stays the same but θ_{II} excitation is now defined as:

$$\theta_{II} = \begin{cases} 0 & \text{for } t \leq t_0 \\ 1.5 \cos \omega(t-t_0) - 1.5 & \text{for } t > t_0 \end{cases} \tag{80}$$

The wind tunnel experiments are conducted with a variety of pitch stirring accelerations. Generally, the computer experiments are conducted with a pitch stirring acceleration of

$$\dot{\omega} = -.1/\pi \tag{81}$$

which is in the progressing sense.

Since in the non-dimensional time units used here the time of one rotor revolution is 2π, the angular pitch stirring velocity one rotor revolution after initiation of pitch stirring is .2, that is one fifth of the rotor angular speed. Figure 5 shows the time history of the blade pitch for about two rotor revolutions ($t_o = 0$, $t = 0$ to 12) in a rotating frame of reference for $\dot{\omega} = -.1/\pi$, corresponding to equation 76. Figure 6 shows the time history of blade pitch in multiblade representation, that is θ_I and θ_{II} vs. time t for the same acceleration corresponding to equations 78 and 80. Figures 5 and 6 refer to the progressing mode. The physical reason why regressing modes are less suited for rotor wake identification is the fact that at a certain regressive excitation frequency the excitation is in resonance with the regressing flapping mode. At this condition no induced dynamic rotor wake exists since aerodynamic excitation and aerodynamic damping cancel each other. Since regressing mode transients include a frequency region with a weak dynamic rotor wake, the identification of the wake parameters is not expected to be as good as it is for progressing mode transients.

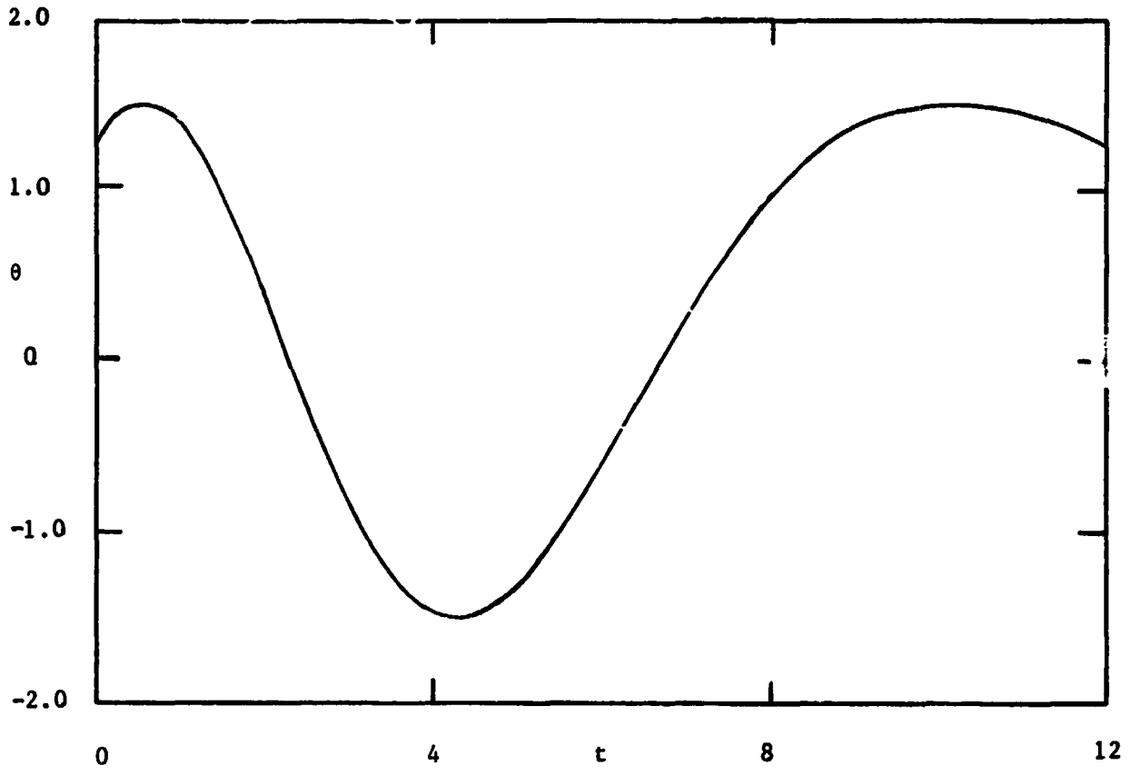

Figure 5. Time History of the Blade Pitch in a Rotating Frame of Reference for $\dot{\omega} = -.1/\pi$ in Equation 76.

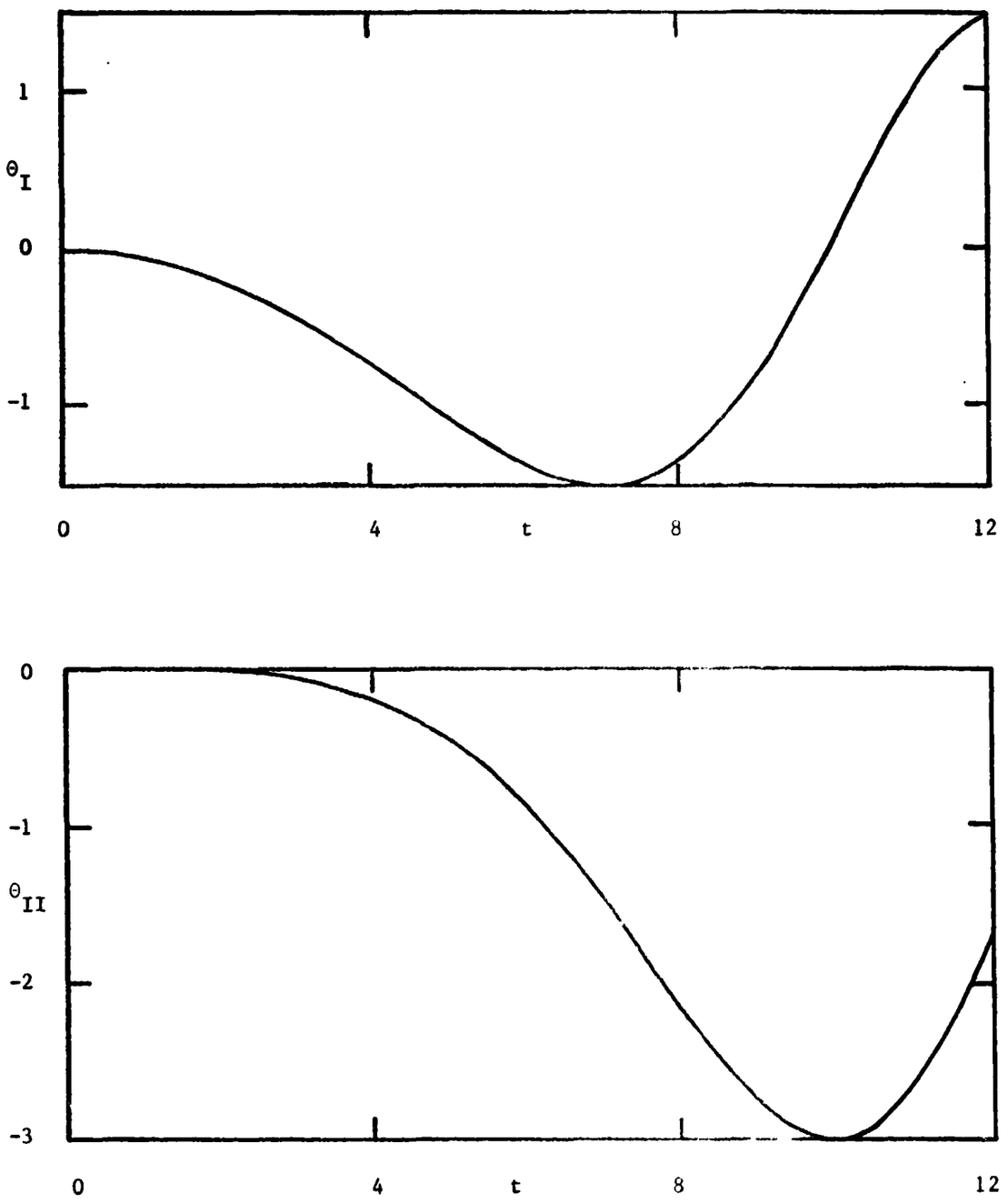

Figure 6. Time History of the Blade Pitch θ_I and θ_{II} for $\dot{\omega} = -.1/\pi$ in Equations 78 and 80.

4. SIMULATION STUDIES

4.1 SELECTION OF IDENTIFICATION METHOD BASED ON PRELIMINARY SIMULATION STUDIES

The selection of the identification method used in this thesis is based on several simulation studies ((5), (22) and (29)).

Simultaneous state and parameter identification in (32) and (33) was conducted using an extended Kalman filter. A major drawback of the method is that the filter can easily diverge unless good initial estimates are available. Particularly in (33) a considerable effort was applied to obtain such good initial estimates. The test data was first processed with a digital filter that took out high frequency noise without distorting the main signals. The data was then processed with a Kalman filter based on the Euler equations, which do not contain the unknown parameters. Thus measurement bias was removed and missing channels were reconstituted. Finally a least squares algorithm was applied to obtain estimates of the unknown parameters. The subsequent application of the extended Kalman filter led to modified parameter estimates, however it is not clear whether or not these modifications represent improvements. In any case the modifications were not large, and the initial estimates appeared to be satisfactory approximations.

In trying to apply the experience from (33) to wind tunnel model transients a difficulty arises, in that there is no equivalent to the Euler equations for the aircraft. Thus there is no way of using a Kalman filter which is free of the unknown parameters. Instead, if a Kalman filter is to be applied, estimates of the parameters

must be inserted. Another difficulty for our wind tunnel model tests is that only flapping deflection measurements are made, while the rates of deflection and the accelerations are not measured. Thus the Kalman filter with the estimated parameters is called upon to provide both rates and accelerations.

This method as explained before has several disadvantages. A priori parameter covariances being generally unknown, give poor and most often, wrong parameter covariances as solution of the Riccati equation. Wrong estimates of the parameter values often cause the filter to diverge.

Analysis is also made by replacing the least squares algorithm of (33), by linear sequential estimators and a simpler "global" estimator. This has the advantage that finite initial parameter covariances can be used, and that the time history of the parameter covariance provides a measure for the time beyond which no more useful information can be extracted from the test data.

The linear sequential estimator as shown before (used in (22)) requires the simultaneous integration of the filter and of the covariance differential equations. A simpler "global" estimate requires only the inversion of a system of linear equations for the unknown parameters and the evaluation of a number of integrals over the time period of the transient. Therefore, a number of comparisons were made between these two methods.

For a single blade 2 parameter identification, both the linear sequential estimator and the "global" estimator provide quite accurate parameter estimates. For convenience, γ and $\delta \triangleq \gamma\, \theta_o$ instead

of γ and θ_0 were identified. Preliminary analysis and comparison between the Iterated Equation Error estimation with updated Kalman filter and the Maximum Likelihood method had given the following results: For single blade parameter identification from pitch stirring transients the Equation Error method applied in an iterative form using a Kalman filter with the latest parameter updates worked well and required the least computer CPU time. For multiblade parameter identification this method became impractical because of slow convergence and high computer CPU time. The Maximum Likelihood method worked well both for single blade and multiblade applications, though in case of single blade identification it requires somewhat more computer CPU time. The parameter covariances from the Maximum Likelihood method are clearly superior to and more meaningful than the covariances determined with the Equation Error method. The Maximum Likelihood method also gave good parameter identifications in the presence of both measurement and system noise, though most of the computer experiments were conducted with measurement noise only.

The following Table 2 compares the results of the various methods on the single blade model (29). The last 4 rows refer to the Maximum Likelihood method.

The number of iterations indicated in the table is that for which convergence has been achieved. The Iterated Equation Error estimation with updated Kalman filter needs the lowest total computer effort, however, the accuracy of the estimate is worst for γ. The Maximum Likelihood estimation, due to faster convergence, needs only moderately more computer effort and yields better accuracy.

Table 2. Comparison of Various Identification Methods on the Single Blade Model.

	Iterations	γ	δ	Variances of γ	Variances of δ	Total CPU time, sec.
True Value		5.00	10.00			
Iterated equation error, single blade	3	4.52	10.09	.073	.111	4.8
Single blade, correct initial conditions	2	4.91	9.82	.0085	.0146	5.2
Single blade, identified initial conditions	2	4.90	9.85	.0092	.0162	8.0
Multiblade, zero initial values	2	4.87	10.27	.0060	.0111	8.0
Multiblade, zero initial rates identified initial deflections	2	5.01	9.97	.0053	.0210	12.0

During the last decade the Maximum Likelihood method of parameter identification has been successfully applied to airplane and helicopter transient testing. This method does not require preprocessing of the test data and also does not need complete measurements of the deflections, of their rates and of the accelerations. The parameter covariance estimates obtained with this method are more meaningful than those obtained with the linear sequential estimator used in (22).

From the above study, one can conclude that the Maximum Likelihood method in its simplified form in which system noise is not modeled, is, for the applications studied, superior to the Equation Error and other existing methods and thus will represent the method of choice for the parameter identification from wind tunnel rotor model tests.

4.2 SIMULATION STUDIES FOR FORWARD FLIGHT USING MAXIMUM LIKELIHOOD METHOD

The Maximum Likelihood method for our particular case pertains to the system equation (zero system noise)

$$\dot{x} = f(x, u, \theta) \tag{82}$$

θ is the vector of unknown parameters that may include initial values of the state variables, constant measurement bias, etc. The measurement equation is assumed to be linear and of the form

$$y = H x + v \tag{83}$$

y is the vector of observed quantities, H is a matrix relating the state variables to the observations, v is the vector of random measurement errors, assumed to be zero mean white noise with given covariance matrix R

$$E[v(t)v^{T}(\tau)] = R\,\delta(t, \tau) \tag{84}$$

R is assumed to be constant with time. Though the preceding

equations do not show bias terms, bias errors could easily be included in the unknown parameter vector θ.

A sample of measurements $y_1\ y_2\ \ldots\ y_n$ is now made during the time of the transient and the parameter estimate $\hat{\theta}$ is selected such that the conditional probability of this sample of measurements given θ is maximized.

$$\hat{\theta} = \max_{\theta} p(y_1 \ldots y_n/\theta) \tag{85}$$

The following steps lead to the maximum of the likelihood function $p(y_1 \ldots y_n/\theta)$, though there is no assurance that the maximum is global. The method outlined here is called quasilinearization with the modified Newton-Raphson method. It assumes Gaussian distributions of the random variables.

1. Select an initial parameter estimate $\hat{\theta} = \theta_o$.
2. Solve the system equation 14 with this parameter estimate

$$\dot{\hat{x}} = f(\hat{x}, u, \hat{\theta}) \tag{86}$$

   The initial conditions can either be obtained from the measurements, or, where this is not feasible, they can be included in the unknown parameter vector $\hat{\theta}$.

3. Calculate for each measurement the "innovation term"

$$\nu_j = y_j - H\,\hat{x}_j \tag{87}$$

4. Solve the "sensitivity equations"

$$\partial\,\dot{\hat{x}}/\theta_k = \partial f/\partial\theta_k + F(t)\,\partial\,x/\partial\theta_k \tag{88}$$

where $F(t) = \partial F(t)/\partial\,x\Big|_{x\,=\,\hat{x}}$

The initial conditions of $\partial\hat{x}/\partial\theta_k$ are zero except when $x(0)$ is identified as part of the parameter vector $\hat{\theta}$. In this case the initial partials have the value one.

5. The likelihood function for zero system noise is

$$J = \log p(y_1 \cdot \cdot y_n/\theta) = - (1/2) \sum_{j=1}^{N} \nu_j^T R^{-1} \nu_j \qquad (89)$$

Determine now the gradient of this function with respect to θ

$$\partial J/\partial\theta = \sum_{j=1}^{N} \nu_j^T R^{-1} \partial\nu_j/\partial\theta \qquad (90)$$

where $$\partial\nu_j/\partial\theta = - H \partial \hat{x}_j/\partial\theta \qquad (91)$$

6. Compute the information or sensitivity matrix

$$M = \partial^2 J/\partial\theta^2 = \sum_{j=1}^{N} (\partial\nu_j/\partial\theta)^T R^{-1} \partial\nu_j/\partial\theta \qquad (92)$$

The inverse M^{-1} of the information matrix provides a lower bound for the covariance of the updated parameter estimates.

7. The updated parameter estimate is

$$\hat{\theta} = \theta_o + \Delta\theta \qquad (93)$$

where $$\Delta\theta = -M^{-1} (\partial J/\partial\theta)^T \qquad (94)$$

8. Go now back to equation 86 with the updated parameter estimate and repeat the steps to equation 93 . Reiterate until convergence of the information matrix and of the parameter vector is obtained.

The Maximum Likelihood method, which was used quite successfully in the single blade forward flight analysis and in multiblade hovering analysis (29), was extended to the multiblade forward flight analysis with the time delayed rotor inflow L-matrix model as defined before.

To study the question of L-matrix identification, simulation studies were performed for a hypothetical rotor with the characteristics of the model rotor treated in (9), so that the experimental values of the L-matrix determined in (9) could be used. The rotor was assumed to have a blade solidity ratio of .100 and a blade flapping frequency of $\omega_1 = 1.20$. The experimental model rotor has a blade solidity ratio of .154 and is usually run with a rotor speed corresponding to a blade flapping frequency of $\omega_1 = 1.17$. An advance ratio of .4 is the upper limit for a conventional helicopter. The dynamic rotor wake effects are rather small at this rotor advance ratio. The dynamic rotor wake parameter identification should be easier for lower advance ratios where the rotor wake has substantially larger effects. In order to study the feasibility of L-matrix identification, the most unfavorable case of .4 advance ratio was selected.

The inflow model chosen is given by equation 68. The theoretical values of K_M, K_{I_1} and K_{I_2}, using potential flow around a solid disc are $K_M = .849$ and $K_{I_1} = K_{I_2} \triangleq K_I = .113$. Choosing the values of the parameters of the $L_{\underline{E}}$ matrix from (9) at $\mu = .4$, the inflow model is obtained as

$$\begin{bmatrix} \dot{\nu}_o \\ \dot{\nu}_I \\ \dot{\nu}_{II} \end{bmatrix} + \begin{bmatrix} .5 & 0 & 0 \\ 0 & 1.5 & -0.6 \\ 0 & 0.3 & 0.6 \end{bmatrix} \begin{bmatrix} \nu_o \\ \nu_I \\ \nu_{II} \end{bmatrix} = 1.2 \begin{bmatrix} C_T \\ -7.5C_M \\ -7.5C_L \end{bmatrix} \qquad (95,$$

Here the number 7.5 represents the theoretical value of the ratio K_M/K_I. We will assume this value as given and identify only K_M, but not K_M and K_I separately. The inflow model is now assumed to have six unknown parameters θ_1 to θ_6, so that the above equation 95 is written in the form

$$\begin{bmatrix} \dot{\nu}_o \\ \dot{\nu}_I \\ \dot{\nu}_{II} \end{bmatrix} + \begin{bmatrix} \theta_1 & 0 & 0 \\ 0 & \theta_2 & \theta_3 \\ 0 & \theta_4 & \theta_5 \end{bmatrix} \begin{bmatrix} \nu_o \\ \nu_I \\ \nu_{II} \end{bmatrix} = \theta_6 \begin{bmatrix} C_T \\ -7.5C_M \\ -7.5C_L \end{bmatrix} \tag{96}$$

The flapping equations are the perturbation equations derived without reverse flow (equations 64, 65, 66 and 67). The system equations have the given parameters $a\sigma = 2\pi/10$, $\mu = 0.4$, tip loss factor $B = .97$, and the flapping frequency $\omega_1 = 1.20$. The Lock number will be assumed given as $\gamma = 5.0$ for some identification runs and will be assumed an additional unknown in other runs.

The inflow equations represent a feedback system, whereby most of the unknown parameters occur in the feedback loop. The feedback signal, ν, is unknown. The only measured quantities are θ_o, θ_I, θ_{II}, β_o, β_I, β_{II}, and β_d. The four other state variables are also unknown. The identification problem thus has seven unknown parameters if γ is included, four unknown state variables and three unknown feedback variables. One of the unknown parameters (θ_6) is a time constant.

The following studies were made using the above inflow model (equation 95)

a) The angular acceleration of the pitch stirring shaft was considered to be $\dot{\omega} = -.1/\pi$. The time of transient measurement is $t = 0$ to 12 time units, the sampling rate

$\Delta t = 0.1$ and the standard deviation of the measurement noise $\sigma_v = .05$. The average least squares fit $\sigma^2(\text{fit})$ is also noted, to determine the accuracy of the identified fit (Table 3).

From the above identification run it is seen that though most of the parameters converge, the accuracy of the estimates vary. The diagonal terms θ_1, θ_2 and θ_5 of the L matrix converge to more accurate parameter estimates than the off-diagonal terms θ_3 and θ_4. $\gamma \triangleq \theta_7$ is very sensitive to the response and hence converges faster and accurately to the true value.

(b) A priori knowledge of the parameter estimates is added to the likelihood function as a quadratic term involving the weighted difference between the estimated parameter values and the priori parameter values, i.e.,

$$(\hat{\theta}_i - \theta_o)^T \Lambda (\hat{\theta}_i - \theta_o) \qquad (97)$$

where Λ is the weighting matrix. The identification runs were under the same conditions as in (a). Two pitch stirring accelerations of $-.05/\pi$ and $-.1/\pi$ are studied. The weighting matrix Λ was taken to be $200I$. The Lock number, γ, which can be determined quite accurately, is assumed to be known at $\gamma = 5.0$.

The main point of interest in Tables 4a and 4b is the improvement in accuracy of M^{-1} values for the different parameters from $\dot{\omega} = -.05/\pi$ to $\dot{\omega} = -.1/\pi$. The values in the latter are about one-tenth the corresponding values for the M^{-1} values obtained by using the slower acceleration. There does not seem to be any appreciable change in $\sigma^2(\text{fit})$ between the two cases in Tables 4a and 4b and Table 3.

Table 3. Simulation Identification Study Results for the L-matrix Model (Equation 95) using the Maximum Likelihood Method with $\omega = -.1/\pi$; $t = 0 - 12$; $\Delta t = 0.1$; $\sigma_v = .05$.

	θ_1	θ_2	θ_3	θ_4	θ_5	θ_6	$\theta_7=\gamma$	σ^2(fit)
True Value	.5	1.5	-.6	.3	.6	1.2	5.0	
Initial Estimate	.6	1.8	-.7	.4	.7	1.4	4.0	.01703
Iteration 1	.515	.882	-.85	.294	.443	1.003	4.876	.00251
2	.46	1.36	-.83	.283	.615	1.205	4.995	.00246
3	.46	1.283	-.74	.222	.592	1.192	5.001	.00244
4	.46	1.29	-.75	.228	.595	1.197	5.003	
Error	.04	.21	.15	.072	.005	.003	.003	
Percent Error	8.0	20.7	25.0	24.0	0.8	.25	.06	
$M^{-1}/\lvert\theta\rvert$	.232	.225	.311	1.09	.322	.252	.042	
M^{-1}	.0111	.0808	.053	.0754	.0375	.0903	.0448	

Table 4a. Simulation Identification Study Results for the L-matrix Model (Equation 95) using the Maximum Likelihood Method with a Priori Knowledge of the Parameters in form of (97) added to the cost: $t = 0\text{-}12$; $\Delta t = 0.1$; $\sigma_v = 0.05$; $\omega = -.05/\pi$.

	θ_1	θ_2	θ_3	θ_4	θ_5	θ_6	σ^2(fit)
True Value	0.5	1.5	-0.6	0.3	0.6	1.2	
Initial Estimate	0.6	1.8	-0.7	0.4	0.7	1.4	.00251
Iteration 1	.593	1.791	-.727	.396	.737	1.379	.00248
Iteration 2	.586	1.783	-.749	.393	.757	1.391	.00247
Iteration 3	.581	1.714	-.766	.391	.768	1.398	.00247
Iteration 4	.576	1.765	-.78	.388	.776	1 403	
Error	.076	.265	.18	.088	.176	.203	
Percent Error	15.2	17.7	30.0	29.3	29.3	16.9	
M^{-1}	.2114	1.466	.2569	1.103	.362	.647	

Table 4b. Simulation Identification Study Results for the L-matrix Model (Equation 95) using the Maximum Likelihood Method with a Priori Knowledge of the Parameters in form of (97) added to the cost: $t = 0\text{-}12$; $\Delta t = 0.1$; $\sigma_v = 0.05$; $\dot{\omega} = -.1/\pi$.

	θ_1	θ_2	θ_3	θ_4	θ_5	θ_6	σ^2(fit)
True Value	0.5	1.5	-0.6	0.3	0.6	1.2	
Initial Estimate	0.6	1.8	-0.7	0.4	0.7	1.4	.00251
Iteration 1	.572	1.79	-.747	.407	.724	1.374	.00249
Iteration 2	.556	1.755	-.783	.413	.738	1.381	.00247
Iteration 3	.547	1.734	-.811	.419	.746	1.386	.00246
Iteration 4	.542	1.714	-.832	.425	.751	1.39	
Error	.042	.214	.232	.125	.151	.19	
Percent Error	8.4	14.2	38.6	41.6	25.	15.8	
M^{-1}	.0149	.1217	.0452	.0988	.047	.0657	

A priori weighting does not seem to have helped in obtaining better estimates of the parameter values. In cases of parameters θ_5 and θ_6, the identified values are much worse. The accuracy of most of the identified parameters don't seem to be very good.

(c) Another study of interest is the case where the induced flow is represented by the equivalent Lock number, γ^*. The simulated measurement data is obtained by using the full L-matrix induced flow model in determining the flapping response. This response is polluted with zero mean, Gaussian white noise of $\sigma_y = .05$ to obtain the measurement data (as before). The identification results are given in Table 5. Other conditions are the same as in (a) and (b).

The equivalent Lock number, γ^*, was identified and converges rapidly. The M^{-1} value obtained is low which shows the goodness of the identified value; but incomplete modeling (i.e., lack of an inflow model) gives rise to a $\sigma^2(\text{fit})$ value which is approximately twice as much as that obtained by using a complete inflow model in Table 4.

(d) In order to identify the elements of the L_E^{-1} matrix directly and also to identify the three mass and inertia terms separately, the inflow model as given by equation 68 is used rather than the simplified equation 96.

Table 5. Equivalent Lock Number γ^* Identified from Data Generated from the Full L-matrix Induced Flow Model $t = 0 - 12$; $\Delta t = 0.1$; $\sigma_v = .05$; $\dot{\omega} = -.05/\pi$.

	γ^*	σ^2 (fit)
Value of γ	5.0	
Initial Estimate	4.2	.00636
Iteration 1	3.863	.00504
2	3.85	.00504
3	3.849	.00504
4	3.849	
M^{-1}	.0013	

$$\begin{bmatrix} \dot{\nu}_O \\ \dot{\nu}_I \\ \dot{\nu}_{II} \end{bmatrix} + \mu \begin{bmatrix} \theta_6 & & \\ & -\theta_7 & \\ & & -\theta_8 \end{bmatrix} \begin{bmatrix} \theta_1 & 0 & 0 \\ 0 & \theta_2 & \theta_3 \\ 0 & \theta_4 & \theta_5 \end{bmatrix} \begin{bmatrix} \nu_O \\ \nu_I \\ \nu_{II} \end{bmatrix} = \begin{bmatrix} \theta_6 & & \\ & -\theta_7 & \\ & & -\theta_8 \end{bmatrix} \begin{bmatrix} C_T \\ C_M \\ C_L \end{bmatrix} \qquad (98)$$

where: $\theta_6 \triangleq 1/K_M$

$\theta_7 \triangleq 1/K_{I_1}$

$\theta_8 \triangleq 1/K_{I_2}$

The identification program was run under the same conditions as in (a) except that length of the identified data length is t = 0 to 18 instead of t = 0 to 12. The increase in data length was justified on account of the poor accuracy of the identified parameters and the high values of the Cramer-Rao lower bounds for the parameters. This increase in data length was verified in a later chapter on "Optimal Data Utilization". The results are tabulated in Table 6.

Once again, the off-diagonal terms of the L_E^{-1} matrix, show poor identifiability. The σ^2(fit) value does not show noticeable change from the results in (a). The improvement in the Cramer-Rao lower bounds with increase of the data length was expected.

The simulated measured responses together with the identified responses are given in Figures 7, 8, 9 and 10. The perturbation identified inflow is plotted in Figures 11, 12 and 13.

Detailed analysis of the simulation studies for pitch stirring acceleration of $\ddot{\phi} = .05/\pi$, $-.1/\pi$ and $.2/\pi$ are given in (34).

Table 6. Simulation Identification Study Results for the L-matrix Model (Equation 98) using the Maximum Likelihood Method with $\omega = -.1/\pi$; $t = 0 - 18$; $\Delta t = 0.1$; $\sigma_v = 0.05$.

	θ_1	θ_2	θ_3	θ_4	θ_5	θ_6	θ_7	θ_8	γ	σ^2(fit)
True Value	1.0	-.416	.167	-.083	-.167	1.18	8.84	8.84	3.2	
Initial Estimate	.83	-.333	.142	-.067	-.142	1.35	7.0	7.0	4.5	.0303
Iteration 1	1.163	-.296	.056	-.084	-.164	1.148	3.823	8.078	3.136	.0033
Iteration 2	.969	-.353	.122	-.065	-.179	1.41o	4.605	8.565	3.237	.00249
Iteration 3	.995	-.37	.11	-.059	-.167	1.438	4.818	8.522	3.242	
Error	.005	.036	.057	.024	.0	.258	4.022	.318	.042	
Percent Error	.5	8.6	34.	29.	0.	17.9	45.	3.6	1.3	
$M^{-1}/\lvert\theta\rvert$	.1206	.0794	.708	.17o	.11	.132	.418	.104	.014	

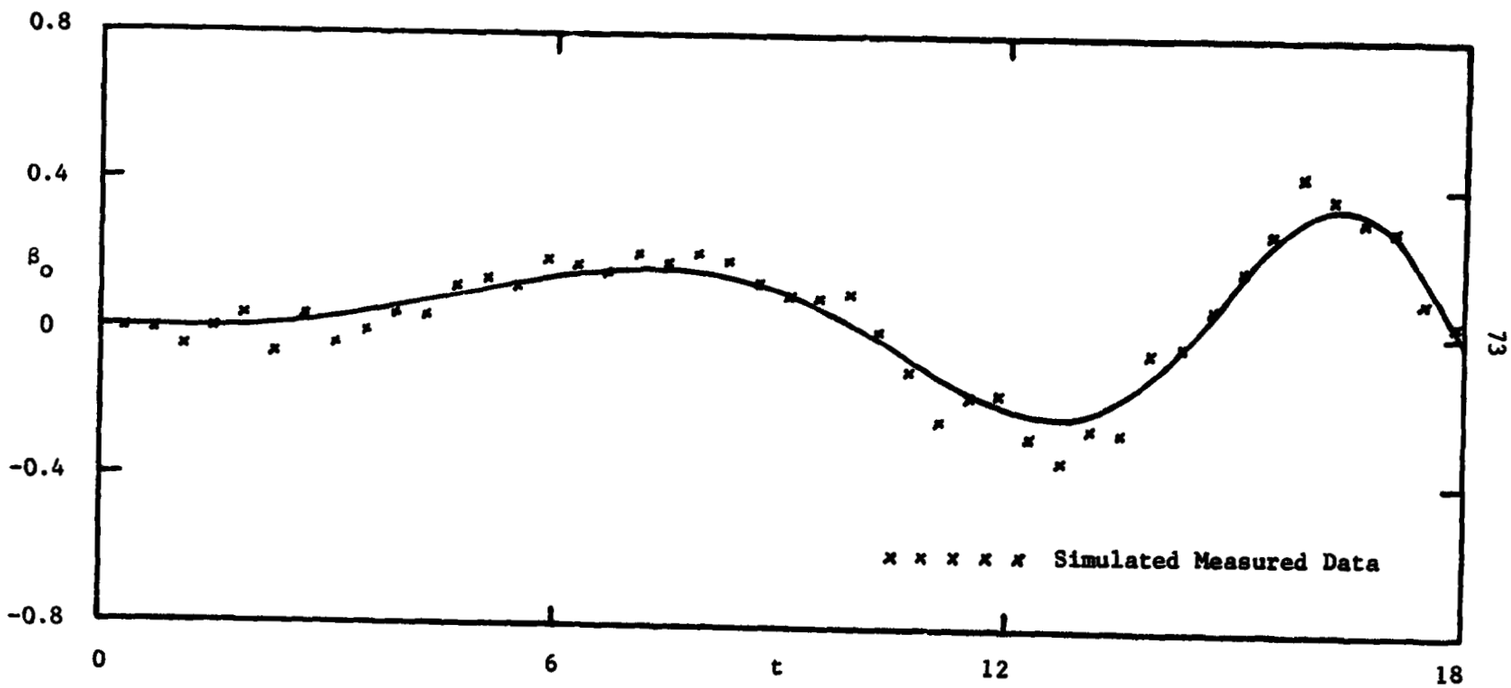

Figure 7. Simulated Measured and Identified Results of the Flapping Response β_o corresponding to Conditions in Table 6.

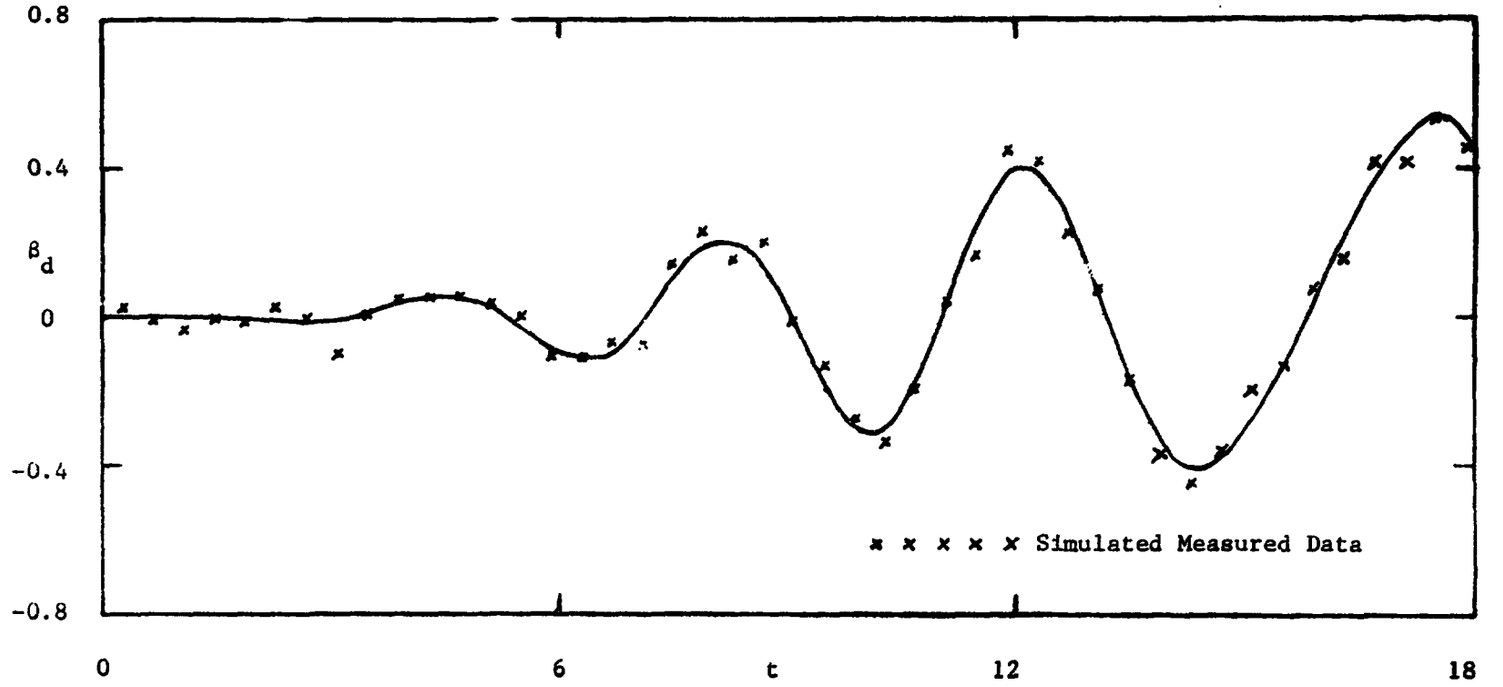

Figure 8. Simulated Measured and Identified Results of the Flapping Response β_d Corresponding to the Conditions in Table 6.

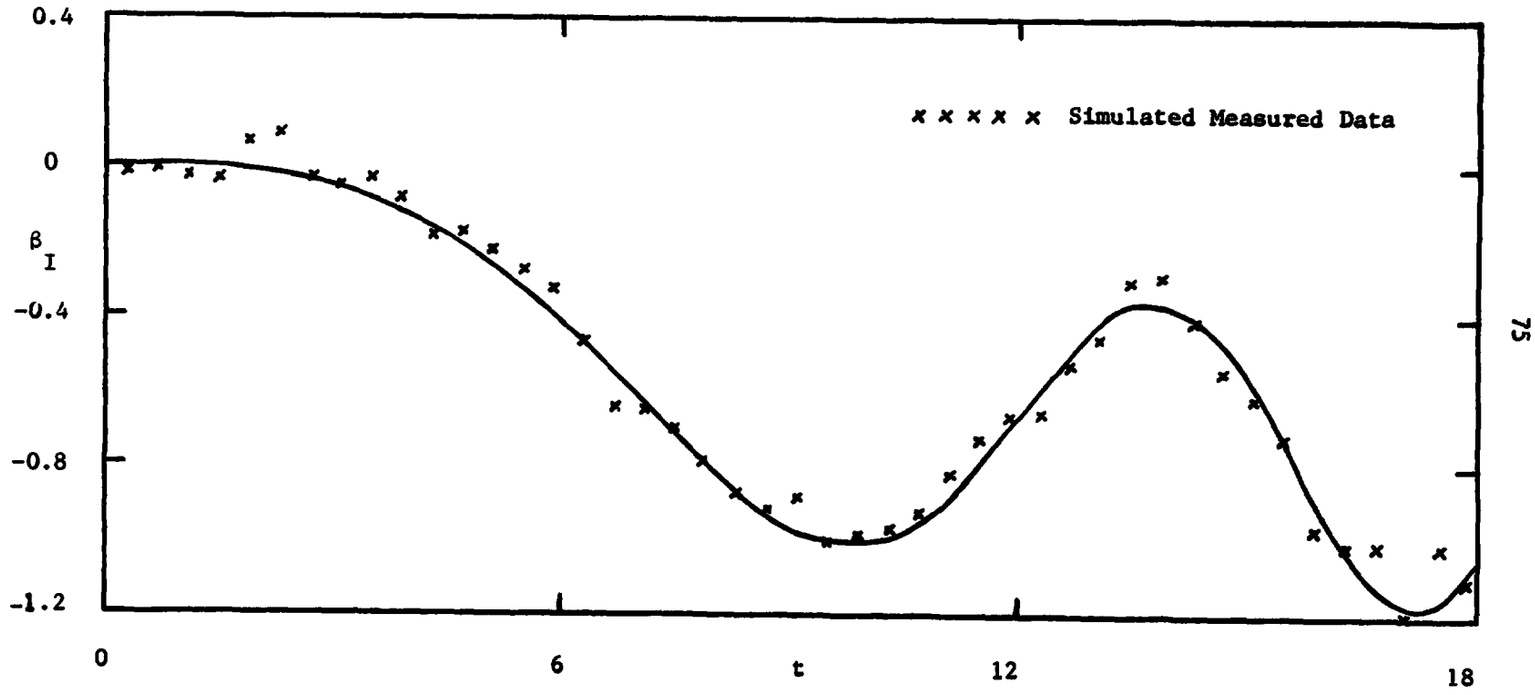

Figure 9. Simulated Measured and Identified Results of the Flapping Response β_I Corresponding to the Conditions in Table 6.

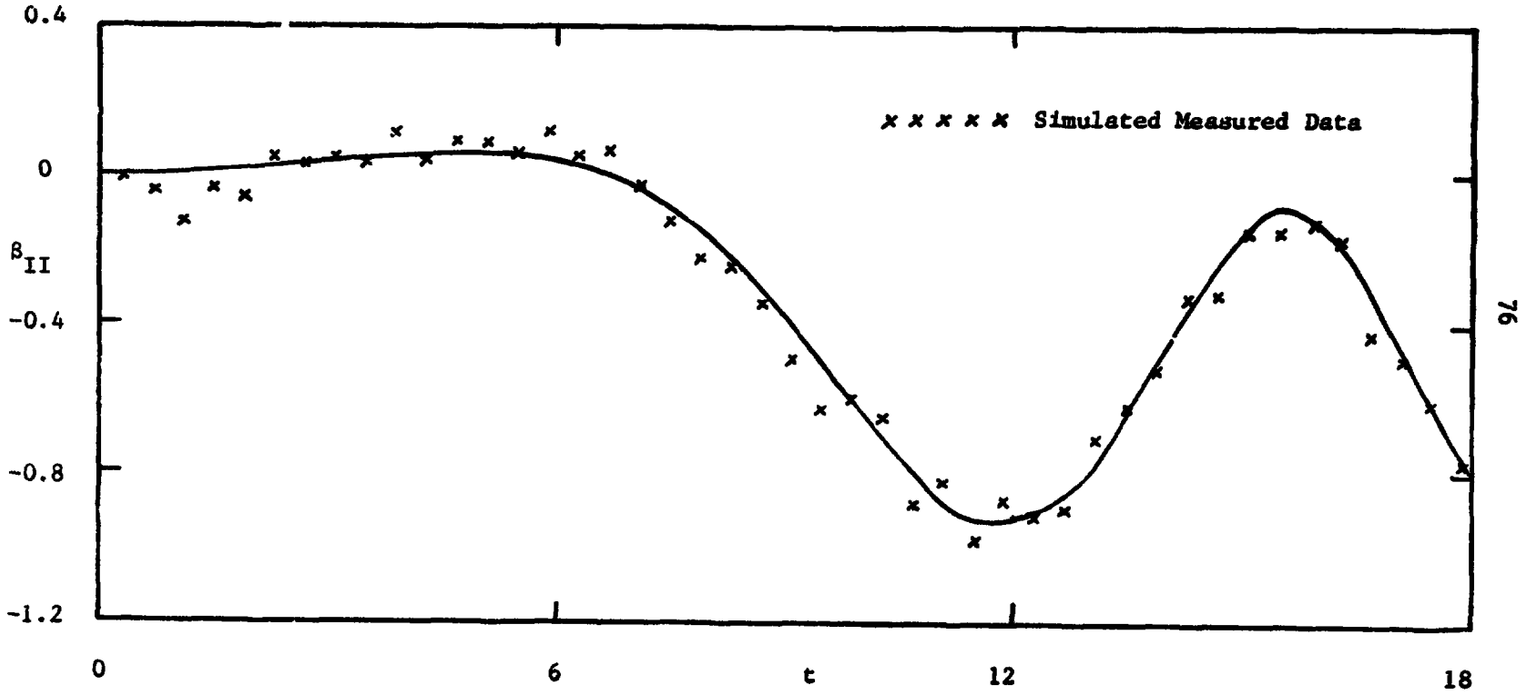

Figure 10. Simulated Measured and Identified Results of the Flapping Response β_{II} Corresponding to the Conditions in Table 6.

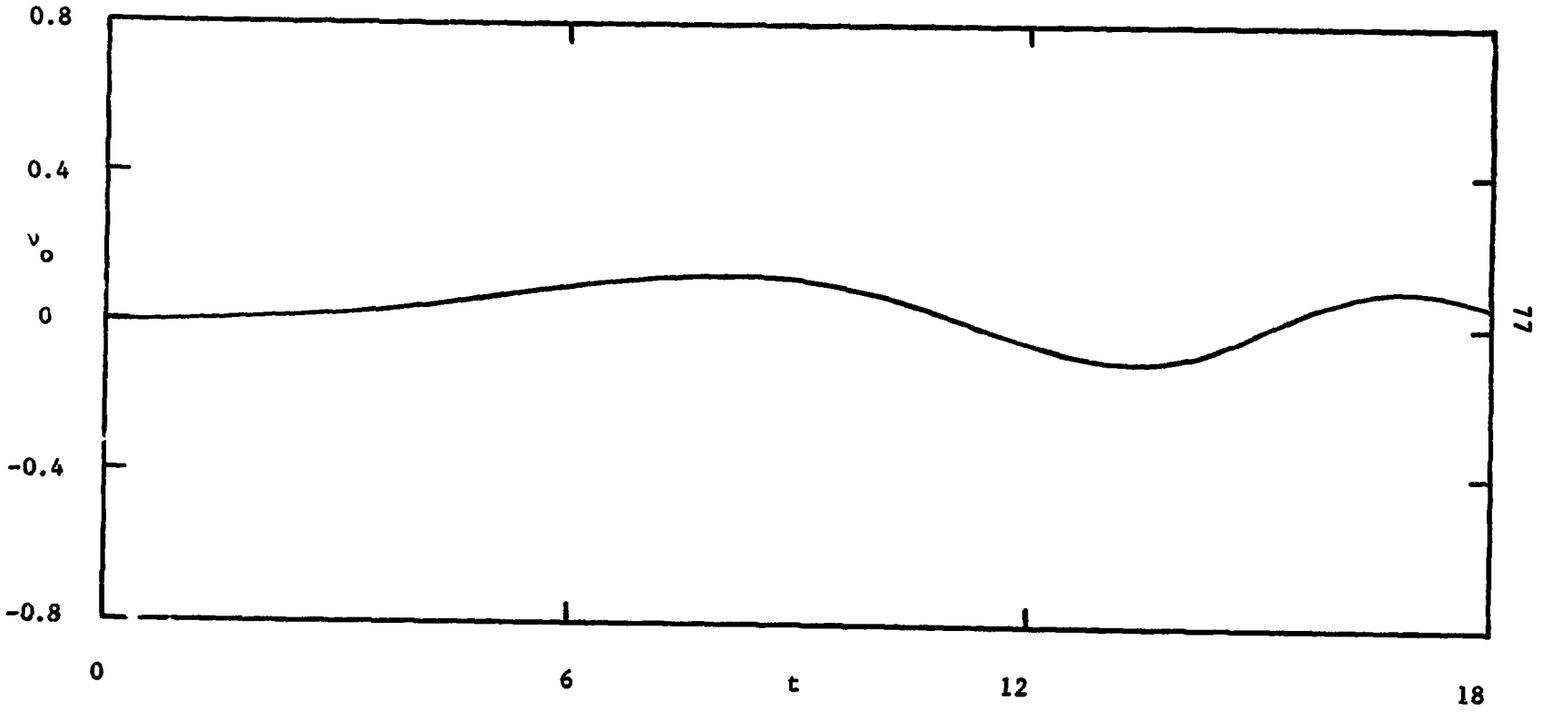

Figure 11. The Perturbation Induced Inflow ν_o for the Identified Model in Table 6.

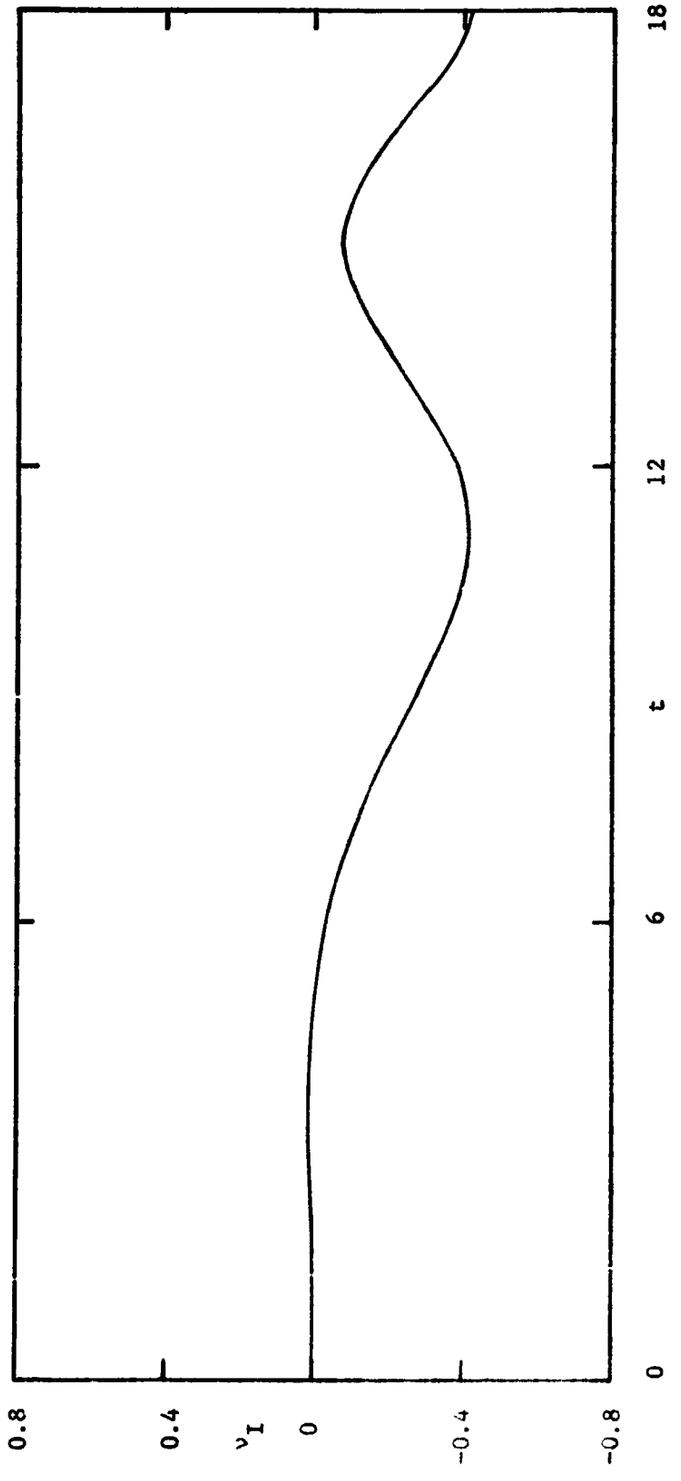

Figure 12. The Perturbation Induced Inflow v_I for the Identified Model in Table 6.

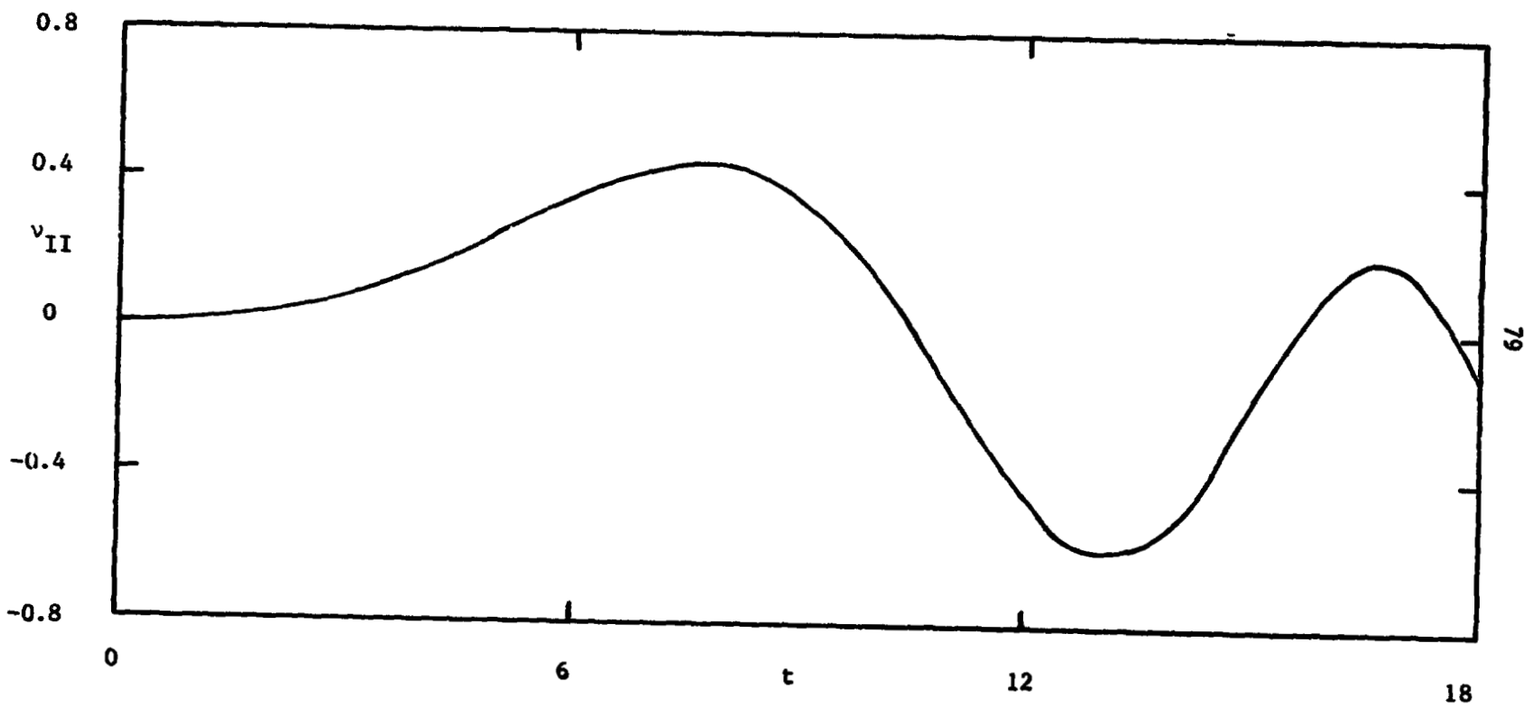

Figure 13. The Perturbation Induced Inflow ν_{II} for the Identified Model in Table 6.

4.3 EIGENVALUE ANALYSIS

The non-uniform downwash is strongly coupled to the moment response of hingeless rotors (9) and (11). This led to the study of the effect of the unsteady downwash on the rotor transient response and also rotor stability. Study of rotor transient response is made in the identification analysis of dynamic rotor response in the previous chapter. Stability studies are made by eigenvalue analysis of the dynamic flapping response of a rotor model.

As mentioned before, it was seen in (14) that, in hovering, the damping of the regressing flapping mode is substantially reduced by dynamic inflow effects at low collective pitch angle. In the following, results of the forward flight eigenvalue analyses are presented using different analytical models.

A detailed study was conducted using the forward flight model given by equations 64, 65, 66 and 67. The parameters of the inflow model given by equation 68 is obtained from Figure 4 of (9). Several important aspects of this analysis are:

The eigenvalue analysis is first conducted at $\mu = 0.4$ using a complete flapping transient model (including the feedback downwash model) with and without the periodic terms. The comparison of the eigenvalues is given in Table 7. Another interesting comparison with the above are the eigenvalues obtained by neglecting the downwash in the constant model. For the constant system, the eigenvalues are obtained directly by taking the Laplace transform of the system equation and then solving for the roots of the characteristic equation. The periodic system equations on the other hand, have to be solved by

Floquet theory as outlined in (35). According to the Floquet theory, the imaginary parts of the eigenvalues are indeterminate and in their multiples of one can be added or subtracted.

From Table 7 one can see that the error in representing the periodic system by a constant system (obtained by neglecting the periodic terms) is small, and therefore, the constant system is in our case, an accurate representation for the set of parameters used. The error in the eigenvalues in the above comparison are all within 2%. In contrast, the flapping model without the dynamic inflow model is significantly in error. The dynamic inflow reduces the damping of the regressing mode (fourth row of Table 7) by 40%.

The sensitivity of the eigenvalues with variation in parameter values was also studied for the constant model. The flapping eigenvalues seem to be insensitive to changes in values of the L-matrix parameters in the downwash model. Variation in value of the Lock number γ caused the real part of the eigenvalues to move closer to the imaginary axis with decrease in the value of γ.

The sensitivity of the eigenvalues to the parameters γ (Lock number) and ω_1^2 (blade natural frequency) is determined. The model chosen was the constant system without downwash. Change in ω_1^2 only changes the frequency component of the eigenvalues. The real part of the eigenvalue stays steady at A/2 (i.e., approximately $\gamma/16$). Table 8 shows the details.

Table 7. Comparison of the Eigenvalues Between the Three Different Forward Flight Models of the Flapping Response.

Eigenvalues at $\mu = 0.4$ ($\gamma = 5.0$; $\omega_1^2 = 1.4$)

Periodic System	Constant System with Downwash	Constant System without Downwash
-0.256±0.137j	-0.253±2.134j	-0.274±2.16j
-0.245±0.131j	-0.246±1.130j	-0.276±1.161j
-0.275±1.162j	-0.277±1.168j	-0.277±1.168j
-0.200±0.190j	-0.201±0.194j	-0.280±0.167j
-0.681+0.0j	-0.682+0.0j	
-1.299+0.0j	-1.316+0.0j	
-1.682+0.0j	-1.665+0.0j	

Table 8. Sensitivity of the Eigenvalues to Variation in ω_1^2 and γ in a Constant Forward Flight Mathematical Model Without Downwash.

Parameters	Eigenvalues			
$\omega_1^2 = 1.44$; $\gamma = 3.0$	-0.165±2.186j	-0.166±1.186j	-0.166±1.188j	-.167 ±.188j
$= 4.0$	-0.220±2.175j	-0.221±1.175j	-0.221±1.179j	-.223 ±.179j
$= 6.0$	-0.327±2.143j	-0.331±1.143j	-0.332±1.153j	-.337 ±.151j
$\gamma = 5.0$; $\omega_1^2 = 1.15$	-.274±2.030j	-0.276±1.029j	-0.277±1.037j	-.280±0.025j
$= 1.44$	-.274±2.160j	-0.276±1.161j	-0.277±1.168j	-.280±0.167j
$= 1.73$	-.274±2.278j	-0.276±1.279j	-0.277±1.285j	-.279±0.286j

The variation in the eigenvalues from hover to an advance ratio of $\mu = 0.4$ is given in Table 9. The constant system model with the complete downwash model is used. The parameter values used are those at $\mu = 0.4$, and given in equation 95. According to (9) the dynamic inflow parameters do not change much between $\mu = 0$ and $\mu = .4$.

Surprisingly, there is negligible change in the eigenvalues with change in advance ratio. The variation may be more pronounced if the changes of the inflow parameter values with change in advance ratio were taken into account.

At higher advance ratio the effect of reverse flow and periodic terms becomes important. To study this effect a comparison between three cases is made as shown in Table 10 for $\mu = 0.8$. Eigenvalues are compared for the following three models:

(1) A rotor model with the periodic terms, reverse flow effects and the complete inflow model

(2) The above complete model neglecting the reverse flow and periodic terms

(3) The model given in (1) with the downwash equations neglected.

From Table 10 it is seen that, neglecting the reverse flow and periodic terms did not affect the flapping eigenvalues significantly. The eigenvalues corresponding to the downwash were changed greatly. At high advance ratio, the feedback due to the dynamic inflow becomes relatively unimportant which is clearly seen in Table 10.

Table 9. Sensitivity of the Eigenvalues to Variation in Advance Ratio in a Constant Forward Flight Mathematical Model with Downwash.

Advance Ratio (μ)	Constant System with Downwash
0.0	-0.259±2.143j; -0.277±1.168j; -0.257±1.137j; -0.717+0j; -1.245+0j; -1.673+0j; -0.197±0.197j.
0.1	-0.259±2.142j; -0.277±1.168j; -0.256±1.137j; -0.715+0j; -1.25+0j; -1.672+0j; -0.198±0.197j.
0.2	-0.258±2.140j; -0.277±1.168j; -0.254±1.136j; -0.708+0j; -1.264+0j; -1.671+0j; -0.198±0.196j.
0.3	-0.256±2.138j; -0.277±1.168j; -0.251±1.133j; -0.697+0j; -1.286+0j; -1.669+0j; -0.199±0.196j.
0.4	-0.253±2.134j; -0.277±1.168j; -0.246±1.130j; -0.682+0j; -1.316+0j; -1.665+0j; -0.201±0.194j.

Table 10. Comparison of the Eigenvalues Between the Three Different Forward Flight Models at High Advance Ratio (μ = 0.8; ω_1^2 = 1.4; γ = 3.2).

Model (1)	Model (2)	Model (3)
-.181±2.143j	-.167±2.143j	-.187±2.148j
-.187±1.126j	-.174±1.147j	-.187±1.151j
-.187±1.147j	-.177±1.166j	-.187±1.151j
-.176±0.190j	-.180±0.175j	-.187±0.154j
-.580+0j	-.268+0j	
-2.451±0.151j	-5.148+0j	
	-17.937+0j	

4.4 OPTIMAL DATA UTILIZATION FOR PARAMETER IDENTIFICATION PROBLEMS WITH APPLICATION TO LIFTING ROTORS

In aircraft or wind tunnel transient testing the question comes up as to what kind of transient should be selected. If the transient is too short, the parameters will be identified with inadequate accuracy. If the transient is too long, an unnecessary amount of data must be processed. The question we pose here for the Maximum Likelihood method is – given a required accuracy of the parameter estimate, and given an input function, what is the minimal quantity of measured data necessary to achieve this accuracy? There are some recent studies where certain criteria were used to define an optimum input. We will first briefly discuss two of these optimal input proposals, and then proceed to develop the method of optimal data utilization for a given type of input.

4.4.1 Two Proposals for Optimal Input Design

General questions of input design are:

(a) What type of input function should be used?

(b) For what time period should the response data be processed to enable identification of the system parameters with a specified accuracy? Are certain time periods of the response particularly rich in information contents and should they, therefore, be preferably used?

There usually are some constraints on the input design like amplitude constraints, smoothness constraints (step or impulse inputs are mathematical idealizations but often practically not realizable),

instrumentation constraints, and constraints imposed by the selected analytical model that usually filters out the higher frequency contents of the input.

Analytical solutions of the problem of optimal input design require the minimization of a cost function. Stepner and Mehra (1) use the sensitivity of the system response to the unknown parameters as the performance criterion for optimal input design. The time of the transient is assumed to be fixed. Thus questions (b) are not involved. The measurement equation is

$$y_m(t) = y(x, \theta, u, t) + v(t) \tag{99}$$

We write the Taylor expansion with respect to the parameter θ about the a priori estimate θ_o of θ and neglect higher order terms:

$$y_m(t) = y(x, \theta_o, u, t) + \frac{\partial}{\partial \theta_o} y(x, \theta_o, u, t)(\theta - \theta_o) + v(t) \tag{100}$$

In the output error method $(\theta - \theta_o)$ is determined by a least squares solution of equation 100 for a fixed time period (t_o, t_f). For a high degree of accuracy in determining $(\theta - \theta_o)$ the sensitivity function $\partial y/\partial \theta$ must be large. The scalar performance index selected in (1) is

$$J = \text{Trace } (WM) \tag{101}$$

where

$$M = \int_{t_o}^{t_f} (\partial y/\partial \theta)^T \, R^{-1} (\partial y/\partial \theta) dt \tag{102}$$

Due to the introduction of R^{-1} in M, the performance criterion favors the measurements which are more accurate. The weighting matrix W is based on the relative importance of the parameter accuracies.

If we assume linear system and measurement equations

$$\dot{x}(t) = F\,x(t) + G\,u(t) \tag{103}$$

$$y_m(t) = H\,x(t) + v(t) \tag{104}$$

together with an "energy constraint" for the input

$$E = \int_{t_o}^{t_f} u^T u\, dt \tag{105}$$

the optimum input u can be determined as a two point boundary value problem whereby the Hamiltonian includes the term

$$(1/2)\mu_0\,(u^T u - E/t_f)\ .$$

The scalar μ_o is the time invariant Lagrange factor to be evaluated from the Euler differential equations of the optimization problem. It should be noted that the " energy constraint" equation 105 has no physical significance but is a convenient device to obtain smooth input functions. Physically, the input will usually be limited by amplitude rather than by the quadratic criterion (equation 105) and quite different "optimal" inputs can then be expected.

(36) attacks the problem of optimal input design in an entirely different way as a time-optimal control problem by minimizing

$$J = \int_{t_o}^{t_f} dt \tag{106}$$

under the following constraints:

System Equations

$$\dot{x} = f(x, u, \theta, t) \quad , \quad x(t_o) = x_o \tag{107}$$

Sensitivity equations

$$\partial\dot{x}/\partial x_o = (\partial f/\partial x)(\partial x/\partial x_o) \; , \; \partial x(t_o)/\partial x_o = I \tag{108}$$

$$\partial\dot{x}/\partial\theta = (\partial f/\partial x)(\partial x/\partial\theta) + \partial f/\partial\theta, \; \partial x(t_o)/\partial\theta = 0 \tag{109}$$

Information matrix equations

$$\dot{M}^{-1} = -M^{-1}(\partial v/\partial\theta)^T R^{-1}(\partial v/\partial\theta)M^{-1} \tag{110}$$

where v is the innovation:

$$v = y_m - y \tag{111}$$

and where the information matrix M is given by equation 102.

Finally, Chen assumes an amplitude constraint

$$|u| \leq V \tag{112}$$

and he prescribes the trace of the information matrix for time t_f

$$C_{ii}(t_f) = \sigma_i^2 \tag{113}$$

One can show that for linear input $u(t)$ into the system equation and for an input matrix independent of any unknown parameter, the optimal input is of the "bang-bang" form between the amplitude constraints. The solution of this problem requires a computer search which was not performed (36). Rather, an arbitrary set of bang-bang inputs in the form of Walsh functions was shown to

result in a specific case in lower values of $M^{-1}(t_f)$ (given t_f) than those obtained by using Mehra's "optimal input". This apparent contradiction can be explained by the differential equation 110 governing M^{-1}. For a particular value of M^{-1} the rate of decrease of M^{-1} with time is dependent on <u>all</u> elements of

$$(\partial y/\partial \theta)^T R^{-1}(\partial y/\partial \theta)$$

while Mehra, in his criterion (equation 101) optimizes only the trace of WM.

While the input amplitude constraint (equation 112) used by Chen is physically more significant than the quadratic constraint (equation 105) used by Mehra, the actual constraints are usually still more complex. In cases of airplanes or lifting rotors one usually wishes to limit the response to the linear sub-stall regime, since the analytical model to be identified is often a linear one. The stall boundary is, however, a complex function of the input and cannot be represented by an amplitude constraint for the input transient. This is particularly relevant for the lifting rotor, so that neither the Mehra nor the Chen input optimization criteria is useful for lifting rotor applications, quite apart from the excessive computer effort involved in obtaining the optimal inputs. Furthermore, the input matrix usually contains unknown parameters. In this case,Chen's optimum solution would not be of the bang-bang type and would be still more difficult to obtain. For all of these reasons it was concluded that at the present state of optimal input design methods an attempt to compare our selected inputs with an

"optimum input" would not be practical. Instead, a more limited approach has been taken described in the following section.

4.4.2 Optimal Data Utilization for given Input Function

We first point out the difference between the continuous and the discrete case. In the Maximum Likelihood (output error method for zero process noise) using the Newton-Raphson approach with quasi-linearization, one obtains for the parameter update increment the following expressions:

Continuous case:

$$\Delta\theta = \left[\int_{t_o}^{t_f} \left(\frac{\partial \nu}{\partial \theta}\right)^T R^{-1} \left(\frac{\partial \nu}{\partial \theta}\right) dt\right]^{-1} \int_{t_o}^{t_f} \left(\frac{\partial \nu}{\partial \theta}\right)^T R^{-1} \nu \, dt \quad (114)$$

Discrete case:

$$\Delta\theta = \left[\sum_{i=1}^{N} \left(\frac{\partial \nu}{\partial \theta}\right)_i^T R^{-1} \left(\frac{\partial \nu}{\partial \theta}\right)_i\right]^{-1} \sum_{i=1}^{N} \left(\frac{\partial \nu}{\partial \theta}\right)_i^T R^{-1} \nu_i =$$

$$= M^{-1} \left(\frac{\partial J}{\partial \theta}\right) \quad (115)$$

The Cramer-Rao lower bound has been defined only for a vector of sampled measurements and not for the continuous case (2) and (18).

For high sampling rate, one can define an approximate differential equation for M from equation 115 in the following way:

$$\text{Set} \qquad S_i \triangleq (\partial \nu / \partial \theta)_i \quad (116)$$

then

$$M = \sum_{i=1}^{N} S_i^T R^{-1} S_i = \frac{1}{\Delta t} \sum_{i=1}^{N} S_i^T R^{-1} S_i \, \Delta t \quad (117)$$

As N increases, Δt gets smaller and the right hand side of equation 117 can be approximated by

$$M \approx (1/\Delta t) \int_{t_o}^{t_f = N\Delta t} S^T R^{-1} S \, dt \tag{118}$$

$$M^{-1} \approx \Delta t \left[\int_{t_o}^{t_f} S^T R^{-1} S \, dt \right]^{-1} \tag{119}$$

Taking the derivative of M^{-1} with respect to t_f:

$$dM^{-1}/dt_f = -M^{-1}(\partial M/\partial t_f)M^{-1}$$

or with equation 118

$$dM^{-1}/dt_f = -(1/\Delta t)M^{-1} S^T R^{-1} S M^{-1} \tag{120}$$

The point is that even in a continuous formulation the time increment Δt between samplings must occur. Equation 119 is the correct formulation for the Cramer-Rao lower bound of the covariance matrix for the parameters. (36) has a recursive formulation corresponding to equation 120.

We can now use the approximately valid differential equation 120 to obtain some insight into ways of best data utilization. Let us assume that we wish to prescribe certain values for the parameter standard deviations σ_i and that we wish to compare the Cramer-Rao lower bound with these standard deviations. Since we are dealing not with the unknown actual parameter covariances but only with their lower bounds, we should apply some conservatism to the selected σ_i.

that is we should select σ_i smaller than we really need for the specific data processing case. We thus require

$$0 \leq M_{t_f}^{-1}(i, i) \leq \sigma_i^2 \qquad (121)$$

whereby $M_{t_f}^{-1}$ is the value of M^{-1} at time t_f. For non-zero values of S, the right hand side of equation 120 is negative definite and hence $M_{t_f}^{-1}$ (i, i) are monotonically decreasing functions of t_f. There will, thus, be a minimum time for which the constraints of equation 121 are satisfied.

Another way of reducing the amount of measured data for the parameter identification is to select for the data processing those time periods for which the components of the matrix

$$S^T R^{-1} S$$

have significant values. It follows from equation 119 that the Cramer-Rao lower bound M^{-1} then will be particularly small. The components of M^{-1} also decrease with decreasing time element Δt between samples.

Since it is impractical to use for the integration of equation 120 infinity as initial condition, it is recommended to determine M^{-1} for a small time period, say for $N = 10$, from equation 119 and integrate equation 120 with the solution to equation 119 as initial conditions. Since S includes parameter estimates, one needs a preliminary estimation of the unknown parameters in order to use equation 120.

4.4.3 Application to a Case of Lifting Rotor Parameter Identification

The simplest mathematical model of the single blade flapping equation as expressed in equation 52 is used to identify the two unknown parameters: the collective pitch angle θ_o and the equivalent Lock number γ. The angular acceleration, in the pitch stirring transient, is assumed to be $\dot{\omega} = .1/\pi$ and $t_o = 12$.

Here we are concerned with the problem of designing the tests in such a way that the test data will be sufficient to determine the two unknown parameters γ and θ_o with good accuracy, i.e., to determine a suitable value of T that allows an accurate identification of parameters.

The simulated identification analysis was performed under the assumption of a random zero mean white noise sequence superimposed on the analytical flapping transient. This transient was obtained for $\theta_o = 2^\circ$, $\mu = 0.4$ and $\gamma = 5.0$. For convenience, the parameters $\delta = \gamma\theta_o$ and γ instead of θ_o and γ were identified.

System and measurement equations corresponding to equations 103 and 104 are:

$$\begin{bmatrix} \dot{x}_1 \\ \dot{x}_2 \end{bmatrix} = \begin{bmatrix} 0 & 1 \\ -(\omega_1^2 + (\gamma/2)\,K(t)) & -(\gamma/2)C(t) \end{bmatrix} \begin{bmatrix} x_1 \\ x_2 \end{bmatrix} + \begin{bmatrix} 0 \\ (\gamma/2)m_{\theta_o} \end{bmatrix} \theta \tag{122}$$

$$y_m = [1 \quad 0] \begin{bmatrix} x_1 \\ x_2 \end{bmatrix} + v(t) \tag{123}$$

where

$$E\{v(t)\} = 0 \qquad E[v(t)\, v(\tau)] = 0.2\, \delta(t - \tau)$$

and $[x_1 \quad x_2] = [\beta \quad \dot{\beta}]$

We first show in Table 11 the effect of data length on the parameters and their associated M^{-1} (i, i) values. The iteration of the Maximum Likelihood method was begun with a 20 percent error in the parameter values. It is seen that a data length of $t = 12 - 14$ is quite inadequate, a data length of $t = 12 - 18$ gives reasonably good parameters, while a data length of $t = 12 - 24$ is much better and leads to a very small lower bounds of the parameter covariance matrix. Figure 14 shows the correct flapping response together with the simulated measurement data. Pitch stirring is initiated at $t = 12$. Figures 15 and 16 show $M^{-1}(\gamma)$ and $M^{-1}(\delta)$ from equation 120 between $t = 16$ and $t = 24$. Two curves are plotted, one for the initial crude estimate of the parameters ($\gamma = 4$, $\delta = 8$), and one for the final estimate of the parameters for $t = 24$, ($\gamma = 4.91$, $\delta = 9.83$). The two curves are in this case not much different. Note the steep descent of the curves to about $t = 17.5$. It would, therefore, not be acceptable to use the data up to less than the time $t = 17.5$. However, there is another descent to $t = 23.0$, causing the improvement shown in Table 11. From Figures 15 and 16 it is clear that the selection of $T = 24.0$ is a good one, that the use of fewer data would result in substantial decrease in parameter accuracy, and that the use of additional data is unnecessary.

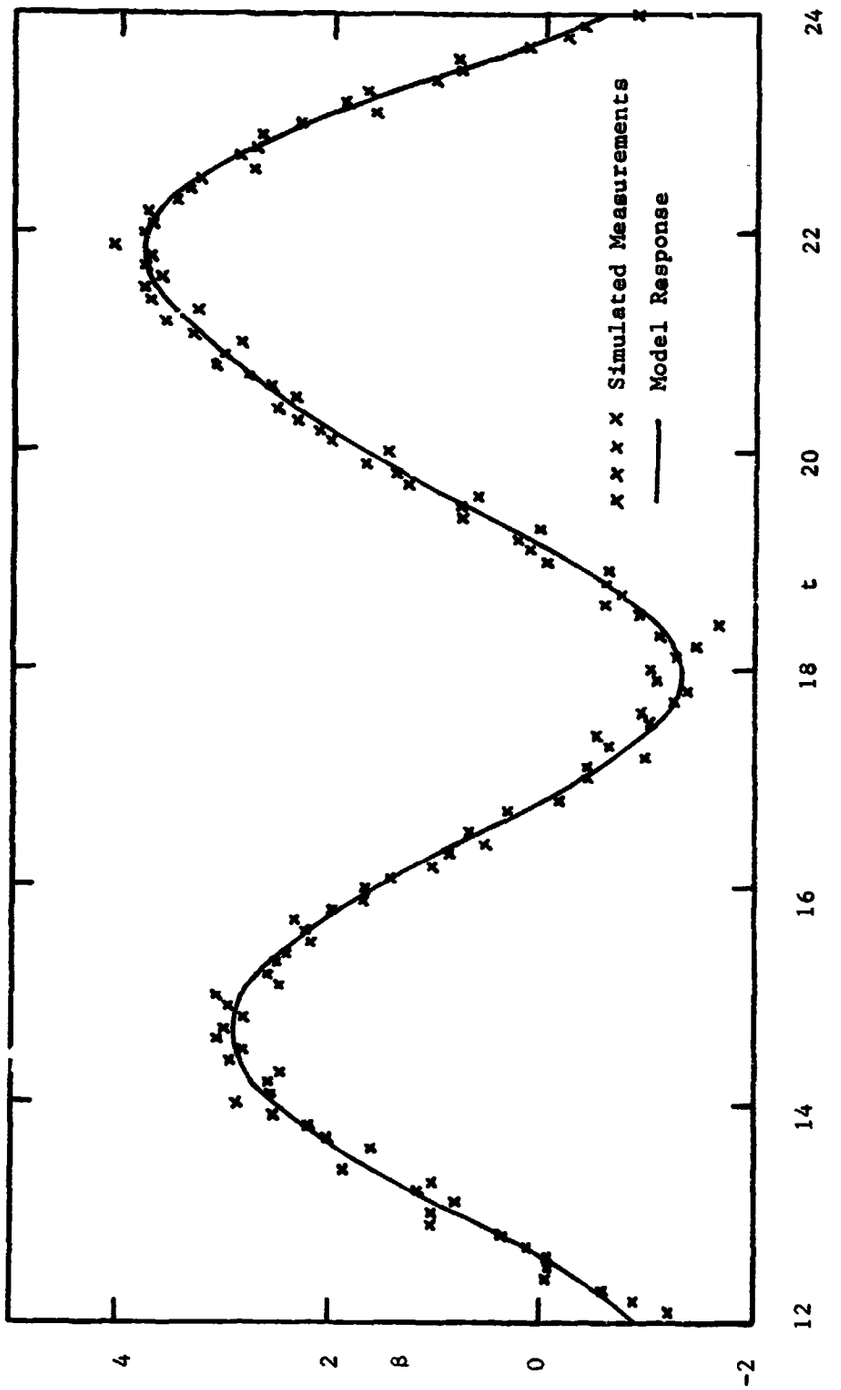

Figure 14. Plot of the Correct Flapping Response and the Simulated Measured Data Corresponding to Equations 122 and 123.

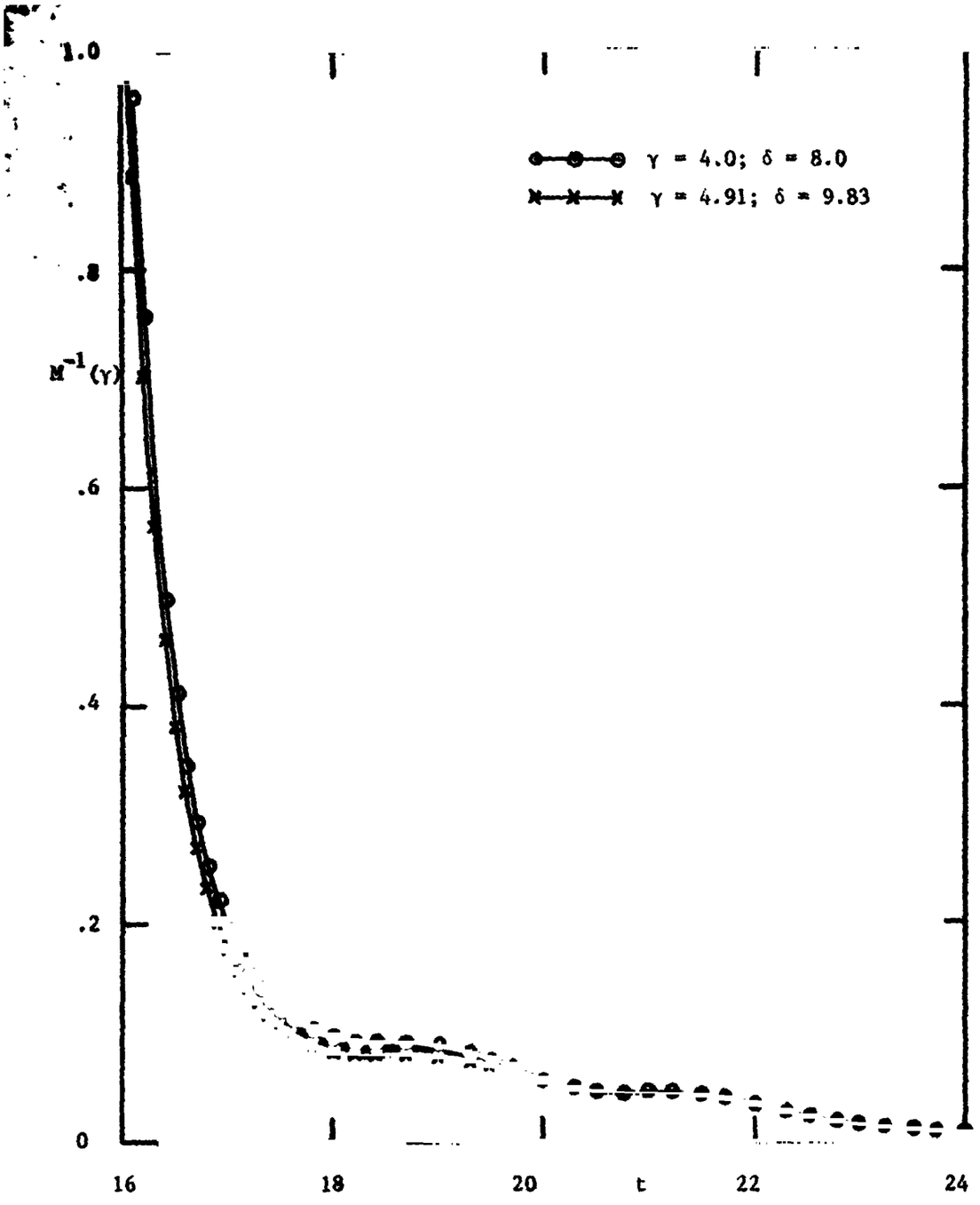

Figure 15. Plot of the Cramer-Rao Lower Bound of the Parameter covariance for the Parameter γ from the continuous Formulation given by Equation 120.

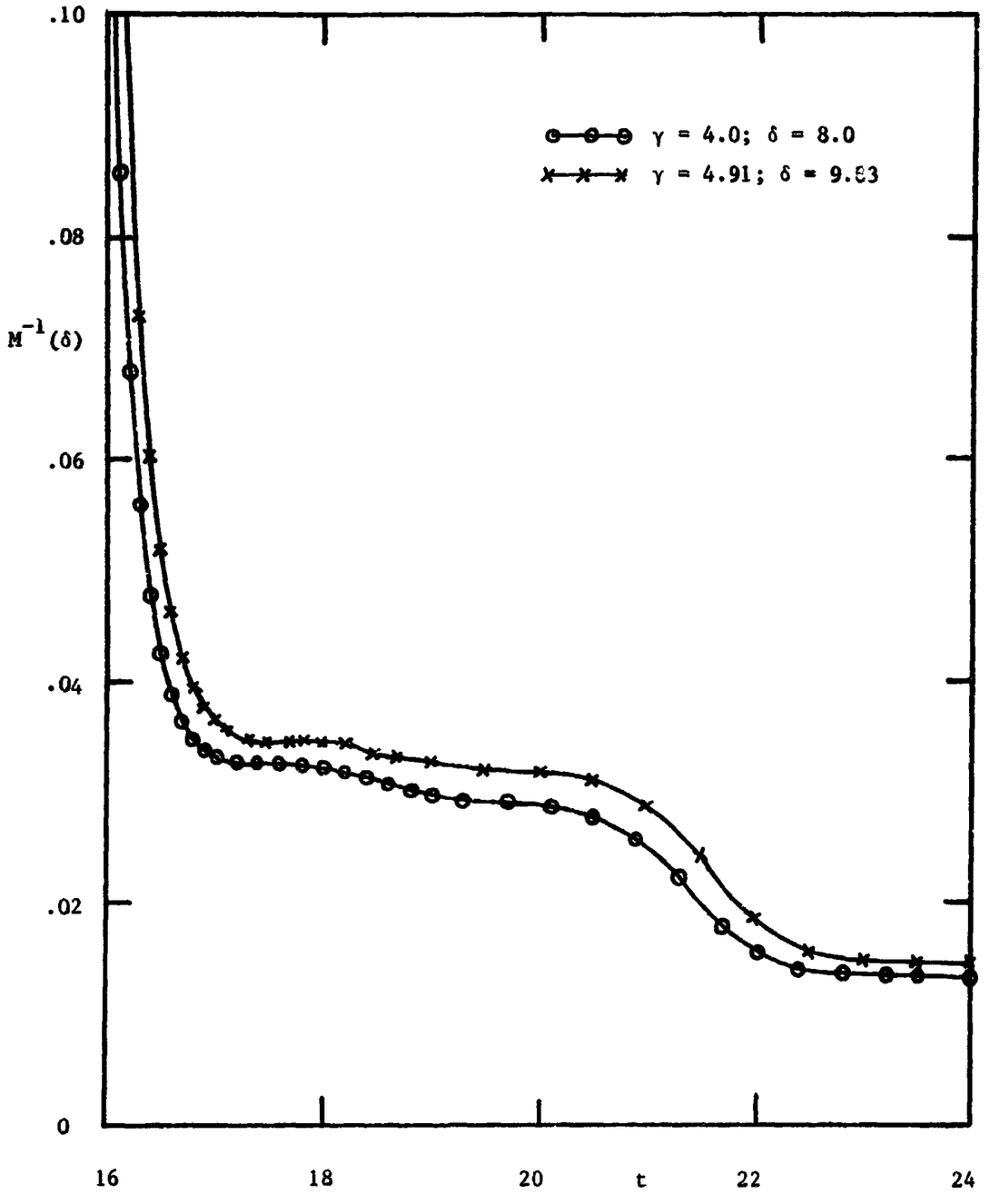

Figure 16. Plot of the Cramer-Rao Lower Bound of the Parameter covariance for the Parameter δ from the continuous Formulation given by Equation 120.

Table 11. Parameter Identifiability for Different Data Length — Single Blade Model (Equations 122 and 123) with Parameters γ and $\delta \underset{\sim}{\Delta} \theta_0 \gamma$.

i) t = 12 - 14

Parameter		γ	δ	$M^{-1}(\gamma)$	$M^{-1}(\delta)$
Initial Estimates		4.00	8.00		
Iteration	1	4.29	9.73	48.0	6.5
	2	4.17	9.71	37.0	8.1
	3	4.10	9.67	37.0	8.0

ii) t = 12 - 18

Parameter		γ	δ	$M^{-1}(\gamma)$	$M^{-1}(\delta)$
Initial Estimates		4.00	8.00		
Iteration	1	5.36	9.67	.096	.032
	2	5.23	9.73	.100	.035
	3	5.23	9.73	.094	.035

iii) t = 12 - 24

Parameter		γ	δ	$M^{-1}(\gamma)$	$M^{-1}(\delta)$
Initial Estimates		4.00	8.00		
Iteration	1	4.94	9.69	.007	.013
	2	4.91	9.85	.008	.015
	3	4.91	9.83	.008	.015

An analogous analysis was made for a forward flight condition, assuming the same pitch stirring transient and the same measurement noise. Now seven instead of three parameters must be identified.

Figure 17 is a plot of the standard deviation (square roots of the Cramer-Rao lower bound) of the various parameter estimates versus the time of identification. The standard deviation is plotted as a percentage of the parameter value. The graphs are drawn under the following specifications:

Parameter values chosen:

$\theta_1 = .5$

$\theta_2 = .9$

$\theta_3 = -.8$

$\theta_4 = .3$

$\theta_5 = .5$

$\theta_6 = 1.0$

$\theta_7 = \gamma = 4.9$

$$\begin{bmatrix} \dot{v}_o \\ \dot{v}_I \\ \dot{v}_{II} \end{bmatrix} + \begin{bmatrix} \theta_1 & 0 & 0 \\ 0 & \theta_2 & \theta_3 \\ 0 & \theta_4 & \theta_5 \end{bmatrix} \begin{bmatrix} v_o \\ v_I \\ v_{II} \end{bmatrix} = \theta_6 \begin{bmatrix} C_T \\ 7.5C_M \\ 7.5C_L \end{bmatrix} \tag{124}$$

Pitch stirring excitation:

$$\begin{aligned} \theta_I &= 1.5 \sin [\omega(t - t_o)] \\ \theta_{II} &= 1.5 \cos [\omega(t - t_o)] \end{aligned} \tag{125}$$

where $$\omega = \begin{cases} 0 & t < t_o \\ -(0.1)(t - t_o)/\pi & t_o < t \leq T \end{cases}$$

Measurement noise statistics: Mean = 0
Std. deviation = .05

Sampling time $\Delta t = 0.1$ time units

Advance ratio $\mu = .4$

The plot gives us the degree of identifiability of the parameter as a function of time length of identification. The Lock number $\gamma = \theta_7$ is identifiable with a much higher degree of accuracy than the various parameters in the perturbation downwash equations. This was seen clearly in the simulation studies for the identification of the parameters. Beyond a time length of $T = 18$ the curves flatten out, indicating that measurement beyond that time does not improve the accuracy of the parameters identified. This is in agreement with the result for zero advance ratio. The above time length seems to be necessary and also adequate for identification purposes, for the given sampling rate and excitation.

In our previous simulation studies we have used a sampling time of $T = 12$ time units. From Figure 17 it appears that inaccuracies in our identified parameters could be attributed to inadequate data length for identification purposes. This factor will be taken into consideration in parameter identifications using test data.

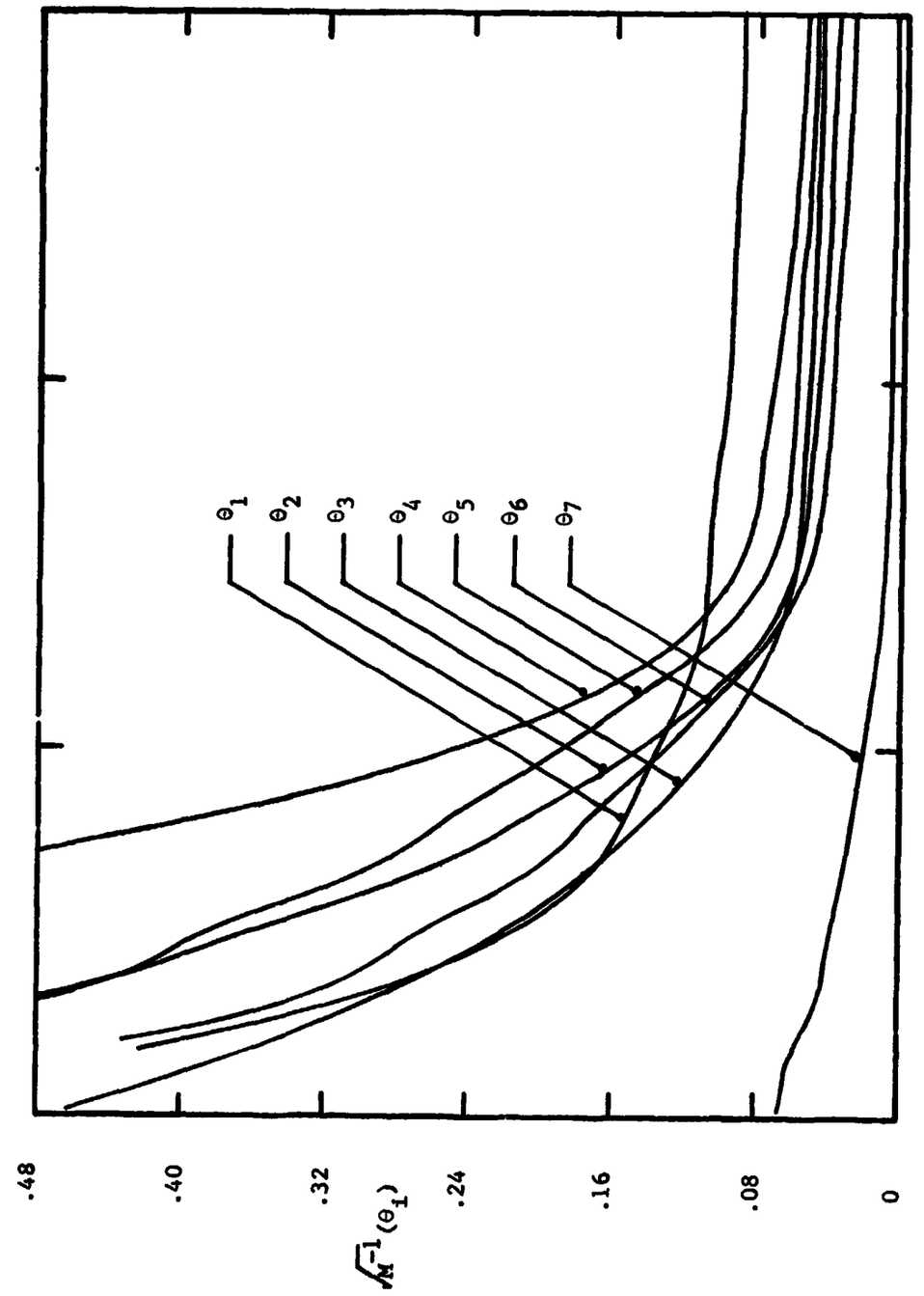

Figure 17. Plot of the Square Root of the Cramer-Rao Lower Bound Versus Length of Transient for the Forward Flight Model with a Downwash Mathematical Model given by Equation 124 and Input Conditions by Equation 125.

5. BRIEF DESCRIPTION OF THE EXPERIMENTAL SET-UP

The basic purpose of the experimental set-up is to measure continuously the flapping response of the rotor blades to cyclic pitch stirring excitation. A sampled length of the response, together with the input excitation, is used to identify the dynamic inflow parameters and hence determine the feedback effect of the rotor wake on the flapping response.

The experiment can be split up into three independent circuits:

1. The strain gauge (the flapping response measurement) circuit
2. The pitch resolver circuit
3. The rotor resolver circuit

A brief description of the above circuits are given below. For a detailed description of the experimental equipment and procedure see (12).

5.1 STRAIN GAUGE CIRCUIT

Four strain gauges are mounted on the flexure of each blade to form a Wheatstone bridge. Two strain gauges on the top and two strain gauges at the bottom of each flexure are so connected that the torsional and the lead-lag motions, if any, are annulled. The rotor is considered to be very stiff in torsion and lead-lag. A schematic diagram of the strain gauge circuit is shown in Figure 18.

Power is supplied to two arms of the bridge through two slip rings. The signal is taken out through two other slip rings from the other two arms of the bridge. The signal is passed through medium-gain amplifiers and recorded on a six channel FM tape-recorder.

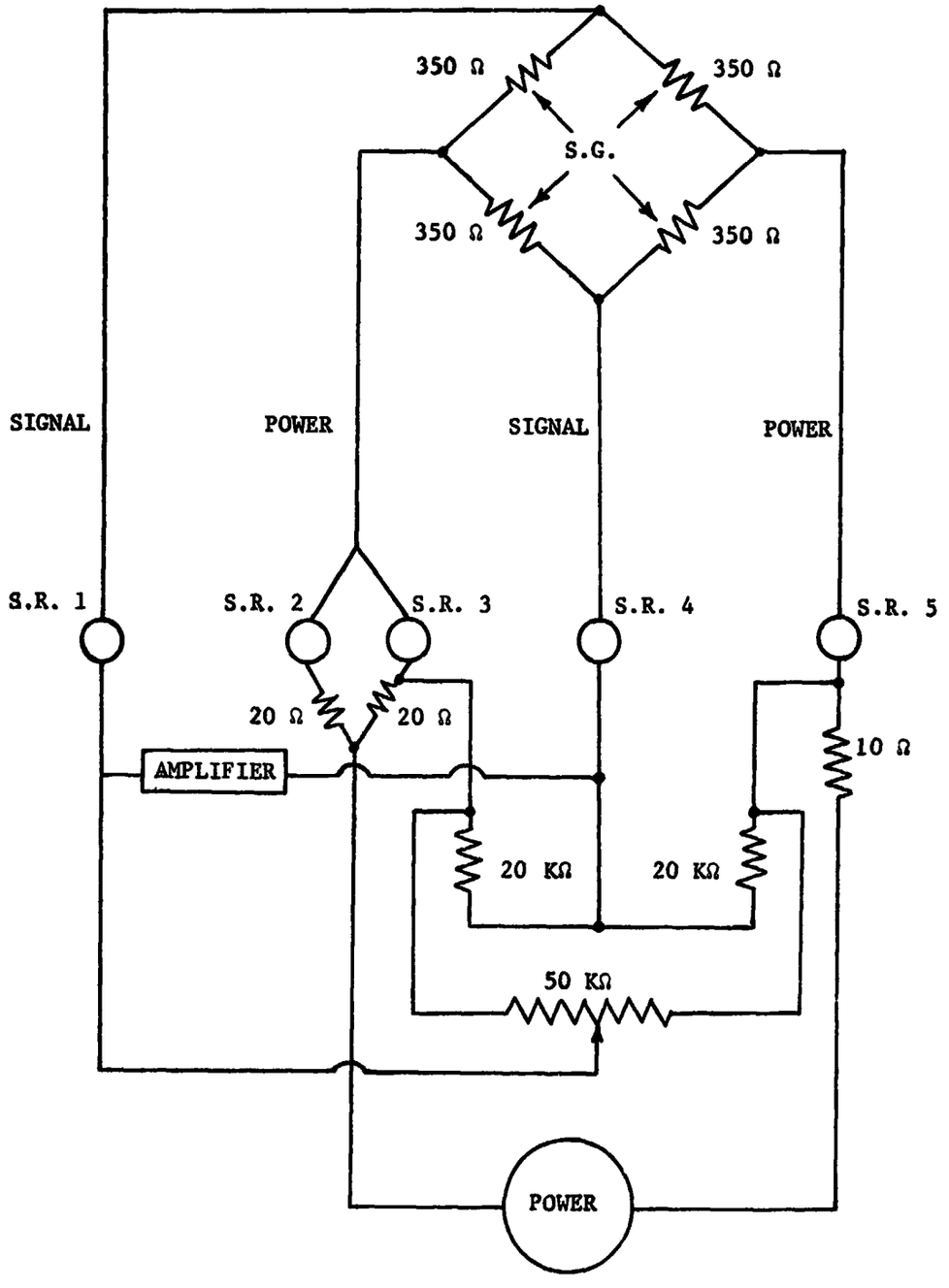

Figure 18. Schematic Diagram of the Balancing Network for each Strain Gauge Circuit (S.G. - Strain Gauge; S.R. - Slip Ring).

5.2 PITCH RESOLVER CIRCUIT

The resolver is a rotating transformer whose output varies sinusoidally with the angular position of the resolver shaft. The resolver shaft is connected by means of a sprocket drive to the inner shaft Figure 19 . The relative velocity of the rotor and the inner shafts provide the pitch stirring excitation. A brief description of the drive mechanisms will be given later. The input to the resolver is an oscillator whose frequency and amplitude can be varied to get desirable output signal from the resolver. The output signal is of a varying amplitude depending on the angular position of the resolver shaft with a carrier frequency corresponding to the input (oscillator) frequency. The signal is then passed through a full-wave rectifier-low pass filter circuit to remove the carrier frequency. The signal is then fed into a low-gain amplifier to adjust the output level of the signal. It then goes through a 3-way, 2-position switch which works as follows (Figure 20):

When the switch is in the "OFF" position, the input to the recorder is a 2.5 volt D.C. battery signal. When the switch is flipped to the "ON" position, the following events occur simultaneously:

a. The motor drive to the inner shaft is activated
b. The signal sent to the resolver is now the resolver signal
c. The solenoid that retains the inner shaft at a fixed (trim) condition, is released

5.3 ROTOR RESOLVER CIRCUIT

An oscillator provides the input to the resolver which provides the angular position of the main rotor shaft in a manner similar to the input to the resolver on the inner shaft. The output of the rotor

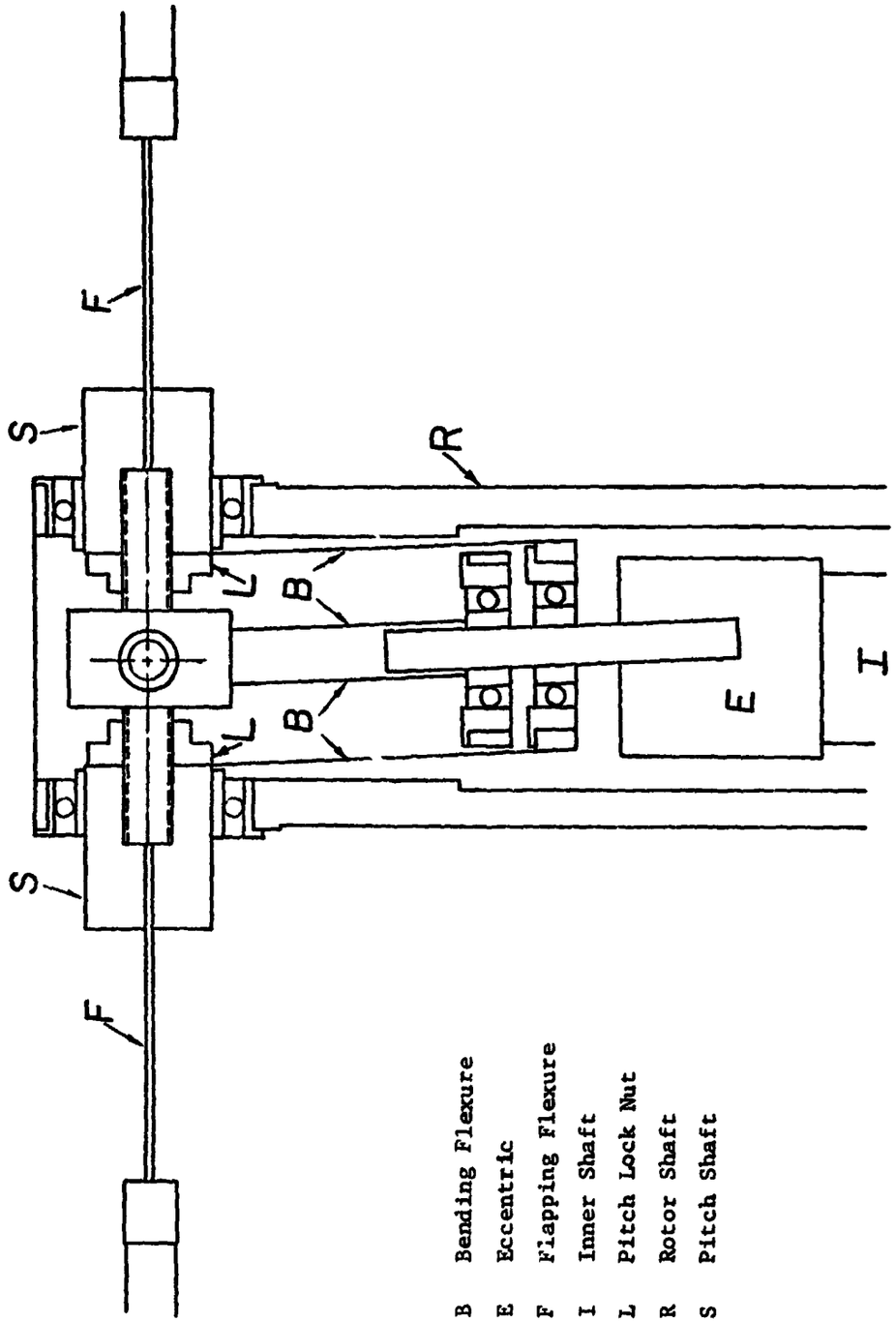

Figure 19. Schematic Diagram of the Blade-Hub-Shaft Assembly.

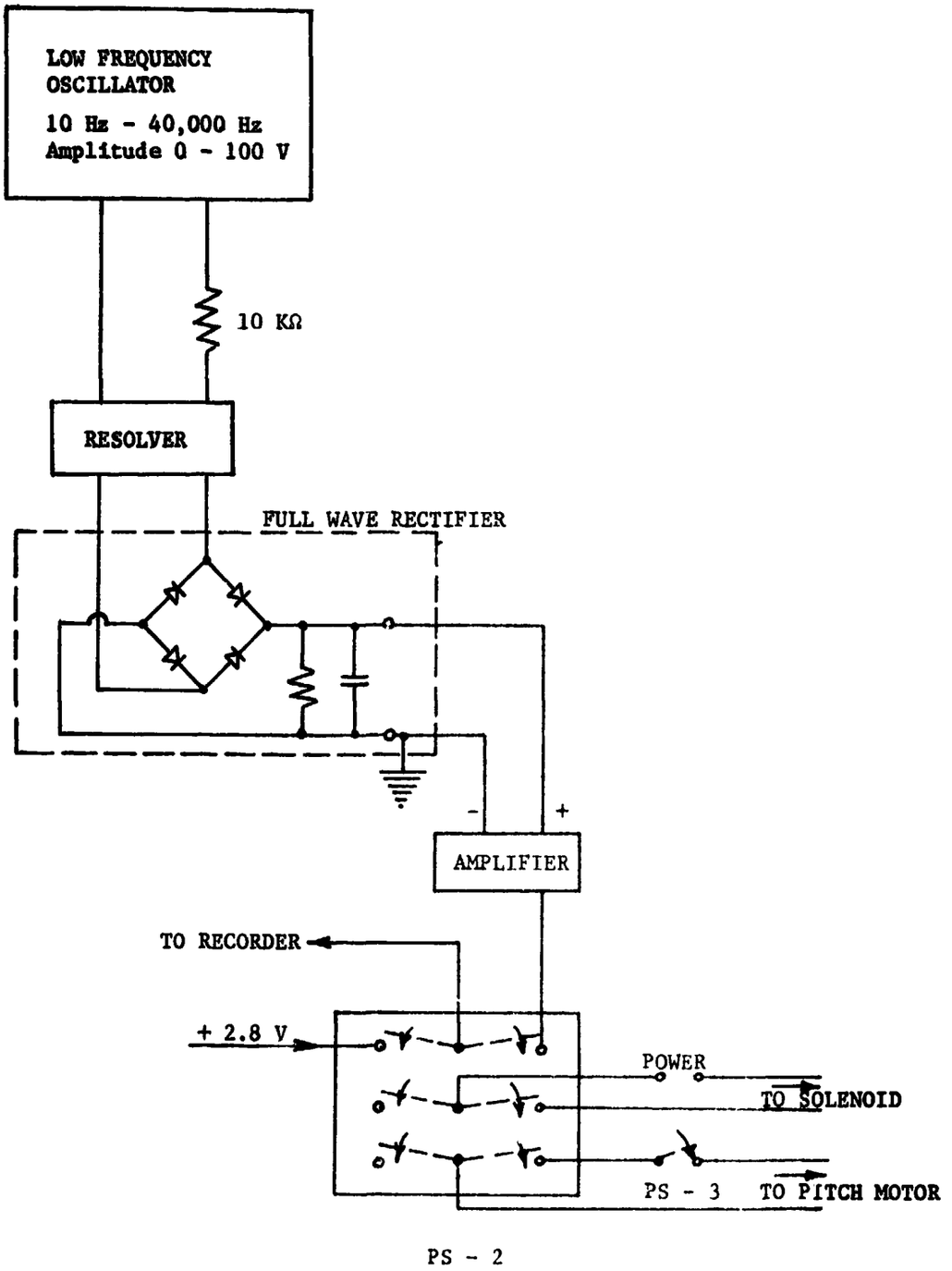

Figure 20. The Resolver Circuit of the Pitch Stirring Excitation.

resolver is then passed through a full wave rectifier circuit. It is then input into a low gain amplifier for output level adjustment as before. It is then sent to a two-way, two-position switch, the output of which is input to the tape recorder. In the "OFF" position the tape recorder input is a 2.5 volt D.C. signal. When the switch is flipped to the "ON" position, the motor that drives the rotor shaft is energized and also the rotor resolver signal is input to the tape recorder. A schematic diagram of the circuit is shown in Figure 21.

5.4 PITCH STIRRING EXCITATION

The inner shaft is a cylindrical rod which passes through the hollow shaft with an eccentric pin mounted at the end as shown in Figure 19. Two sets of pitch control flexures are mounted on the pin. Each set of flexures is clamped to two opposite blades. Rotation of the inner shaft is effectively the same as rotating a tilted swash plate. The collective pitch of the blades is adjusted by loosening the pitch lock nut adjusting the blade pitch on the pitch screw and then relocking the pitch lock nut. The drive is mounted on the other end of the inner shaft. Basically two drive mechanisms are used:

1. A motor is used to drive the inner shaft using a sprocket drive. The acceleration of the motor provides the required transient excitation. This is seen in Figure 22a.
2. A coil spring mounted on the base of the inner shaft is used to drive it through 90, 180 and 270 degrees. The acceleration of the shaft would be proportional to the

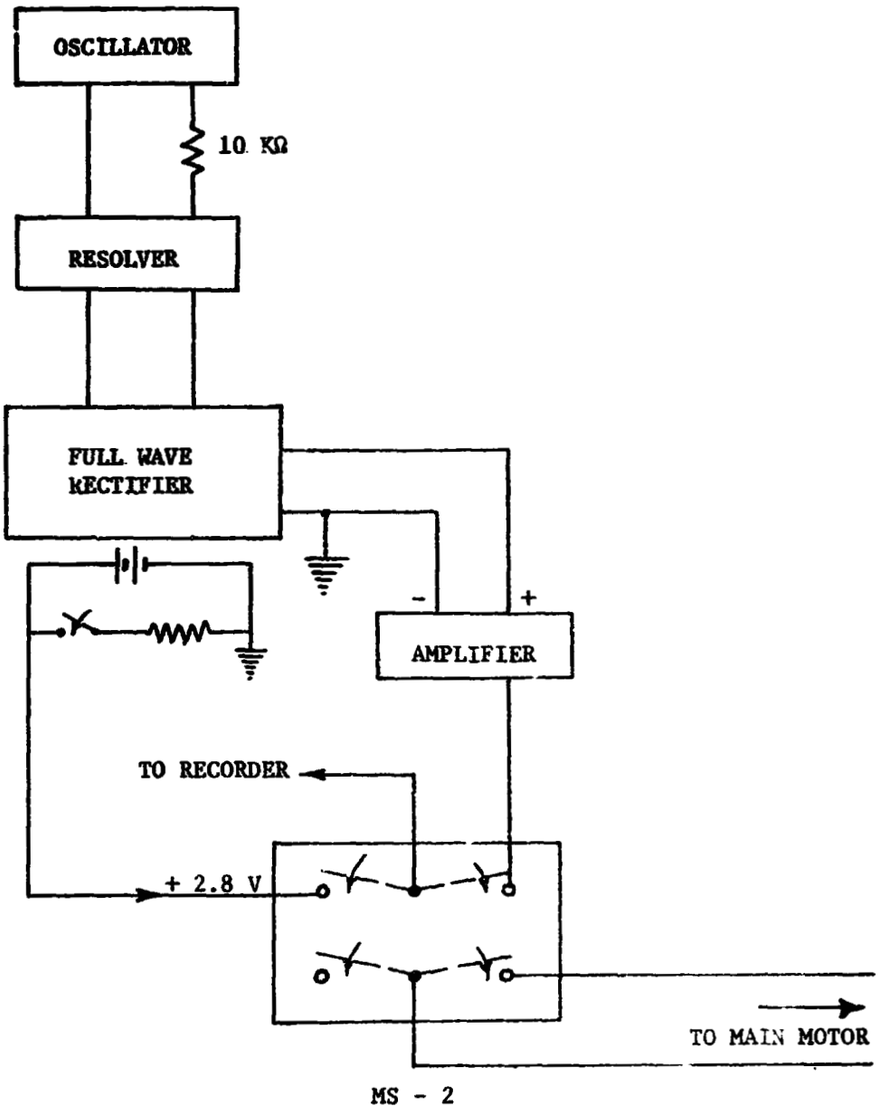

Figure 21. The Rotor Resolver Circuit.

amount that the coil spring was wound prior to its release.

A view of the spring excitation is shown in Figure 22 b.

5.5 BRIEF DESCRIPTION OF THE EXPERIMENTAL PROCEDURE

The stands are adjusted so that the rotor plane is parallel to the base of the wind tunnel for study of the flapping response for zero angle of attack. The collective pitch of each blade is set in the following manner:

In order to make relative collective pitch changes, a beam of light is focused on the small mirror glued to the root of each rotor blade as shown in Figures 23a and 23b. At zero collective pitch setting, the beam striking the mirror at an angle of incidence of 30^{o} is reflected to a position marked X^{*} on the calibrated scale. On changing the collective pitch Figure 23b, the angle of incidence of the beam changes, which is reflected to the position marked X_1, which directly reads the change in the collective pitch setting from the position X^{*}.

To set the collective pitch to zero degrees, the zero degree eccentric is mounted on the inner shaft. The pitch angles of the blades are adjusted till each of the blades have a minimum flapping response. This is studied on the scope.

A qualitative judgement regarding the relative accuracy of the collective pitch settings is made by using the stroboscope. A photocell reflecting off thin reflecting strips (corresponding to each blade) on the rotor shaft is used to trigger the stroboscope. The blades can be observed to have the same flapping angle. If not, small adjustments have to be made in the collective pitch settings.

Figure 22a. Motor Drive for the Pitch Stirring Excitation.

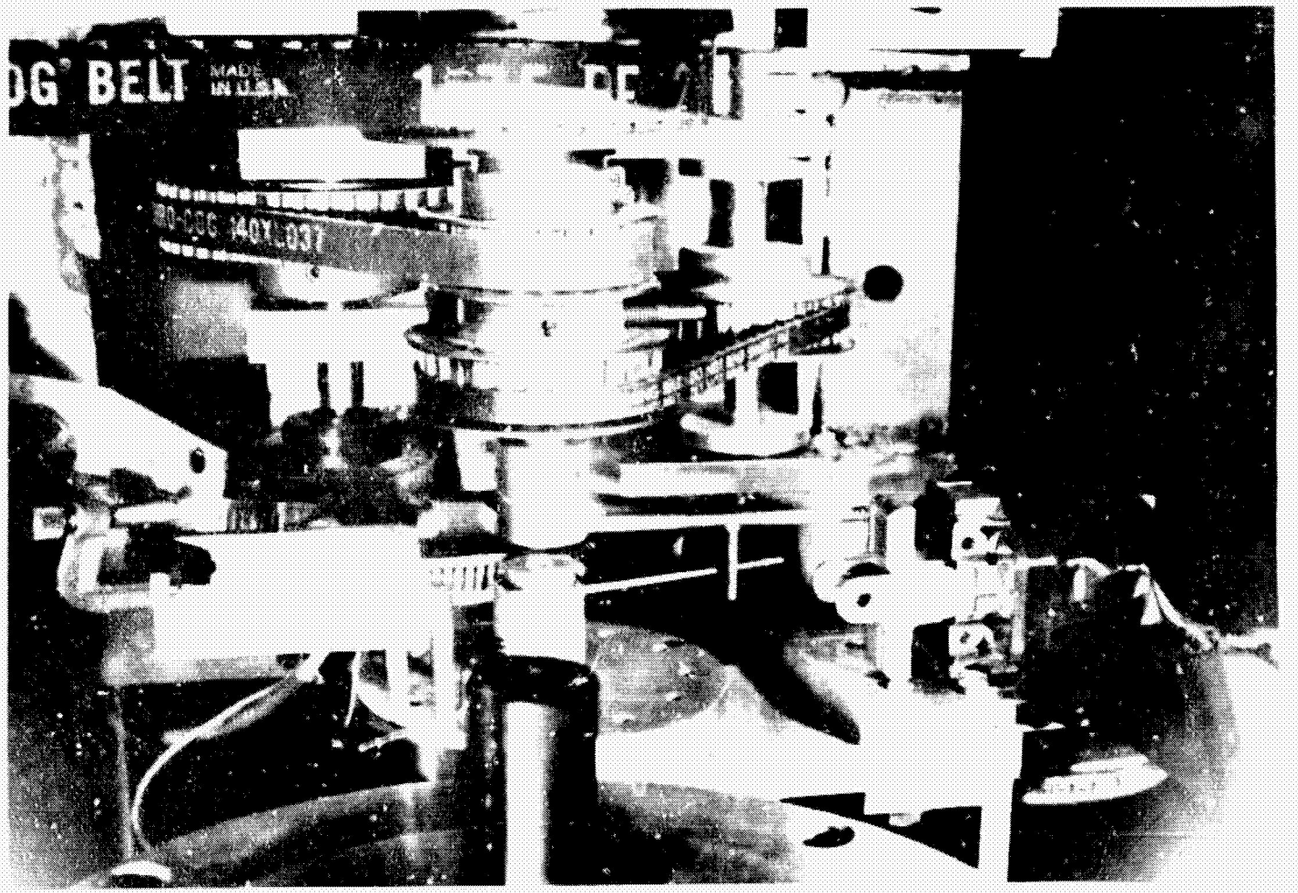

Figure 22b. Picture of the Spring Control for the Pitch Stirring Excitation.

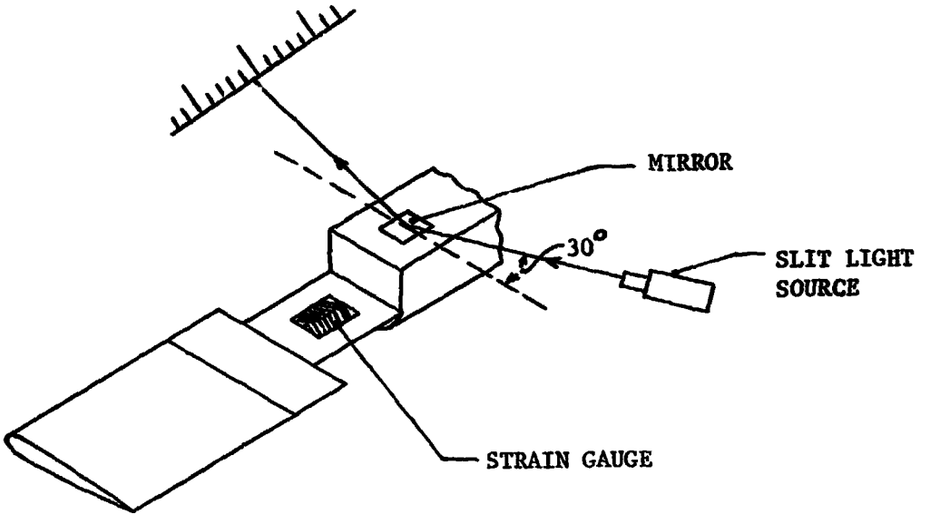

Figure 23a.

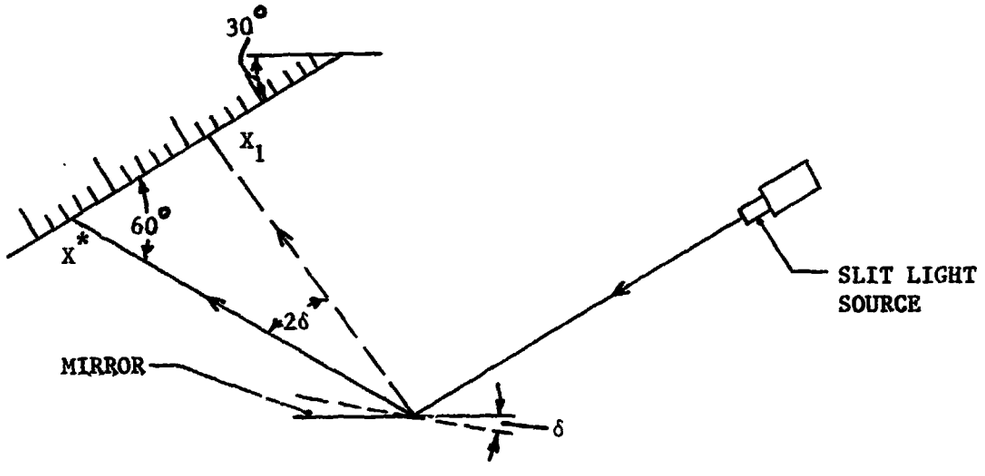

Figure 23b.

Figure 23 a-b. Reflective Principles used in Relative Collective Pitch Setting of the Rotor Blades.

The zero eccentric on the inner shaft is replaced by the ± 1.4 degree eccentric. The inner and the rotor shaft resolvers are now synchronized. This is done by first locking the rotor shaft and the inner shaft by a locking pin. A screw on the rotor shaft which is located at the zero azimuth angle is used to activate a magnetic pick-up which generates a voltage blip. The inner and the rotor shafts are run in the locked position. The rotor and the inner shaft resolvers are adjusted such that their zeros pass through the center of the blip of the magnetic pick-up. The inner and the rotor shaft resolver positions are now synchronized. Since the resolver output amplitudes are not exactly sinusoidal for constant rotational speed, the resolver signals of both the inner and the rotor shafts are recorded with the two shafts locked. This provides information for calibration of the resolvers.

The shafts are uncoupled and the drive for the inner shaft is set up. The strain gauge circuits are balanced as described before. The flapping deflection has now to be calibrated. This is done by using the following blade specifications:

(a) one inch of tip deflection corresponds to 6.23^{o} flap

(b) one inch of tip deflection requires a moment of .562 lbf-in

With the above information, a 10 gram mass at 7.17 inch (blade tip) distance is found to create a deflection of 1.746^{o} flap. The amplifier gain is adjusted for an output of 1.746 volts, thus giving a one volt/degree flap deflection. The tape recorder is zeroed and then calibrated by recording two known levels of D.C. voltages.

The rotor structure is mounted on a swiveling base so that the rotor shaft can be tilted for different angle of attack positions. The rotor shaft tilted at $\alpha = -3^{o}$ is shown in Figure 24a and 24b. A fairing is mounted on the rotor shaft for a streamline flow past it and to avoid the effect of the rotor shaft on the blade wake effects.

The motor that drives the rotor shaft is turned on by the switch MS-2 (Figure 21). The inner shaft is held in position mechanically by means of a solenoid. The rotor shaft speed is adjusted by a potentiometer, thereby changing the rotational flap-bending stiffness ω_1 of the rotor blade. The wind tunnel speed is adjusted for tne required advance ratio. The tunnel speed is measured by a manometer.

A six channel FM tape recorder, which measures the response of the four blades and the two resolver signals, is turned on to record the signals. Switch PS-3 (Figure 20) is in the closed position and PS-2, the inner shaft drive motor, is in the "OFF" position. When the switch PS-2 is flipped, the inner shaft drive motor is turned on and the solenoid that holds the inner shaft is released at the same time. The acceleration of the inner shaft drive provides the transient excitation. Switches PS-3 and PS-2 are turned off in sequence and the recording stopped. A view of the experimental set-up is seen in Figure 25.

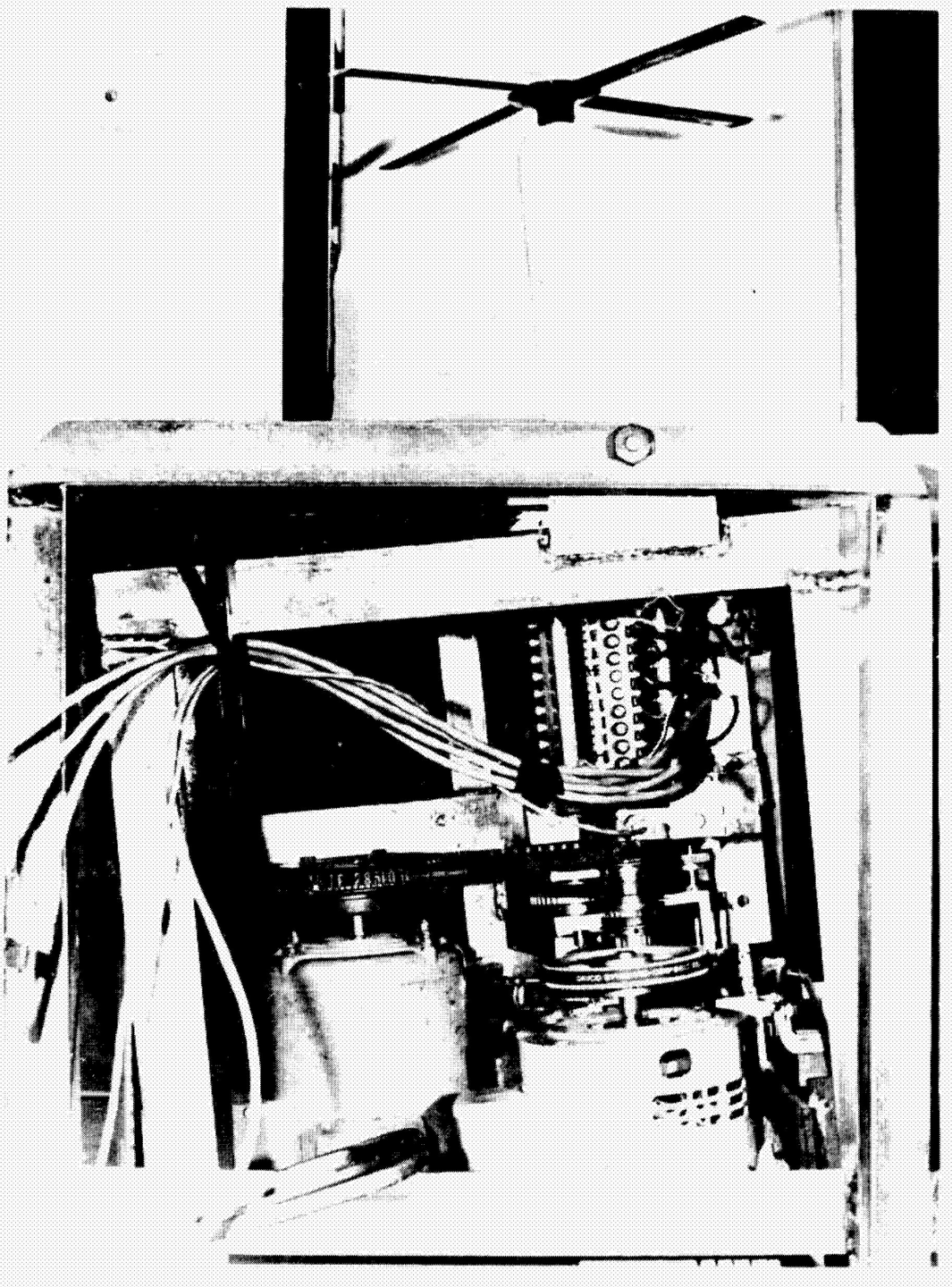

Figure 24a. Photograph of the Rotor Shaft Tilted at $\alpha = -6^{\circ}$ in the Wind Tunnel Test Section.

Figure 24b. Close-up View of the Tilted Rotor Shaft in the Wind Tunnel.

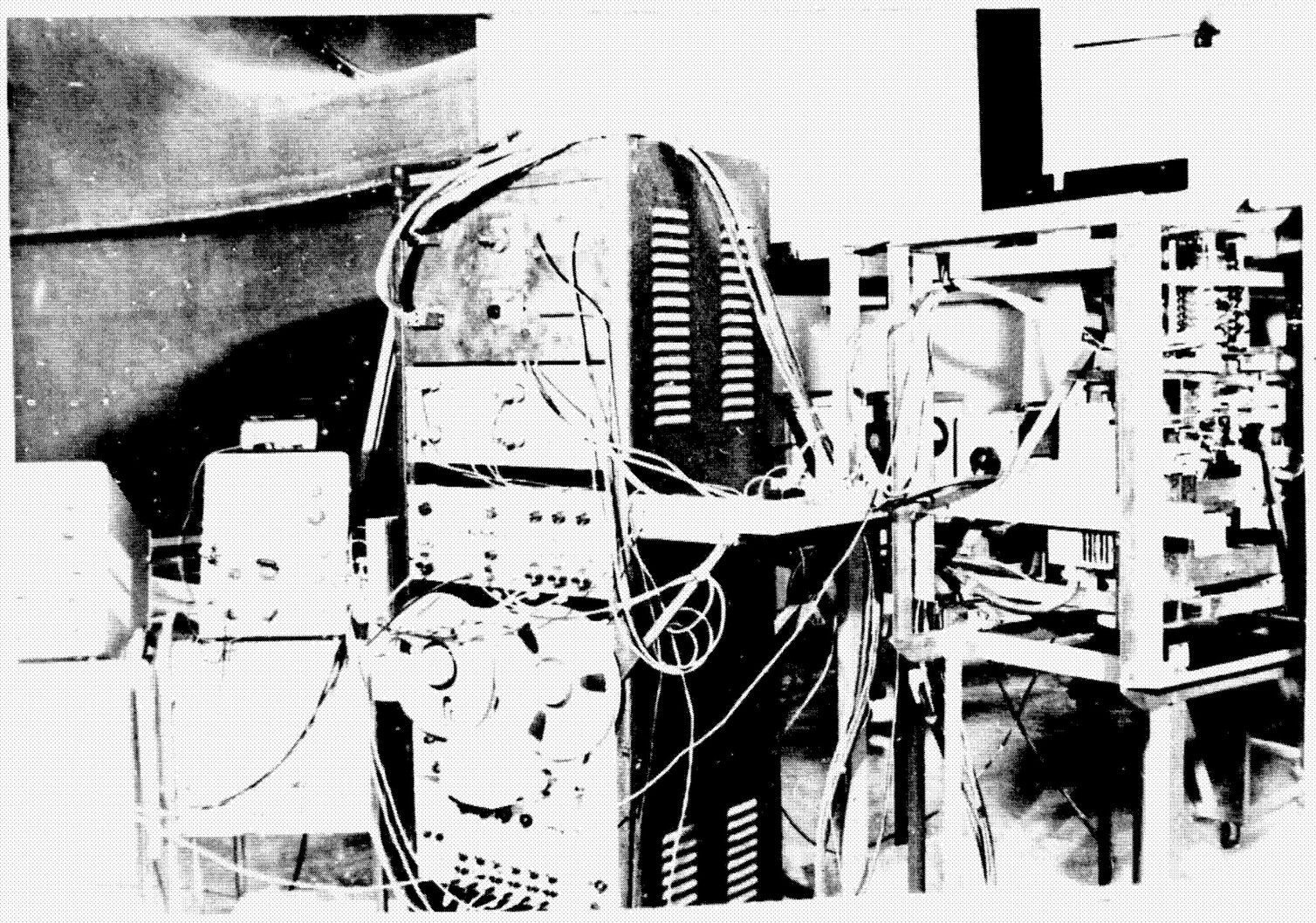

Figure 25. Photograph of the Complete Experimental Set-up.

6. EXPERIMENTAL DATA ANALYSIS

The transient test results together with the trim conditions are recorded in analog form on magnetic tape. The two resolver signals and the signals from the blade flapping strain gauges are processed on a PDP-8 and PDP-12 mini-computer complex. Prior to the identification analysis, several preliminary raw data manipulations are necessary. The analog data are digitized, the data is transformed from rotating to fixed coordinates and the transient perturbation results are separated from the trim values. The small bias values in the blade flapping measurements are removed by identifying the bias values in each identification run.

For low advance ratios ($\mu \leq .4$), it is seen (from 4.3) that the multiblade formulation gives accurate response with the periodic terms left out. When the periodic terms are neglected, the β_d equation 67 becomes uncoupled from the rest of the equations. Hence the β_d response can be neglected from the identification procedure. Even for $\mu = 0.6$, a comparison of the γ^* identification between a model with the periodic terms, the β_d equation and reverse flow effects included and a model neglecting all of the above effects is surprisingly accurate. These are shown in Table 12 and Table 13. Thus it is seen that neglecting the reverse flow and the periodic terms at low advance ratios is quite acceptable. At low advance ratios the reverse flow regions are restricted near the rotor hub, thus having negligible effect on the flapping response of the rotor blades.

Table 12. - 13. Comparison of the Identified γ^* Values Using a Mathematical Model which Includes Reverse Flow, Periodic Terms and β_d equation (Table 13) with a Model Excluding the Above Effects (Table 12) Using Data at $\mu = 0.6$.

Table 12

	Parameter γ^*	Least Squares fit (R) $\sigma^2_{\beta_0}$	$\sigma^2_{\beta_I}$	$\sigma^2_{\beta_{II}}$
Initial Value	3.00	.01735	.39835	.06648
Iteration 1	3.529	.00184	.00812	.00767
2	3.654	.00163	.00859	.00754
3	3.654	.00163	.00859	.00754
4	3.654			

Table 13

	Parameter γ^*	Least Squares fit (R) $\sigma^2_{\beta_0}$	$\sigma^2_{\beta_I}$	$\sigma^2_{\beta_{II}}$	$\sigma^2_{\beta_d}$
Initial Value	3.654	.00112	.00816	.00716	.01540
Iteration 1	3.630	.00112	.00866	.00719	.01542
2	3.595	.00112	.00795	.00726	.01557
3	3.584	.00112	.00781	.00725	.01562
4	3.580				

An interesting observation is that at higher advance ratios the bias terms are rather large. This is because at high μ, the trim flapping response has (seen experimentally) a small variation of the amplitude of the trim condition with a large time period. This can very well cause the trim subtracted from the transient response to be slightly different from the actual trim at which the transient was measured, thus giving rise to the bias values.

If all the blades were identically set, the trim values for the flapping response of the blades in the non-rotating system would be nearly constant. From equation 67 it is apparent that β_d has a moderate 2/rev. in its trim condition, β_I and β_{II} have a smaller 4/rev. input effect, and β_0 has a very small 4/rev. for its trim response. A typical average trim condition data is given in Figure 26.

If a constant approximation is used for the trim values, it will correspond to the starting values of the transient responses. This would ensure response bias values of approximately zero, though the 2/rev. and the 4/rev. trim conditions show themselves in the transient data. If the periodic trim conditions for data obtained at low advance ratios are used, then the transient responses will be rid of both the bias and the 2/rev. and the 4/rev. trim variations.

6.1 PITCH STIRRING EXCITATION

Two rates of acceleration of the inner shaft are obtained by adjusting the potentiometer setting of the eddy current to the motor that drives the inner shaft. Plots of the slow and the fast excitation are shown for normalized θ_{II} as a function of non-dimensionalized time in Figure 27 and Figure 28 respectively. Care was taken to use

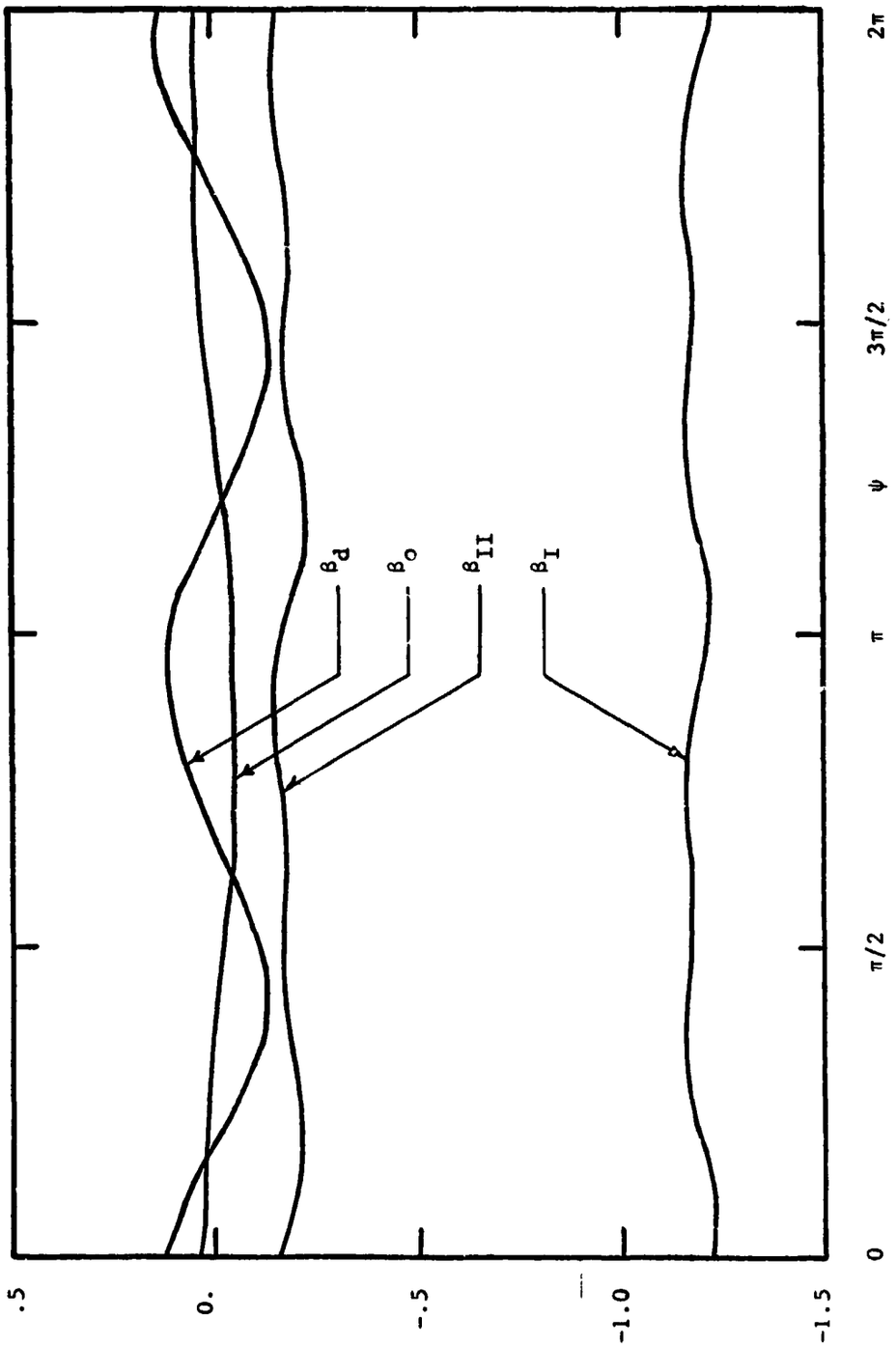

Figure 26. Average Trim Condition for the Flapping Responses of a Typical Data Set: $\theta_o = 5^o$; $\omega_1 = 1.24$; $\mu = 0.2$.

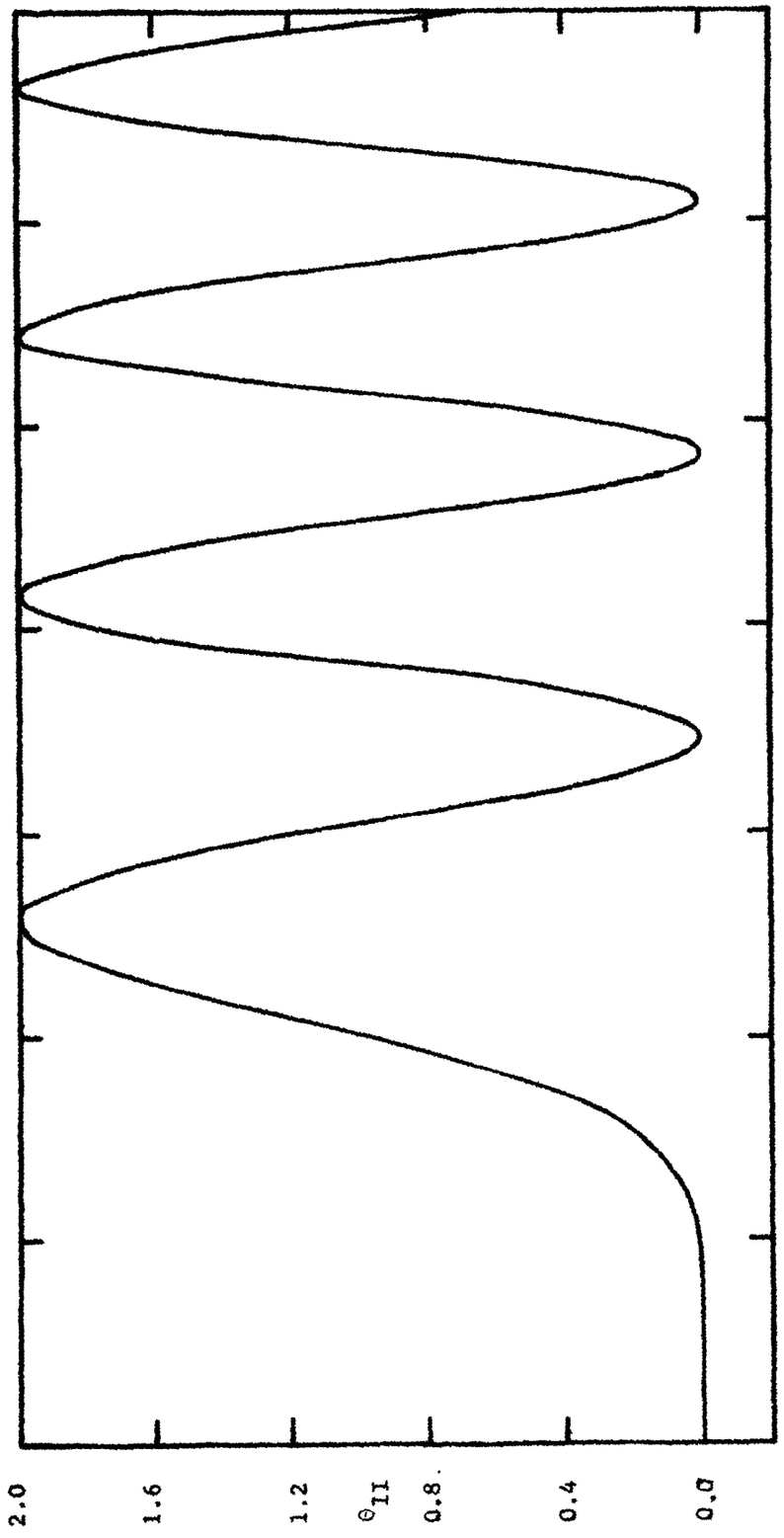

Figure 27. Plot of the Slow Transient Pitch Stirring Progressing Excitation for Normalized Θ_{II} as a Function of Non-Dimensionalized Time.

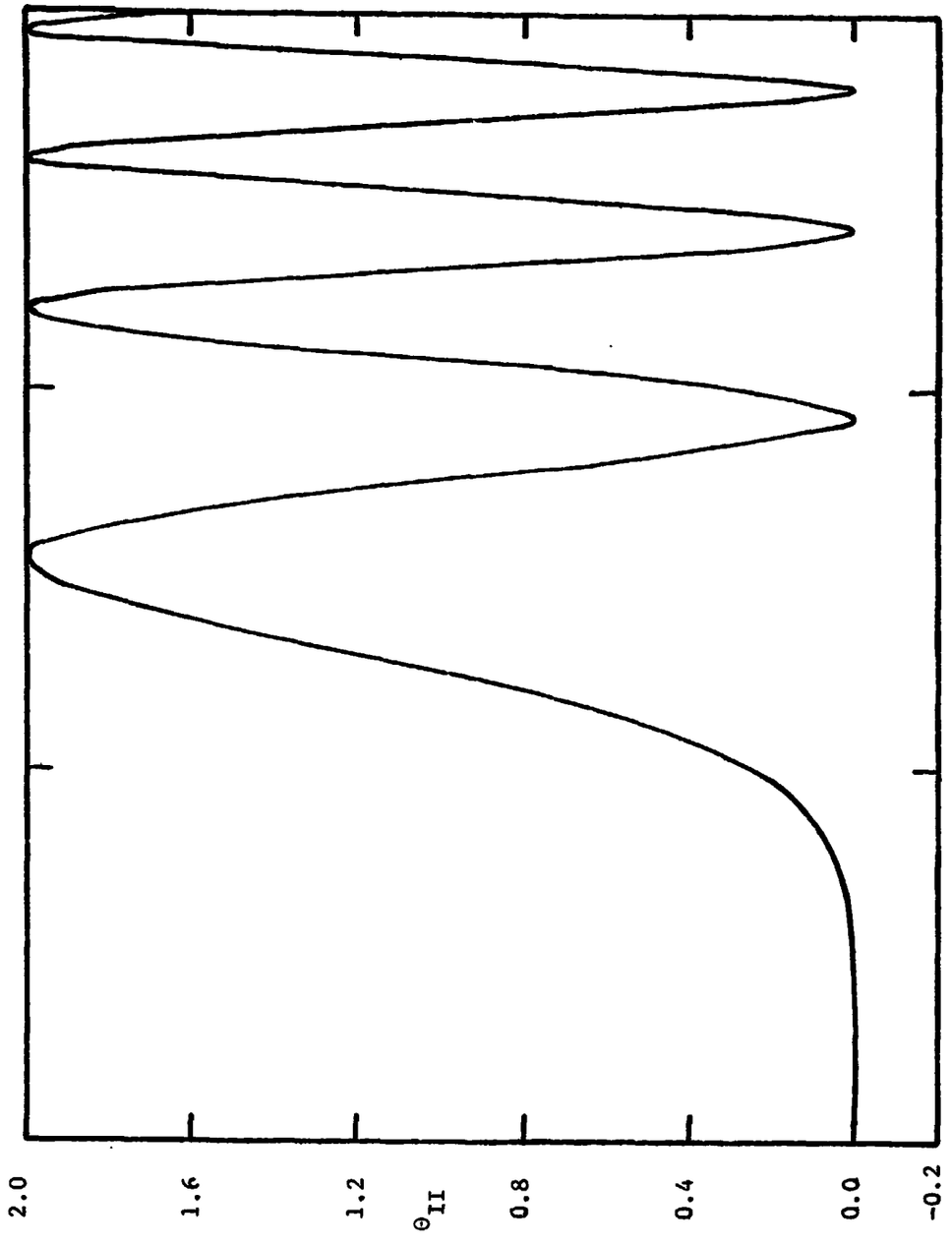

Figure 28. Plot of the Fast Transient Pitch Stirring Progressing Excitation for Normalized Θ_{II} as a Function of Non-Dimensionalized Time.

a length of data in which the excitation velocity is uniformly increasing. For both rates of excitation, the frequency of excitation becomes approximately constant beyond $t = 30$ and any data utilized in this range would tend to give biased parameters whose values depend on this constant excitation frequency.

The inputs are mostly progressive pitch stirring accelerations of the inner shaft. Data is also gathered using regressive pitch stirring acceleration and spring loaded pitch stirring excitation. Details of these inputs are given in (12). These data sets are used for verification of the identified model response prediction.

6.2 γ^* IDENTIFICATION RESULTS

Figure 29 is a plot of γ^* versus advance ratio for different values of the collective pitch setting at $\omega_1 = 1.18$. The values of γ^* from momentum theory ($\theta_o = 0^o$, equation 58) are plotted for comparison. This analytical result is for low collective pitch settings. As the advance ratio increases, the rotor wake gets washed away faster and hence, the feedback effect of the dynamic inflow on the flapping response decreases. This is seen in the increasing value of the identified γ^* with advance ratio for all collective pitch settings.

Figure 30 shows similar results for $\omega_1 = 1.24$. The analytical model approaches the true value of γ asymptotically. The experimental results for $\theta_o = 0^o$ shows that around $\mu = 0.75$, γ^* is approximately equal to the value of the blade Lock number γ. This shows that at this high advance ratio, the effect of the rotor downwash has become negligible.

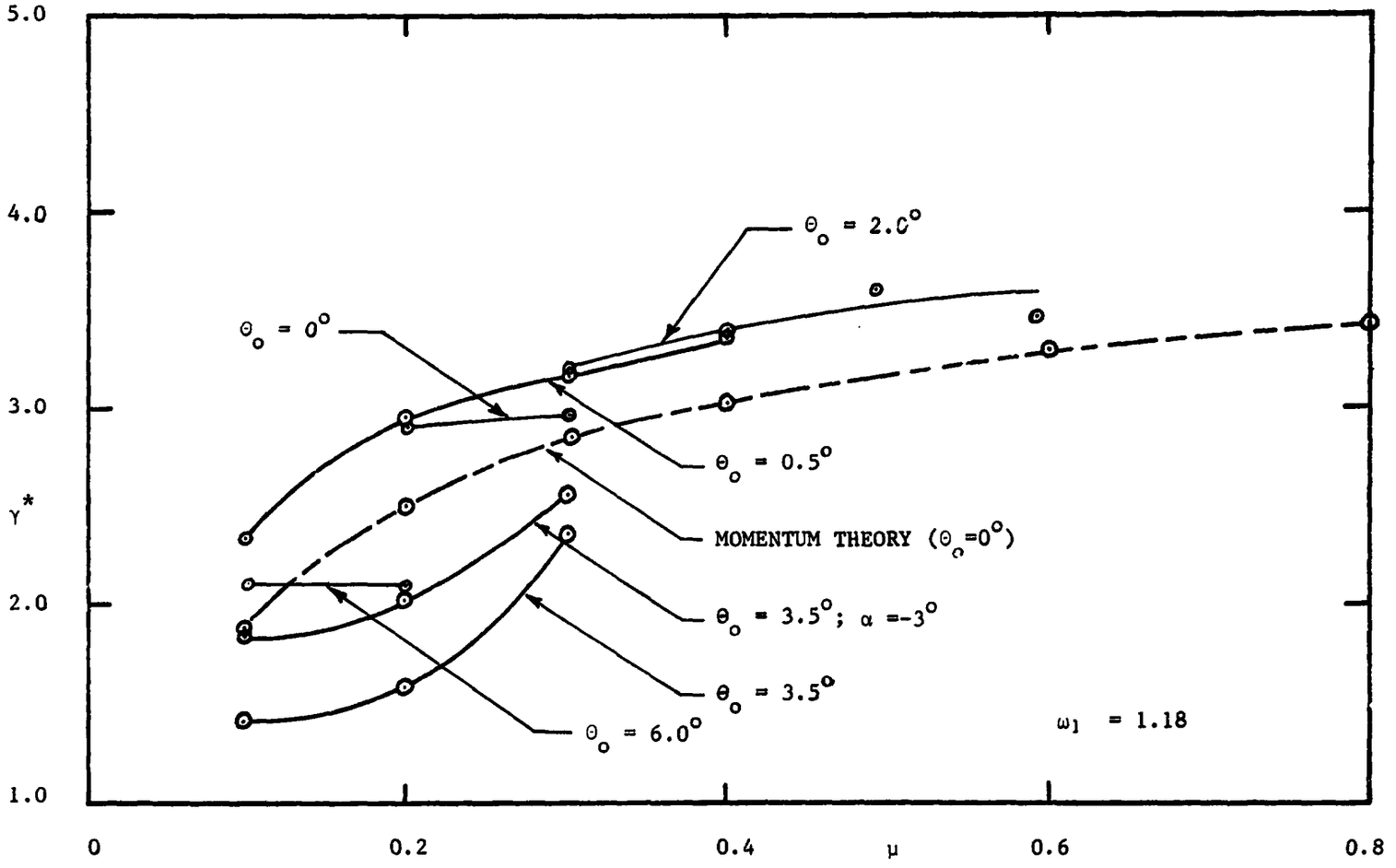

Figure 29. Plot of Identified γ^* versus Advance Ratio for Different Values of Collective Pitch Settings at $\omega_1 = 1.18$.

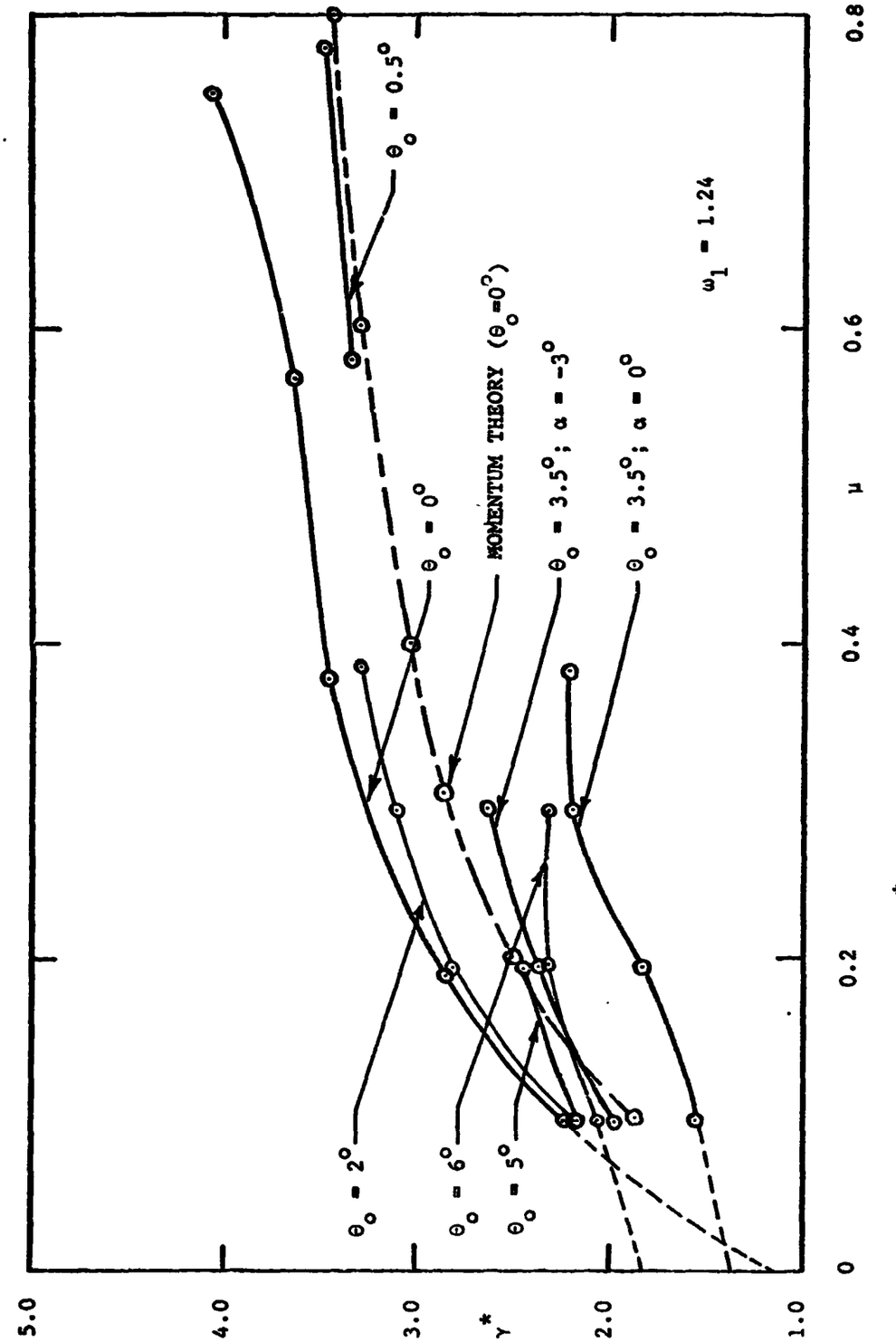

Figure 30. Plot of Identified γ^* versus Advance Ratio for Different Values of Collective Pitch Settings at $\omega_1 = 1.24$.

Figure 29 and Figure 30 are combined and plotted in Figures 31a and 31b, where γ^* is drawn as a function of θ_0, the collective pitch setting. The consistent trend seen in these curves is that, with increasing value of θ_0, the γ^* value first drops and then increases beyond a collective pitch setting of around 3^o. This is in apparent contradiction to the equivalent Lock number formulation given by equation 57, which indicates that, since with increasing collective pitch θ_0 the induced mean downwash $\bar{\nu}$ monotonically increases (11), the equivalent Lock number increases. The discrepancy, however, is due to the fact that the tip loss factor B is decreasing with increasing θ_0, causing an apparent decrease in the value of the Lock number which varies as B^4.

Also plotted in Figure 29 and Figure 30 are graphs of γ^* for trim conditions of $\theta_0 = 3.5^o$; $\alpha = -3^o$. This increases the downwash over the trim condition of $\theta_0 = 3.5^o$; $\alpha = 0^o$, and hence, decreases the effective angle of attack of the blade. This is seen in the higher value of γ^*. This agrees with the trend of γ^* versus θ_0 as found before.

Studies have also been done to determine the effect of a range of α from 0^o to -6^o. The shaft tilt corresponds to a combination of collective and lateral cyclic pitch change of the rotor blades. This is because the changes in the angle of attack ($\Delta\theta$) due to a shaft angle of attack of α are:

At $\psi = 0$ and π (fore and aft positions):

$$\Delta\theta = \mu\alpha/(r/R) \tag{126}$$

At $\psi = \pi/2$ (advancing side):

$$\Delta\theta = \mu\alpha/(r/R+\mu) \tag{127}$$

At $\psi = 3\pi/2$ (retreating side):

$$\Delta\theta = \mu\alpha/(r/R-\mu) \tag{128}$$

Figures 32a and 32b are plots of $\Delta\gamma^*$ versus shaft tilt angles. Since these are essentially plots of γ^* versus collective pitch change (on a different scale), the trend of these graphs should agree qualitatively with those in Figures 31a and 31b. This is an independent verification of the results shown in Figures 31a and 31b.

γ^* has been found to have very good identifiability. Data length study has been done for transient data at $\omega_1 = 1.24$, $\theta_0 = 5^0$, $\mu = 0.3$. γ^* was identified using seven transient data lengths ranging from two to five rotor revolutions. In all of the cases, the γ^* identified to within 4% of one another.

6.3 L-MATRIX MODEL IDENTIFICATION

A simplification in the flapping response of the L-matrix is made when the β_0 equation is neglected from the set of equations used for identification (see equation 64). This is done for the following reason:

Numerous identification tests have shown that both L_{11} and $\tau_0 \triangleq 1/K_M$ have poor identifiability (see equation 71). These are the two parameters associated with λ_0. The primary effect of λ_0 is on the β_0 response and the β_0 transient response is small in comparison to β_I and β_{II} responses. Since β_0 is weakly coupled with β_I and β_{II} responses at low advance ratios, the equations governing the β_0 and the λ_0 responses can be neglected.

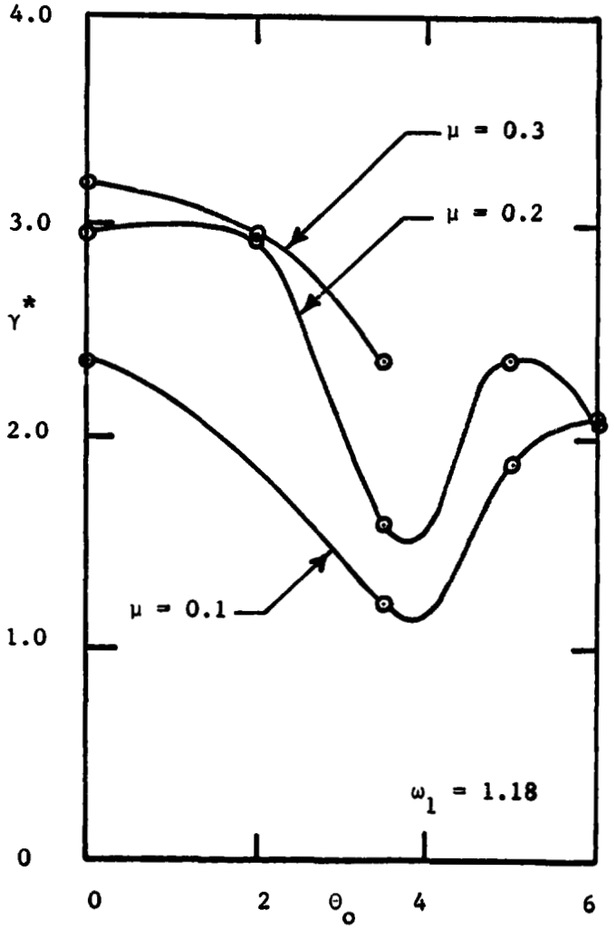

Figure 31a.

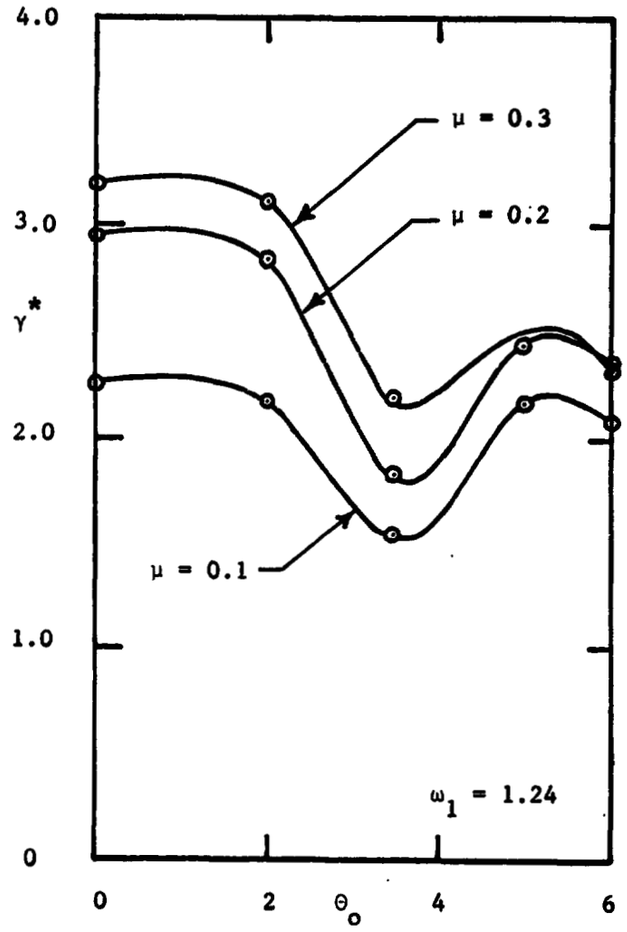

Figure 31b.

Figures 31a-b. Plots of Identified γ^* Versus Collective Pitch Settings at ω_1 = 1.18 and 1.24 Respectively (for Different Advance Ratios).

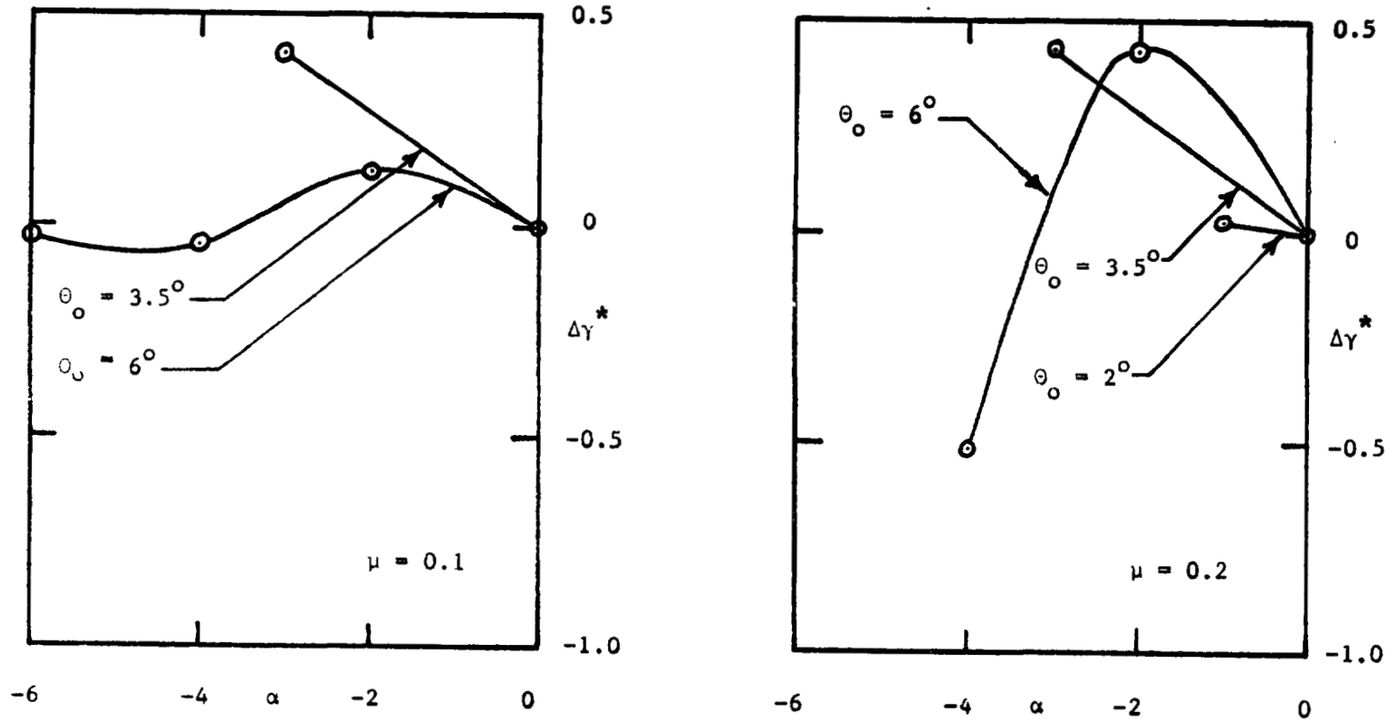

Figure 32a. Plots of $\Delta\gamma^* = \gamma^* - \gamma^*_{\alpha=0}$ Versus Shaft Tilt (α - degrees) for Different Collective Pitch Settings at $\omega_1 = 1.18$.

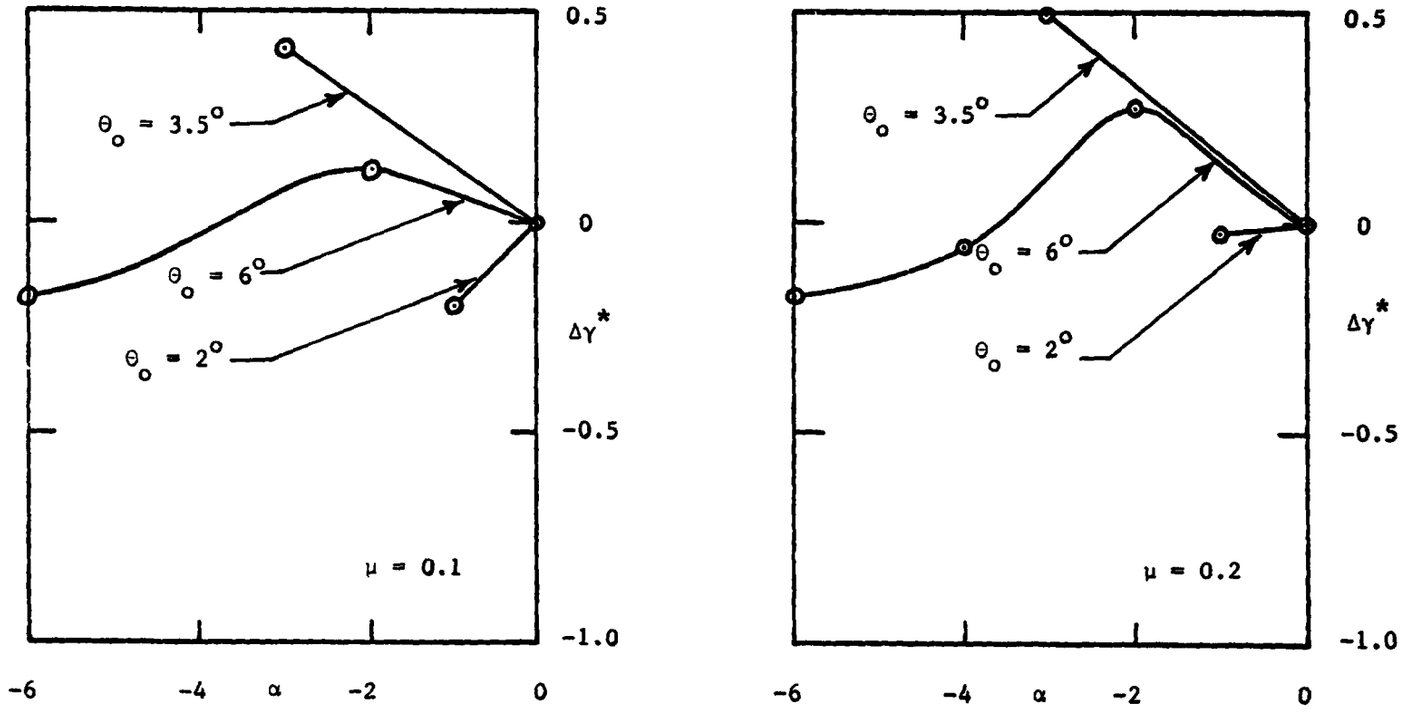

Figure 32b. Plots of $\Delta\gamma^* = \gamma^* - \gamma^*_{\alpha=0}$ Versus Shaft Tilt (α - degrees) for Different Collective Pitch Settings at $\omega_1 = 1.24$.

The reason for the small β_0 transient response, and consequently poor identifiability of the two associated parameters L_{11} and τ_0 seems to be due to the lack of collective pitch excitation. Pitch stirring excitations in the pitch and roll directions generate adequate β_I and β_{II} responses to identify the parameters associated with them.

The above simplification reduces the identification problem to one of identifying the four elements L_{22}, L_{33}, L_{32} and L_{23} of the L-matrix, τ_I, τ_{II} (see equation 71) and γ, based on the measurements β_I and β_{II}, θ_I and θ_{II}. γ appears as a product with B^2, B^3 and B^4 in the flapping equations. The tip loss factor B is not known accurately as a function of the blade pitch angle. Simulation studies have shown that γ identifies very accurately (within 3% of its true value). Hence the value of B is assumed to be 1.0 and the Lock number γ is assumed as a parameter to be identified. The identified γ will thus represent, not the true value of the Lock number, but a product of the Lock number and a power of B between 2 and 4. Roll and pitch time constants τ_I and τ_{II} are assumed to be identical in theory (11), but with increasing advance ratio they are expected to have increasingly different values.

Figure 33 is a plot of γ versus θ_0. The trend of the curve with increasing θ_0, according to steady momentum theory, should be decreasing due to decreasing value of the tip loss factor.

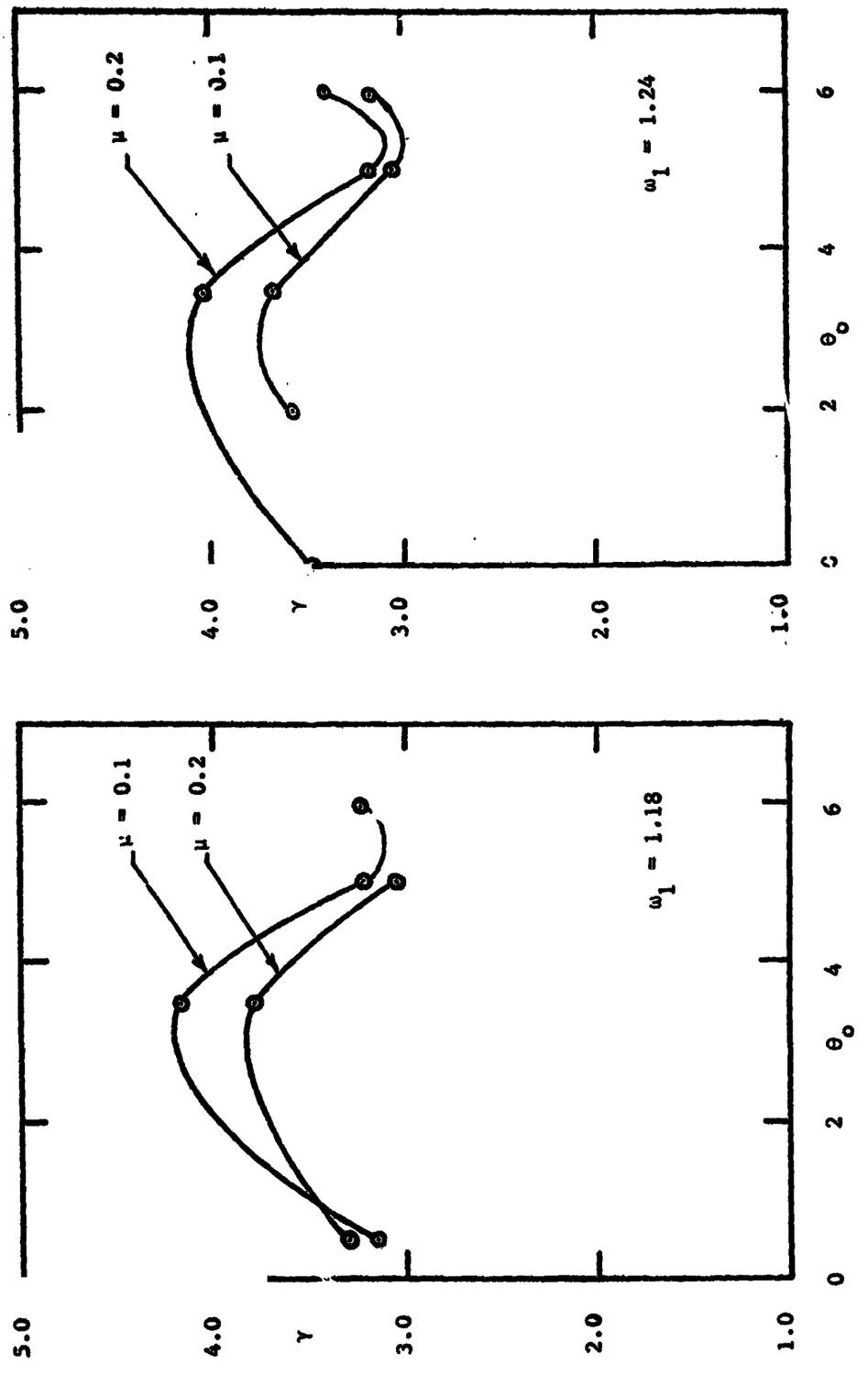

Figure 33. Plot of Identified γ Versus θ_o.

But the value of the Lock number increases and then drops beyond a certain θ_0. This trend is also found in a similar plot for hovering analysis (12). The plot also shows a decreasing variation of γ with increasing advance ratio (graph drawn for $\mu = 0.2$ as compared to the one drawn at $\mu = 0.1$).

Figure 34 shows a plot of the parameter L_{22} as a function of the advance ratio for different identification runs. The corresponding values predicted by momentum theory are plotted for comparison. The experimental values are several times larger than those from momentum theory. L_{33} is similarly plotted for two different ω_1 values in Figure 35.

The parameters L_{23} and L_{32} show no consistent trend with variation of the trim conditions. The values from all the experimental results lie around the value of zero, as predicted by momentum theory. All identified values of L_{23} are between -0.15 and +0.15. All identified values of L_{32} lie between -0.15 and +0.4.

From several studies, it is seen that τ_I and τ_{II} have approximately equal values at $\mu = 0.1$ regardless of their trim conditions. The value is very close to the theoretical value in (9). At $\mu = 0.2$, the value τ_I becomes larger and τ_{II} becomes correspondingly smaller. The ratio of τ_I to τ_{II} ranges from 1.5 to approximately 2.5. A typical comparison is shown in Table 14.

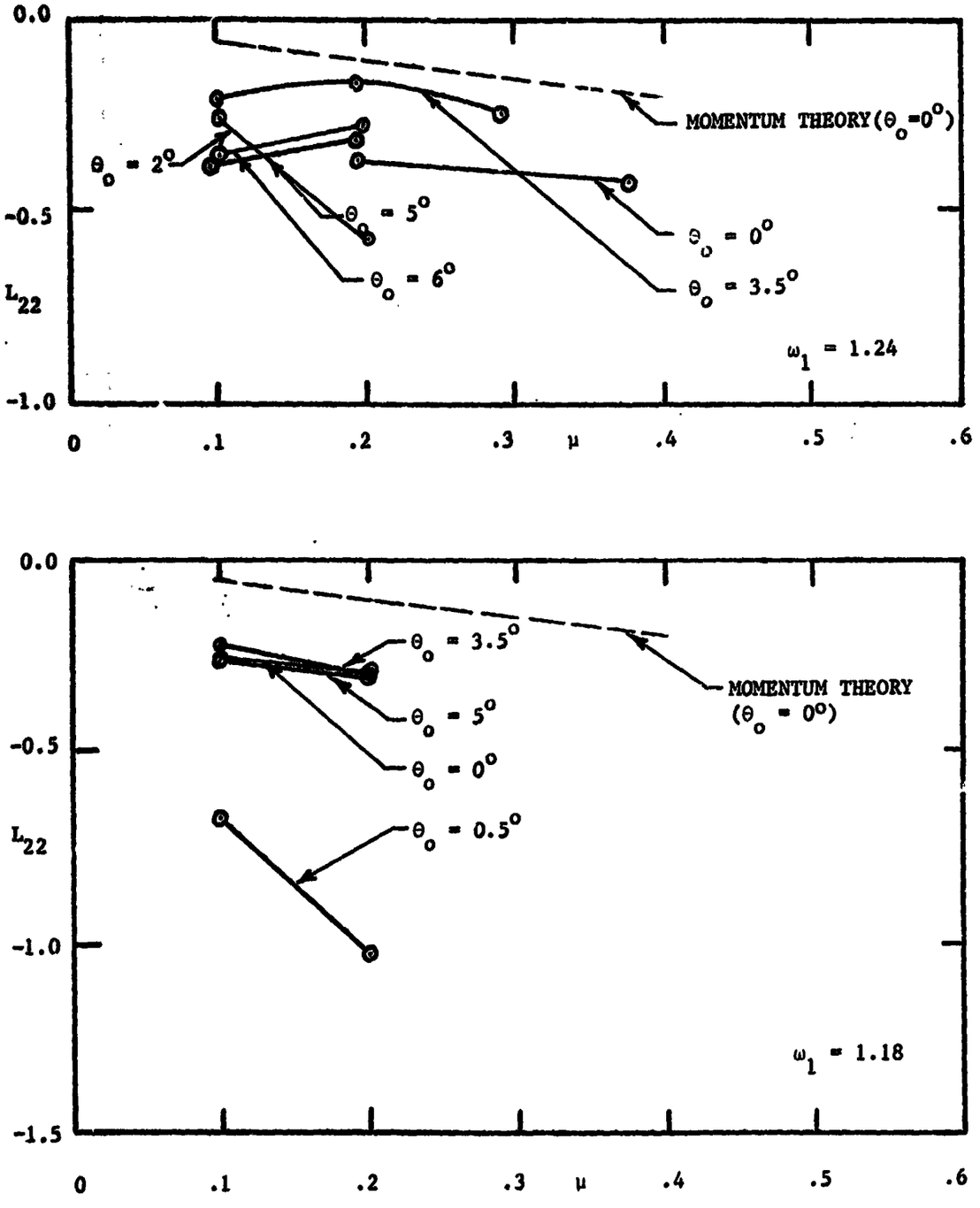

Figure 34. Plot of Identified Parameter L_{22} Versus Advance Ratio.

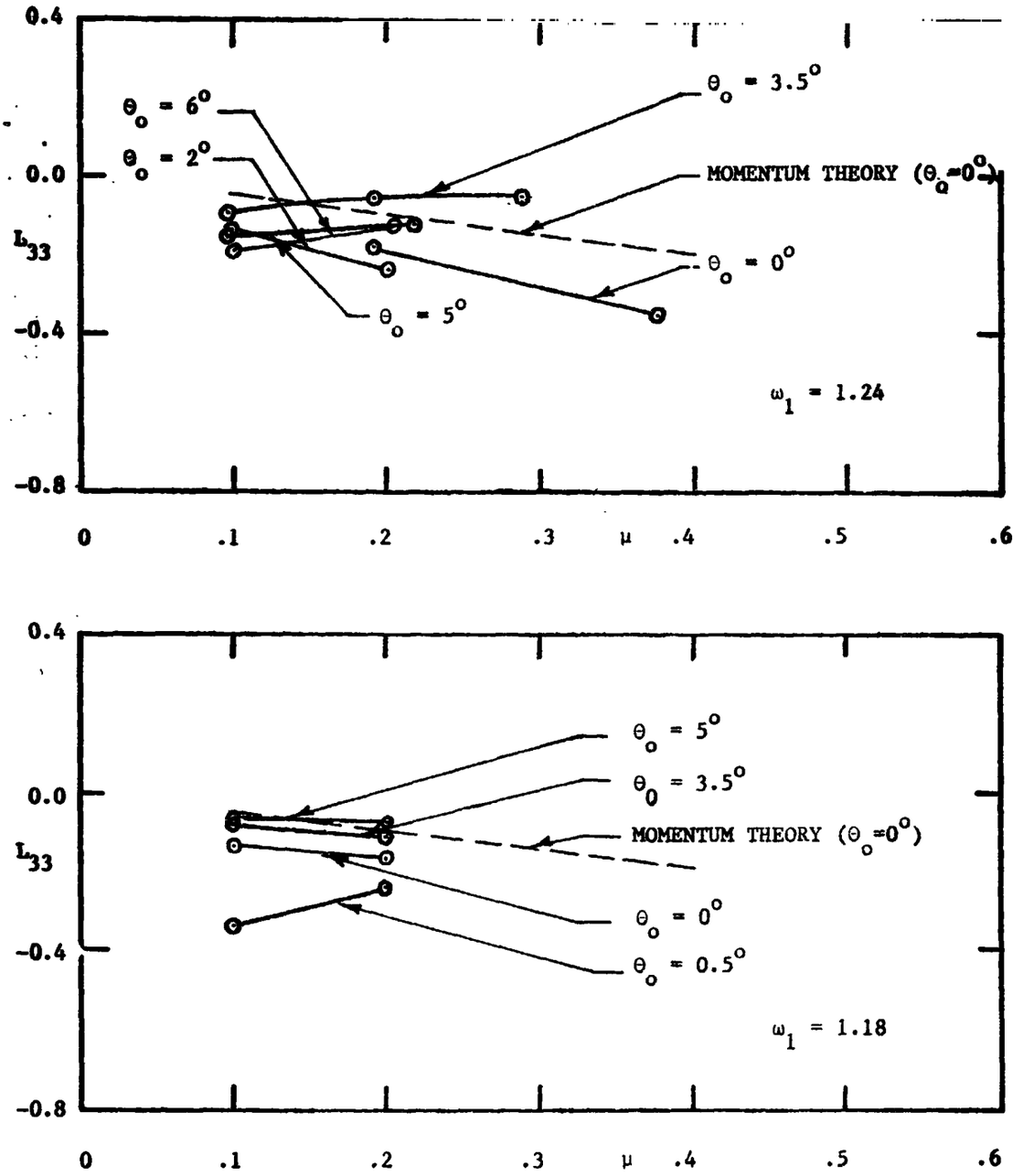

Figure 35. Plot of Identified Parameter L_{33} Versus Advance Ratio.

Table 14. Comparison of Identified τ_I and τ_{II} Values with Advance Ratio.

Trim Values	Advance Ratio	Identified Parameters	
		τ_I	τ_{II}
$\theta_o = 5^o$; $\omega_1 = 1.24$	0.1	8.41	7.35
$\theta_o = 5^o$; $\omega_1 = 1.24$	0.2	13.86	6.45
$\theta_o = 0^o$; $\omega_1 = 1.24$	0.2	14.28	8.86
$\theta_o = 0^o$; $\omega_1 = 1.24$	0.4	10.79	2.78

6.4 COMPARISON OF IDENTIFICATION AND PREDICTION STUDIES

As explained before (page 126), the transient data length used for identification is selected such that the input transient has a uniform increase in velocity. Progressive input excitations of the slower type (Figure 27) and their corresponding responses are generally used for the identification of the parameters.

Once the parameters have been identified, based on a certain length of data, the goodness of these parameter values, and hence, that of the corresponding mathematical model, has to be ascertained. Prediction studies are, hence, required, and are made in the following manner:

The identified parameter values are inserted into the mathematical model. The model is now complete. This complete model together with the faster transient input (Figure 28) is used to determine the response of the mathematical model to be compared with the response of the experimental model to the same faster excitation. This prediction study is done for closely similar trim conditions as those in the corresponding identification study.

Typical examples of studies done are given here.

1. In Figures 36a,36b and 36c, data set with $\theta_o = 0^o$, $\omega_1 = 1.24$ and $\mu = 0.4$ is modelled using the γ^* model and the L-matrix model programs. This data is modelled so well with the γ^* model that there is hardly any improvement by using the more complete L-matrix model.
2. Prediction curves for data with $\omega_1 = 1.116$, $\theta_o = 5^o$ and $\mu = 0.1$. A comparison of the three models is studied for prediction results in Figures 37a and 37b. The three models are:

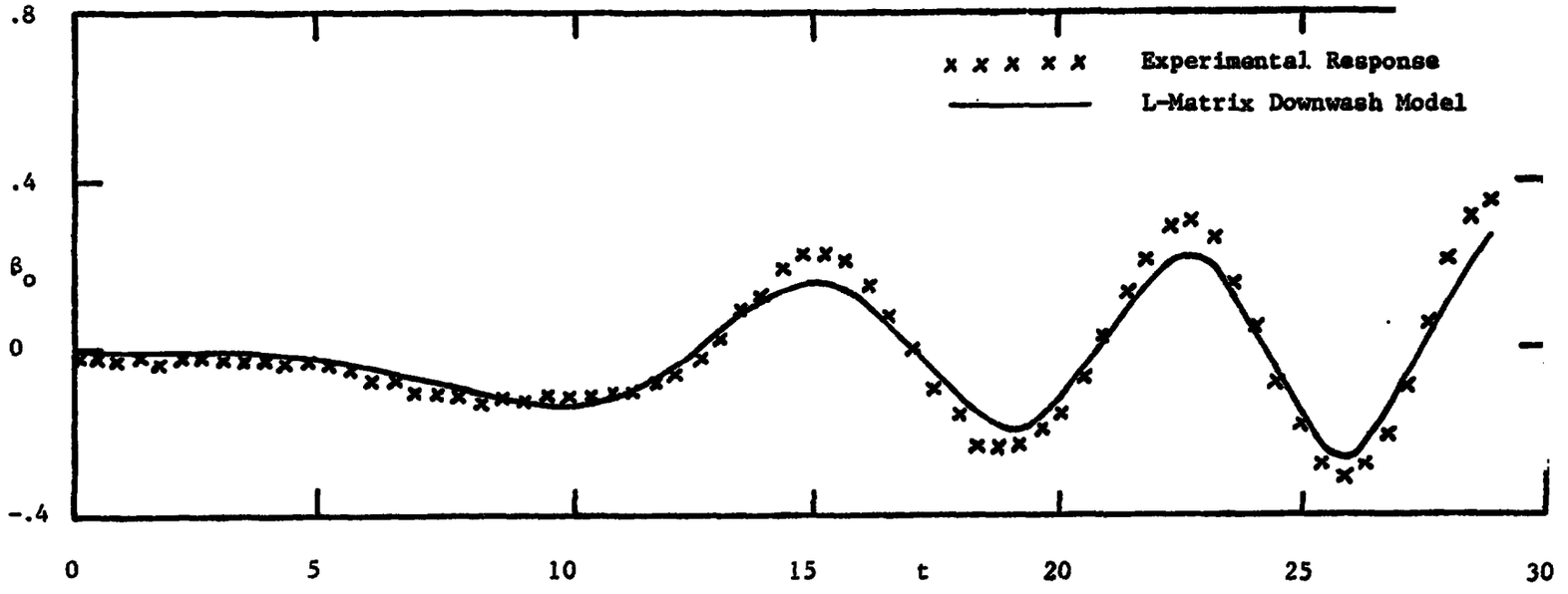

Figure 36a. Plots of β_o Responses for $\theta_o = 0^o$; $\omega_1 = 1.24$ and $\mu = 0.4$.

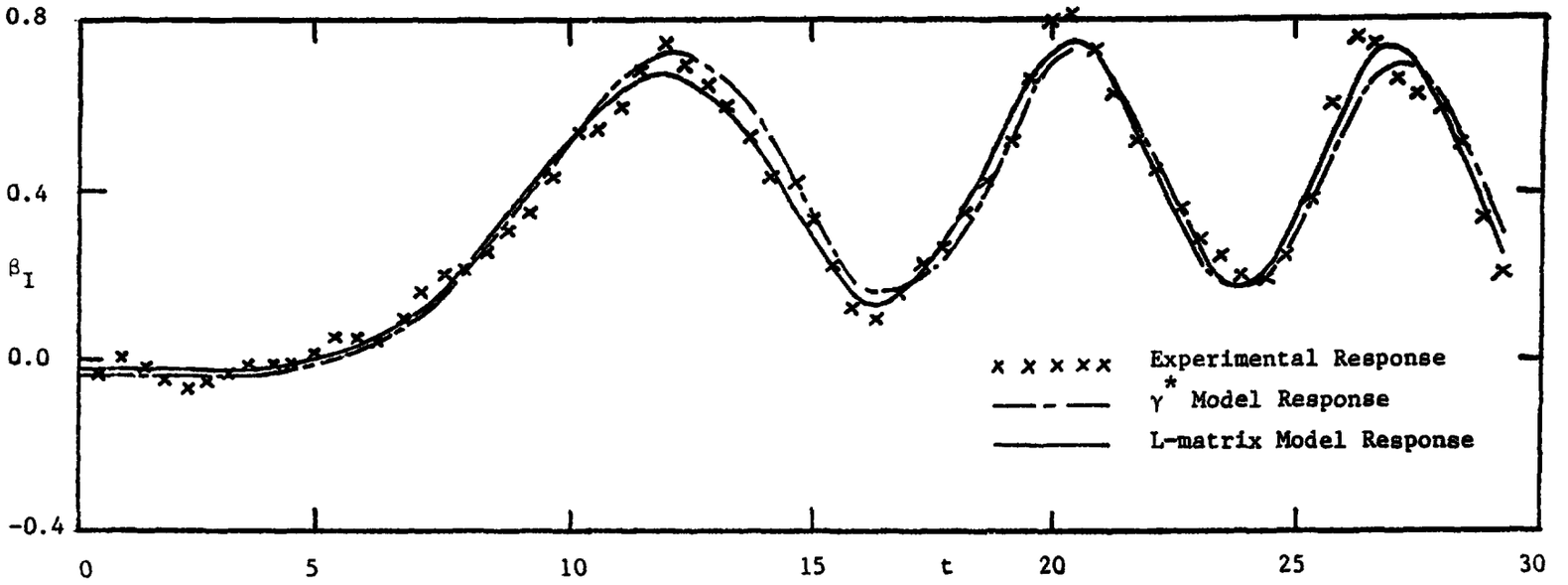

Figure 36b. Plots of β_I Responses for $\Theta_o = 0^o$; $\omega_1 = 1.24$ and $\mu = 0.4$.

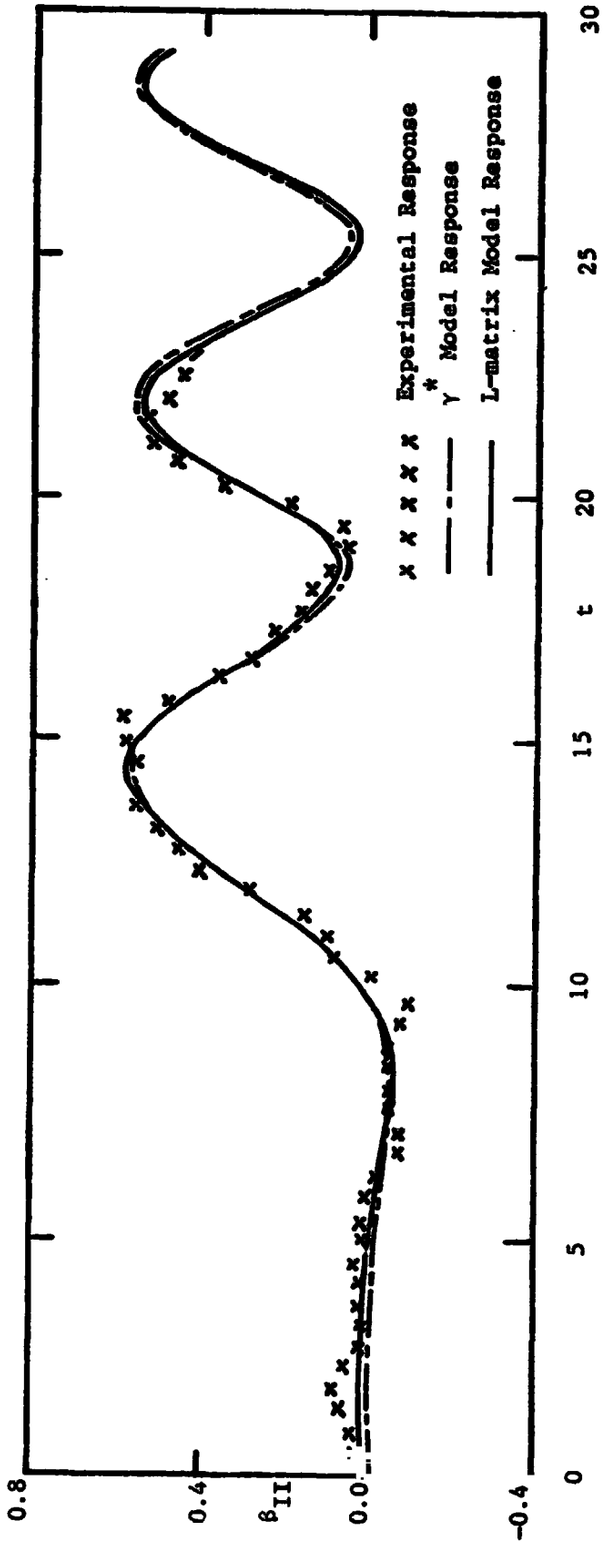

Figure 36c. Plots of β_{II} Responses for $\theta_o = 0^o$; $\omega_1 = 1.24$ and $\mu = 0.4$.

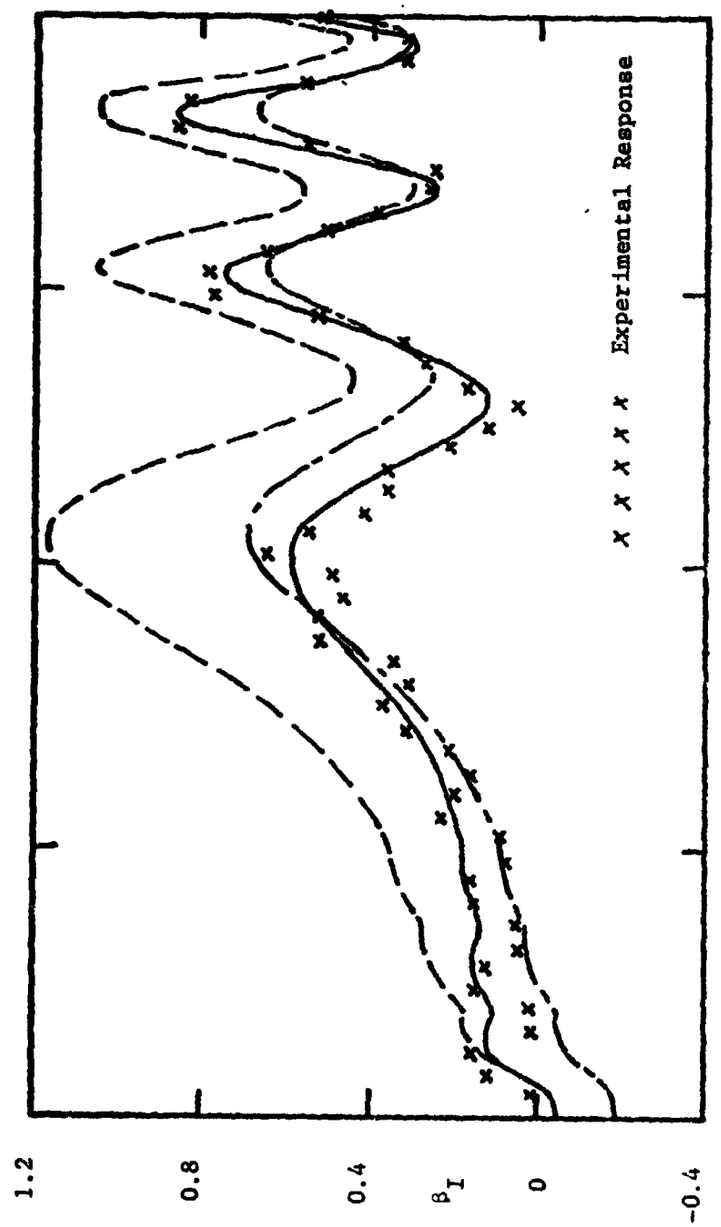

Figure 37a. Prediction Results for β_I Responses for $\Theta_o = 5^o$; $\omega_1 = 1.116$ and $\mu = 0.1$.
——— L-Matrix Downwash Model Obtained from Data with $\Theta_1 = 5^o$; $\omega_1 = 1.24$ and $\mu = 0.1$
— - — - — γ Model Obtained from Data with $\Theta_o = 5^o$; $\omega_1 = 1.24$ and $\mu = 0.1$
— — — — — γ Model (Neglecting Downwash)

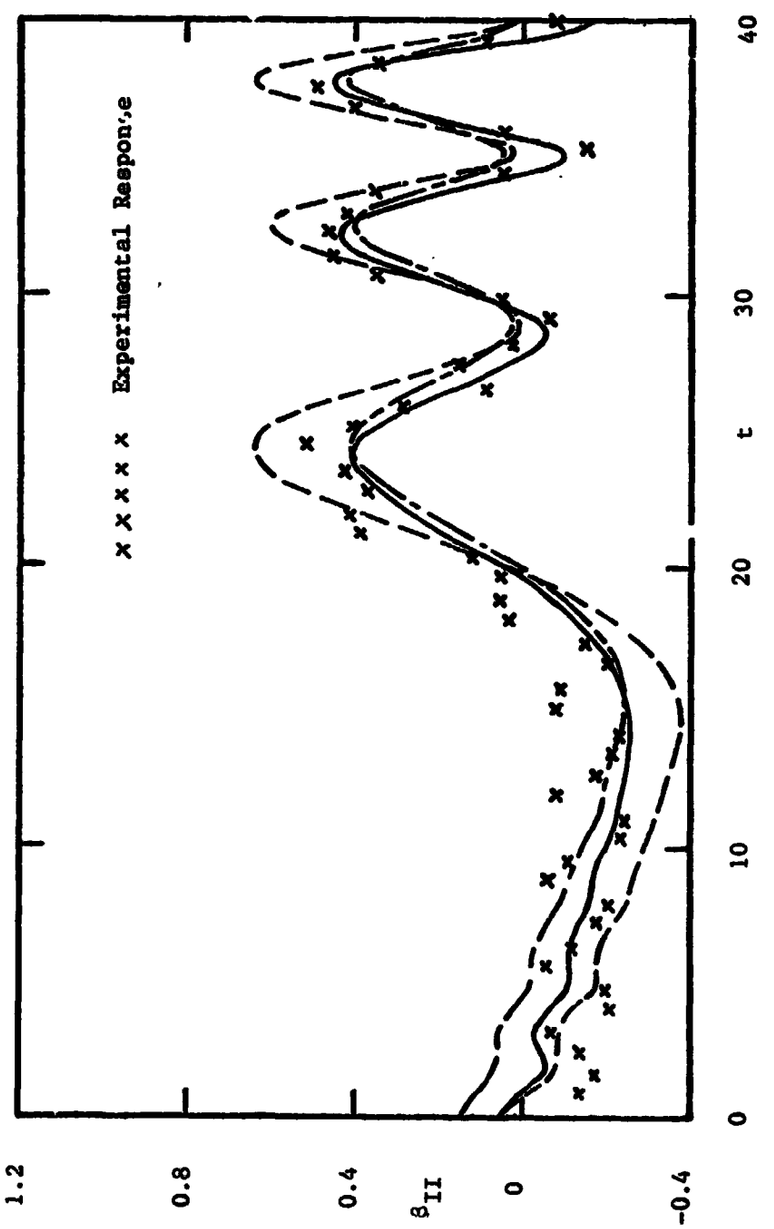

Figure 37b. Prediction Results for β_{II} Responses for Conditions given in Figure 36a.

(a) γ model (neglecting downwash)

(b) γ^* model (obtained from data with $\omega_1 = 1.24$, $\theta_0 = 5^0$ and $\mu = .1$)

(c) the more complete L-matrix model (parameters obtained from data with $\omega_1 = 1.24$, $\theta_0 = 5^0$ and $\mu = 0.1$)

Though the model without downwash shows high r. m. s. fit errors, the other two models give good degree of fit prediction.

The γ model gives larger amplitude responses as compared to the other two. The Lock number γ is the ratio of the aerodynamic forces to the gyroscopic (inertia) forces. Increase in the aerodynamic forces increases the amplitude of the response. Increase in the inertia forces decreases the amplitude of the response. Hence, with increasing value of γ, the response has an increasing amplitude. This is also verified by the flapping equation 52 which shows that, since γ multiplies the forcing function, the response is directly dependent on it, even though the damping of the system is increased by increasing the value of γ.

Frequency response curves show that the γ^* model has a decreasing value of the amplitude response with increasing progressive frequency excitation (beyond a certain frequency), whereas the true response has an opposite trend (37). This gives rise to greater discrepancies at higher progressive frequencies between γ^* model and the physical model. This is clearly seen in the β_I and β_{II} prediction curves, since the prediction studies are made at a much higher frequency of input transient excitation as compared to the frequency range in which the γ^* model was determined.

The initial conditions for these prediction studies were chosen at their corresponding identified values.

3. Prediction curves for data with $\omega_1 = 1.18$, $\theta_0 = 5^0$ and $\mu = 0.2$. The L-matrix parameters and γ were chosen from the data set with $\omega_1 = 1.24$, $\theta_0 = 5^0$ and $\mu = 0.2$. The three models are studied as before (see Figures 38a and 38b). All the features found in the previous prediction study with $\mu = 0.1$ are found in this study. An important observation is that the model neglecting the dynamic inflow (γ^* model) has a significantly smaller error at $\mu = 0.2$ as compared to that at $\mu = 0.1$. This indicates the fact that with increasing advance ratio, the feedback effect of the downwash is diminishing.

4. In Figures 39a,39b and 39c, data set with $\theta_0 = 5^0$, $\omega_1 = 1.24$ and $\mu = 0.2$ is modelled using the γ^* model and the more complete L-matrix model (with diagonal terms). The plot shows a significant improvement in the fit by using the complete L-matrix model.

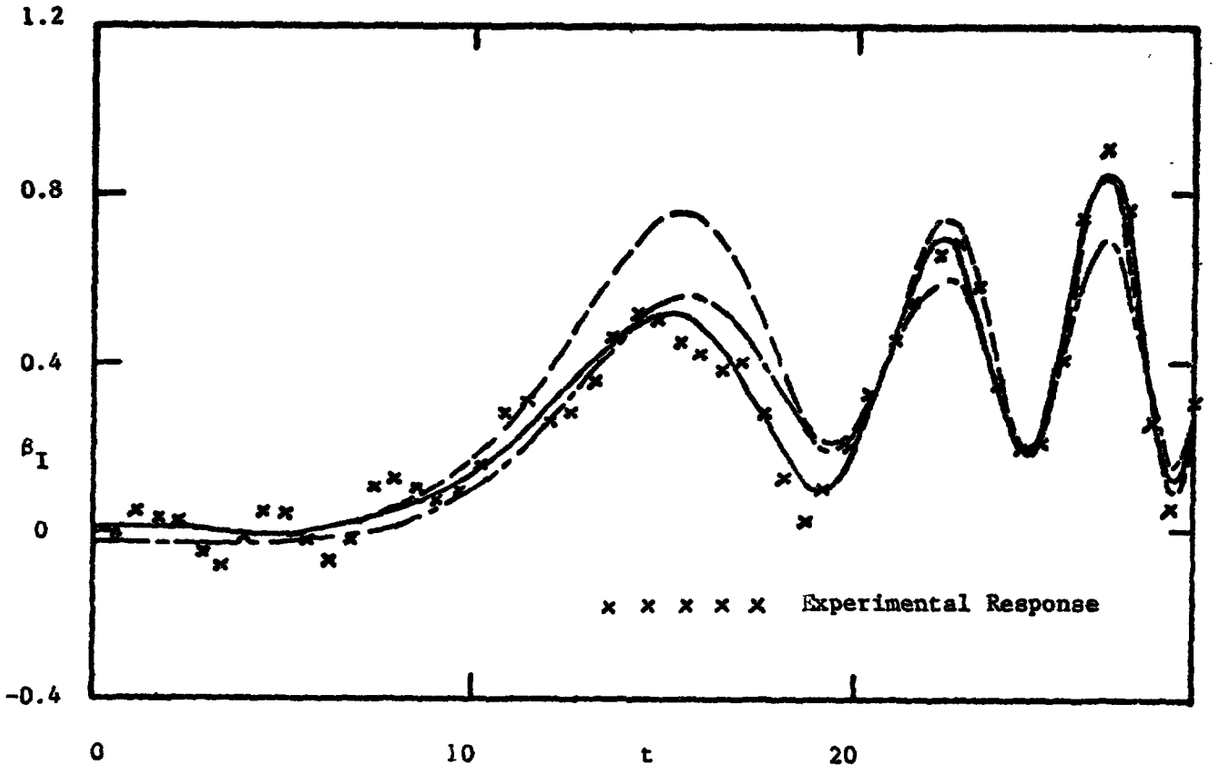

Figure 38a. Prediction Results for β_I Responses for $\theta_o = 5^o$; ω_1 =1.18 and $\mu = 0.2$.
———— L-Matrix Downwash Model Obtained from Data with $\theta_o = 5^o$; $\omega_1 = 1.24$ and $\mu = 0.2$
—— - —— γ^* Model Obtained from Data with $\theta_o = 5^o$; $\omega_1 = 1.24$ and $\mu = 0.2$
— — — — γ Model (Neglecting Downwash)

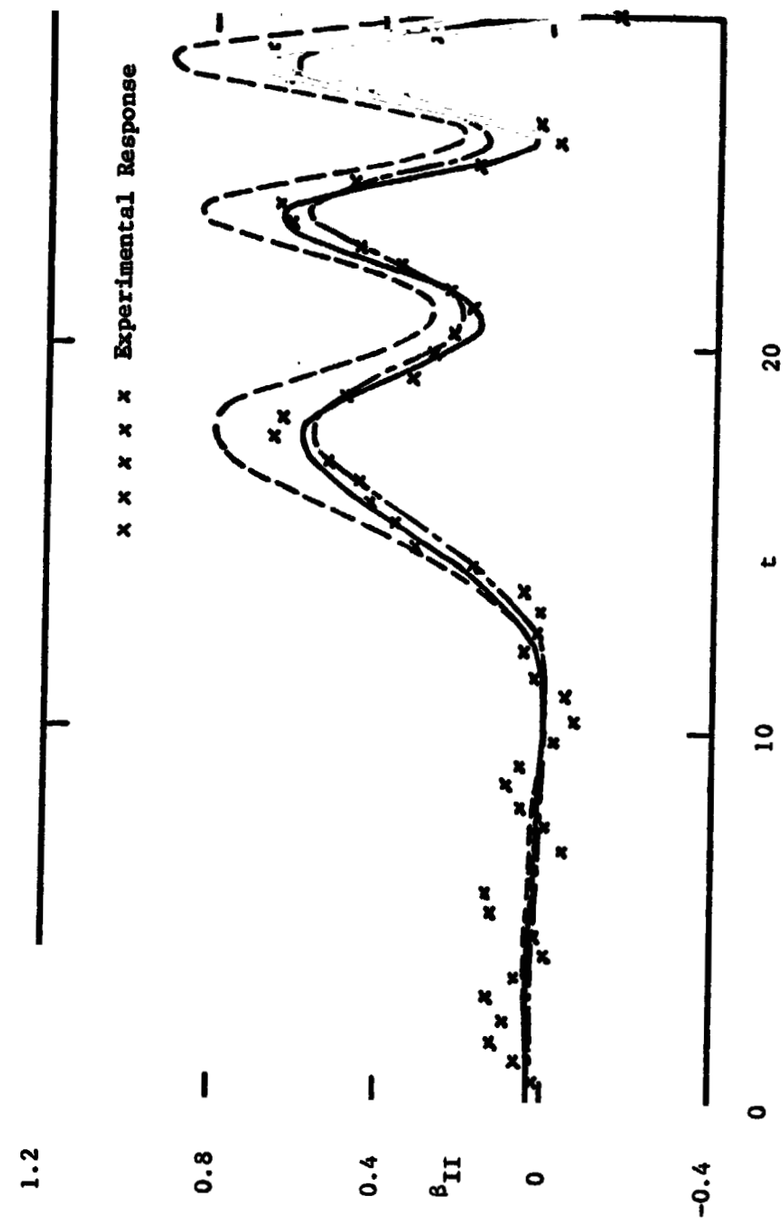

Figure 38b. Prediction Results for β_{II} Responses for Conditions given in Figure 37a.

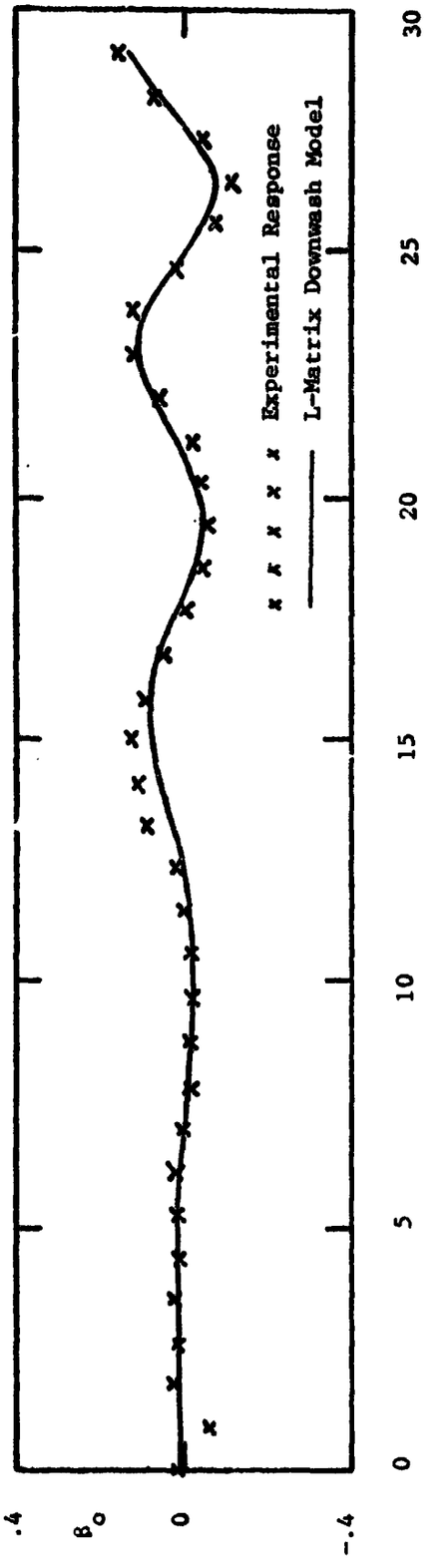

Figure 39a. Plots of β_o Responses for $\theta_o = 5^o$; $\omega_1 = 1.24$ and $\mu = 0.2$.

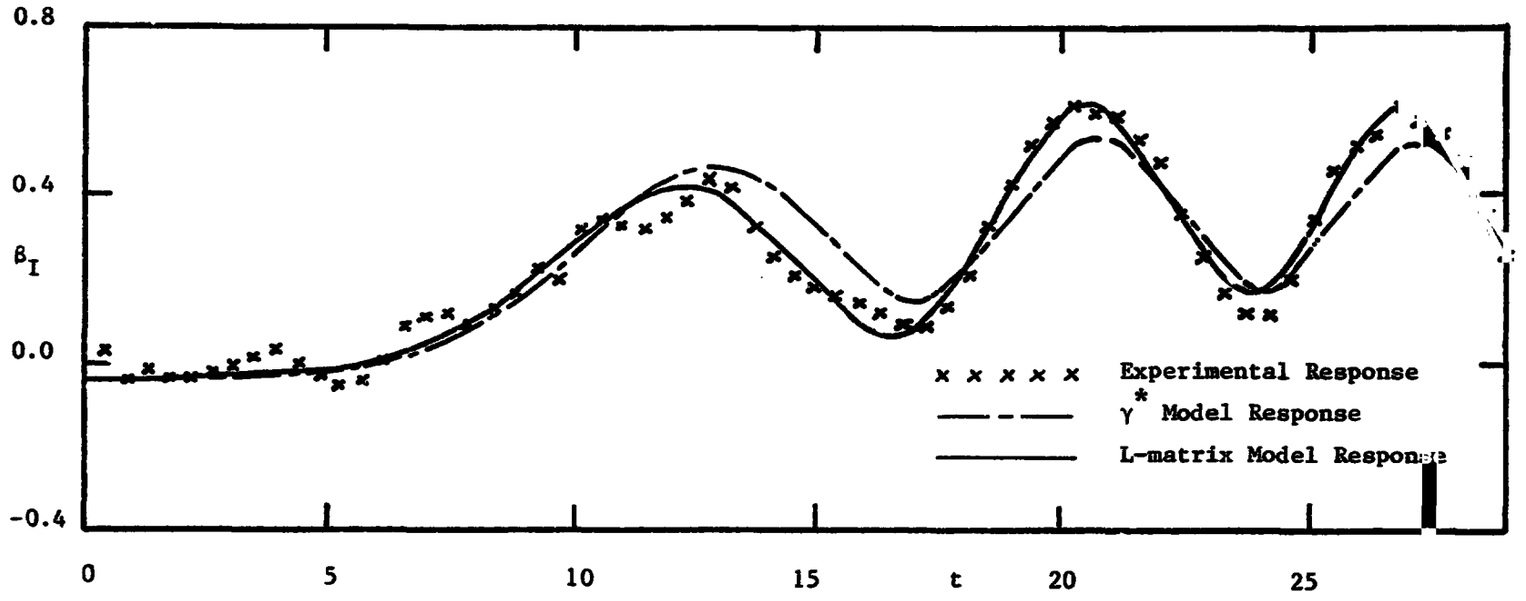

Figure 39b. Plots of β_I Responses for $\theta_o = 5^o$; $\omega_1 = 1.24$ and $\mu = 0.2$.

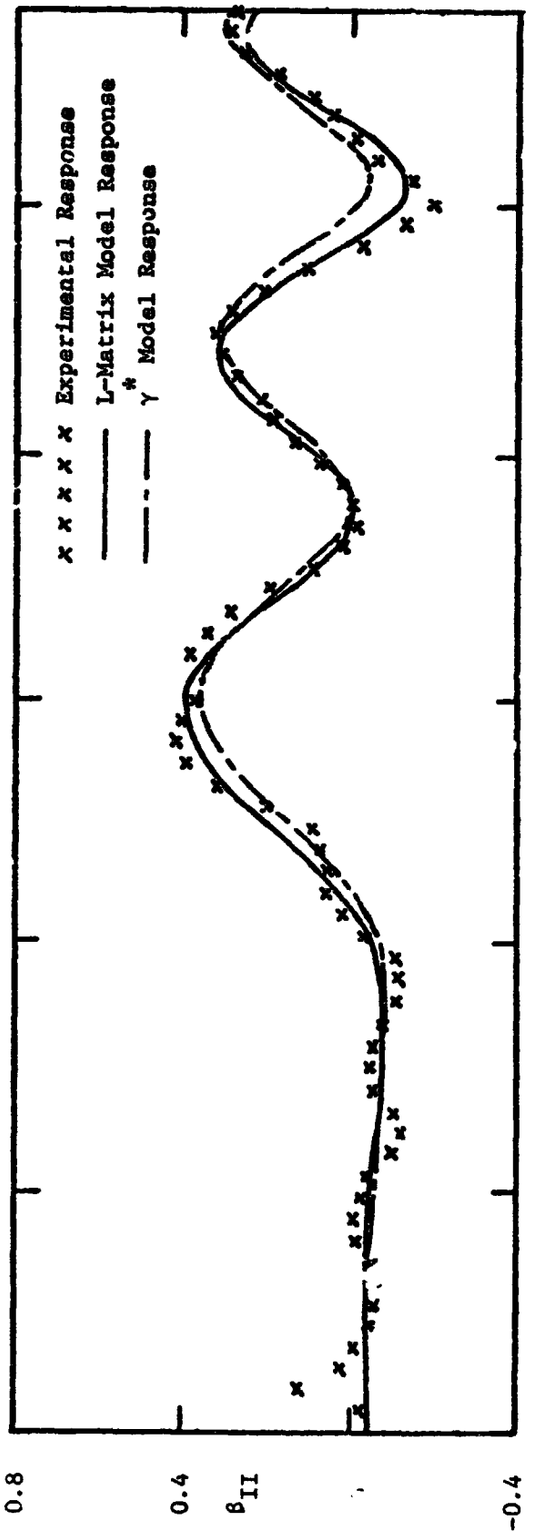

Figure 39c. Plots of β_{II} Responses for $\theta_o = 5^o$; $\omega_1 = 1.24$ and $\mu = 0.2$.

7. CONCLUSION AND DISCUSSION OF RESULTS

Based on the preceding analysis of the feedback effects of the rotor dynamic inflow on the flapping response of the rotor blades to accelerated pitch stirring excitation, several interesting results follow.

7.1 CONCLUSION OF METHOD ANALYSIS

Apart from the several theoretically justifiable properties of the Maximum Likelihood method as outlined in section 2.7, simulation studies and comparison with other identification techniques give the following results:

1. The Maximum Likelihood method works well for both the single blade and the multiblade application in simulation studies.
2. The Cramer-Rao lower bounds for the parameter covariances obtained from the Maximum Likelihood analysis provide a good measure of accuracy of the identified parameters and are clearly superior and more meaningful than the covariance estimates determined with other known methods.

7.2 RESULTS OF THE SIMULATION STUDIES

1. Single blade identification of γ^* and θ_o together with the initial values of the flapping response at $\mu = 0.4$ give good results. This analysis is not used for experimental data because of small differences between the different blade responses.
2. The parameters of the entire L-matrix (as given by equation 96) converge in the simulation identification of the perturbation flapping response model, though with limited accuracy. The

off-diagonal terms L_{23} and L_{32} and the time constants τ_o, τ_I and τ_{II} have been found to provide poor identifiability in certain cases.

3. The γ^* identification study provides consistent and fast convergence under all test conditions.

4. Eigenvalue analysis of different forward flight models show (Table 7) that for the cases studied, at low advance ratios($\mu \leq .4$), the error in neglecting the periodic terms in the flapping equations is negligible (< 2% in the eigenvalue comparisons). On the other hand, neglecting the inflow in the mathematical model gives rise to significant errors.

5. The eigenvalue variation with advance ratio (Table 9) is negligible. This is based on no variation of the inflow parameter values with advance ratio.

6. At high advance ratio (μ=0.8), there is negligible change in the eigenvalues (Table 10) when the feedback effects of the inflow is neglected.

7.3 RESULTS FROM EXPERIMENTAL DATA ANALYSIS

1. The cyclic pitch stirring excitation with approximately constant stirring acceleration is adequate for identification of the parameter γ^* (equation 72) and some of the L-matrix parameters (equation 74). To identify the parameters associated with the ν_o equation accurately (equation 74), collective pitch excitation is probably required.

2. Progressive transient excitation data gives identifiable parameters. The same identification study on regressive cyclic pitch stirring

transient excitation data gives equally good results.

3. γ^* is an accurately identifiable parameter for all trim conditions (the collective pitch setting, the blade rotational stiffness, the rotor shaft angle of attack and advance ratio). This concurs with the findings of the simulation studies. In contrast, the L-matrix parameters identify only upto an advance ratio of μ=0.4. Beyond this advance ratio it is not possible to identify these parameters.

4. The identifiability of the parameters from the experimental data is in close agreement with the findings in the simulation studies. The time constants τ_o, τ_I and τ_{II} have increasing identifiability in that order. Their effects on the flapping responses are lower than those of the parameters of the L-matrix.

5. The γ^* model adequately represents the feedback effects of the induced inflow on the flapping response for advance ratio $\mu \geq 0.4$. At low advance ratios ($\mu < 0.4$), the L-matrix model provides a much better correlation to the experimental flapping responses as compared to the γ^* model. With increasing advance ratio, the difference between the fits of the two mathematical models and the experimental results decreases.

6. The identified values of some of the L-matrix parameters agree reasonably well with those obtained by using momentum theory (Figures 34 and 35). Most of the identified values of L_{22} and L_{33} fall between the values obtained from momentum theory and the empirical values given in (10). Empirical L_{22} and L_{33} values

are approximately -0.5 and -0.2 respectively, for advance ratios between 0 and 0.4.

7. L_{32} and L_{23} identify to values around the momentum theory value of zero. They show no consistency or trend in their variation with the trim conditions. The identified values of L_{23} lie between -0.15 and 0.15; L_{32} lies between -0.15 and 0.4.

8. The accuracy of the identified mathematical model is determined by applying it to tests not used for the identification. Examples shown in Figures 37 a-b and 38 a-b show the adequacy and goodness of the inflow models that have been used.

7.4 AREAS OF FURTHER STUDY

1. The plots of Figures 31 a-b show a consistent trend that has not been explained by theoretical models (see 6.2). This suggests the need for a more complete mathematical model to represent the variation of the equivalent Lock number γ^* with trim condition.

2. The parameters associated with the perturbation equations for ν_o (equation 74) are not identifiable using cyclic pitch stirring excitation. In order to make a complete identification, collective pitch transients will have to be added.

3. In the preceding study, dynamic rotor inflow is coupled to blade flapping only. It is unlikely that blade lead-lag or torsional flexibility will have a substantial effect on the dynamic inflow. However, the effect of the dynamic inflow on lead-lag and torsional deflections is expected to be of importance and should be studied.

8. APPENDICES

8.1 NOMENCLATURE

B	blade tip loss factor
B(j/k)	innovation covariance matrix at time t_j given measurements till time t_k (equation 32)
C(t)	aerodynamic damping (equation 53)
C_T	rotor thrust coefficient, positive up (equation 130)
C_M	rotor pitching moment coefficient, positive nose up (equation 130)
C_L	rotor rolling moment coefficient, positive to right (equation 130)
D(t)	measurement input matrix
E	energy term (equation 105)
E(θ/Z)	expected value for the probability density of θ given the measurements Z
F(t)	rotor state matrix
G(t)	rotor input matrix
H(t)	measurement state matrix
I	identity matrix
J	scalar cost criterion
K_M, K_{I_1}, K_{I_2}	nondimensiona. apparent mass and inertia of impermiable disk
K(t)	aerodynamic stiffness (equation 54)
K(j)	Kalman filter gain at time t_j
L	rotor induced flow gain matrix
L_{11}, L_{12},.., L_{33}	parameters of the L^{-1} matrix (equation 73)
M	information matrix
M_k	moment at the rotor hub of the k th blade
P(t)	the state covariance matrix
K_I	when $K_{I_1}=K_{I_2}=K_I$

NOMENCLATURE (continued)

$P_{\theta x}(t)$	combined covariance matrix, where the parameters θ are included in an augmented state
Q	system equation noise covariance matrix
R	measurement equation noise covariance matrix and rotor radius
S_i	sensitivity matrix at time t_i (equation 116)
T_k	thrust at the rotor hub of the k th blade
U_p	relative blade normal velocity (equation 133)
U_T	relative blade tangential velocity (equation 132)
W	positive definite weighting matrix
Y_j	set of observation vectors till time t_j $(y_1, y_2, \ldots, y_j)$
Z	set of all observation vectors $(y_1, y_2, \ldots, y_N)$
a	blade section lift slope
b, N	number of blades on the rotor
c	blade chord
f(.)	function of variables in paranthesis in the system equation
h(.)	function of variables in paranthesis in the measurement equation
g	vector of measurement bias
$m_\theta(t)$, $m_\lambda(t)$	aerodynamic flapping moments (equations 55 and 56)
p(.)	probability density function
t_o	initial time
t_f, T	final time
s	complex variable in the laplace transform
t	nondimensional time for which the period of one rotor revolution is 2π
u(t)	input control vector

NOMENCLATURE (continued)

$v(t)$	measurement noise vector of covariance R
$w(t)$	system noise vector of covariance Q
$x(t)$	rotor state vector
$y(t)$	rotor output or measurement vector
α	hub pitch angle, positive nose up
β_k	flapping angle of the k th blade, positive up
β_o, β_d, β_I, β_{II}	multiblade flapping coordinates: coning, differential coning (only for even-bladed rotors), longitudinal and lateral cyclic flapping
ψ_k	azimuth angle of the k th blade
$\delta = \gamma\theta_o$	parameter identified in the single blade analysis
$\delta(t)$	delta function
λ	nondimensional normal inflow
λ_o, λ_I, λ_{II}	uniform, longitudinal and lateral inflow components
κ	adaptation factor for the first mode representation
$\eta(x)$	first rotating mode shape of a rotor blade
ω	angular pitch stirring speed
ω_l	blade flapping natural frequency in the rotating system
Ω	rotor angular speed
μ	rotor advance ratio
$\nu(j)$	innovation vector at time t_j (equation 23)
ν_o, ν_I, ν_{II}	uniform, longitudinal and lateral perturbation induced inflow components
ν_k	induced inflow of the k th blade
ρ	air density
γ	blade Lock number
$\Gamma(t)$	system noise matrix (equation 3)

NOMENCLATURE (continued)

θ_o, θ_I, θ_{II}	collective, nose down cyclic and left cyclic pitch angles respectively
θ_b	instantaneous blade pitch angle
θ_1, θ_2,..., θ_6	parameters of the inflow perturbation model (equations 102 and 104)
θ	vector of unknown parameters
σ	rotor solidity ratio ($bc/\pi R$)
σ_i	standard deviation of the i th parameter
Λ	positive definite weighting matrix
ζ	measured states in the system equation

Superscripts

$\dot{}$	time derivative
$\hat{}$	estimated value
$\check{}$	mode of the probability density function
T	transposed matrix
*	equivalent value
$\bar{}$	mean or trim value

Subscripts

m	measured variable
i	i th sample of the variable
k	blade number or iteration number
o, d, I, II	multiblade variables
E	empirical value

Symbols

$\approx$	approximate equality
$\triangleq$	defined by

NOMENCLATURE (continued)

$\lvert\ \rvert$	determinant of a matrix or absolute value of a number
$\sim$	equivalent to
Π	product of the given terms
Δ	increment
Σ	summation of the given terms
$\int_b^a$	definite integral with limits from a to b
$\leq$	less than or equal to
$\geq$	greater than or equal to
$\lVert U \rVert_W = U^T W U$	eucledian norm

8.2 DERIVATION OF THE THRUST AND MOMENT COEFFICIENTS C_T, C_L AND C_M AS A FUNCTION OF THE STATE VARIABLES

The state of the system is

$$X^T = [\beta_o \ \dot{\beta}_o \ \beta_I \ \dot{\beta}_I \ \beta_{II} \ \dot{\beta}_{II} \ \nu_o \ \nu_I \ \nu_{II} \ \beta_d \ \dot{\beta}_d] \tag{129}$$

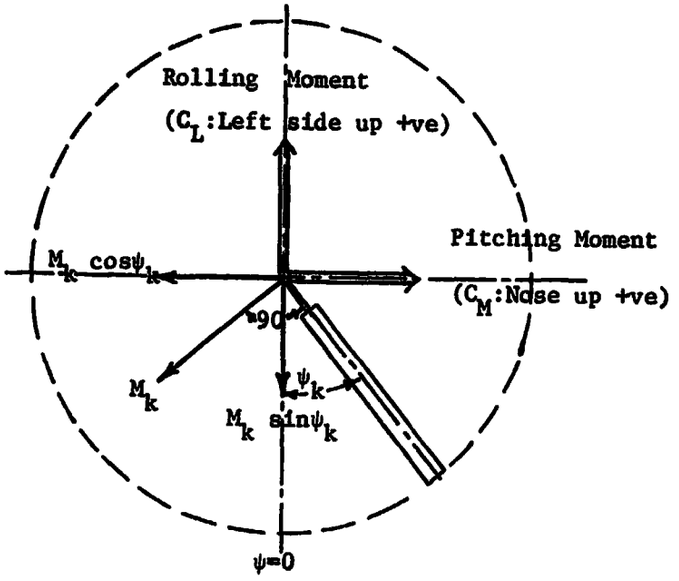

$$C_L = -(1/\rho\pi\Omega^2R^5)\sum_{k=1}^{N} M_k \cos\psi_k$$

$$C_M = -(1/\rho\pi\Omega^2R^5)\sum_{k=1}^{N} M_k \sin\psi_k \tag{130}$$

$$C_T = (1/\rho\pi\Omega^2R^4)\sum_{k=1}^{N} T_k$$

We now determine the thrust and moment of each blade to be substituted into the equations 130.

Blade pitch angle: $\theta = \theta_o - \theta_I \sin\psi + \theta_{II} \cos\psi$

Induced flow: $\nu = \nu_o + \nu_I \, x \cos\psi + \nu_{II} \, x \sin\psi$ (131)

Relative tangential velocity:

$$U_T = x + \mu \sin\psi \tag{132}$$

Relative normal velocity: (+ are up)

$$U_p = \nu - x\dot{\beta} - \mu\beta \cos\psi \tag{133}$$

The thrust and moment exerted by each blade, as given under the assumption of no reversed flow are:

$$T_k = \frac{\rho a c \Omega^2 R^3}{2} \int_0^B (U_T^2 \, \theta + U_p \, U_T)_k \, dx \tag{134}$$

$$M_k = \frac{\rho a c \Omega^2 R^4}{2} \int_0^B (U_T^2 \, \theta + U_p \, U_T)_k x \, dx \tag{135}$$

Equation 132 can be substituted into equation 134 with the aid of the transformation

$$\begin{aligned} \beta_k &= \beta_o + \beta_d(-1)^k + \beta_I \cos\psi_k + \beta_{II} \sin\psi_k \\ \dot{\beta}_k &= \dot{\beta}_o + \dot{\beta}_d(-1)^k + \dot{\beta}_I + \beta_{II})\cos\psi_k + (\dot{\beta}_{II} - \beta_I)\sin\psi_k \end{aligned} \tag{136}$$

The result, after some algebraic manipulation, is:

$$T_k = \frac{\rho a c \Omega^2 R^3}{2} \{(B^3/3 + B\mu^2/2 + B^2\mu \sin \psi_k - B\mu^2 \cos 2\psi_k/2)\theta_o$$

$$- (B^2\mu/2 + (B^3/3 + 3B\mu^2/4)\sin \psi_k - B^2\mu \cos 2\psi_k/2$$

$$- B\mu^2 \sin 3\psi_k/4)\theta_I + ((B^3/3 + B\mu^2/4)\cos \psi_k + B^2\mu \sin 2\psi_k/2$$

$$- B\mu^2 \cos 3\psi_k/4)\theta_{II} + (B^2/2 + B\mu \sin \psi_k)\nu_o$$

$$+ (B^3 \cos \psi_k/3 + B^2\mu \sin 2\psi_k/4)\nu_I + (B^3 \sin \psi_k/3 + B^2\mu/4$$

$$- B^2\mu \cos 2\psi_k/4)\nu_{II} - (B^3/3 + B^2\mu \sin \psi_k/2)(\dot{\beta}_o + \dot{\beta}_d (-1)^k)$$

$$- (B^3 \cos \psi_k/3 + B^2\mu \sin 2\psi_k/4)(\dot{\beta}_I + \beta_{II})$$

$$- (B^3 \sin \psi_k/3 + B^2\mu/4 - B^2\mu \cos 2\psi_k/4)(\dot{\beta}_{II} - \beta_I)$$

$$- (B^2\mu \cos \psi_k/2 + B\mu^2 \sin 2\psi_k/2)(\beta_o + \beta_d (-1)^k)$$

$$- (B^2\mu/4 + B\mu \sin \psi_k/4 + B^2\mu \cos 2\psi_k/4 + B\mu \sin 3\psi_k/4)\beta_I$$

$$- (B\mu \cos \psi_k/4 + B^2\mu \sin 2\psi_k/4 - B\mu \cos 3\psi_k/4)\beta_{II}$$

$$- \kappa ((\beta_o + \beta_d (-1)^k + \beta_I \cos \psi_k + \beta_{II} \sin \psi_k)(.4411\ \mu^2$$

$$\sin 2\psi_k + 1.0676\ \mu \cos \psi_k) + (\dot{\beta}_o + \dot{\beta}_d (-1)^k \qquad (137)$$

$$+ (\dot{\beta}_I + \beta_{II})\cos \psi_k + (\dot{\beta}_{II} - \beta_I)\sin \psi_k)(\mu \sin \psi_k (-.2119) - .0838))\}$$

Equation 130 for C_T is now substituted in the previous equation 137. The signs of the induced downwash ν_o, ν_I and ν_{II} are changed for the proper (positive down) convention.

$$C_T = (a\sigma/2)\{(B^3/3 + B\mu^2/2)\theta_o - (B^2\mu/2)\theta_I$$

$$- (B^2/2)\nu_o - (B^2\mu/4)\nu_{II} - (B^3/3)\dot{\beta}_o + (B\mu^2/2)\sin 2t\ \beta_d$$

$$- (B^2\mu/4)\dot{\beta}_{II} + \kappa((.4411)\mu^2 \sin 2t\ \beta_d$$

$$-.5338\mu\ \beta_I + .0838\ \dot{\beta}_o + (.1059)\mu\ (\dot{\beta}_{II} - \beta_I))\} \qquad (138)$$

Equation 133can now be substituted in equation 135, and using the transformation equation 136and equation 130 , the following expansions for C_L and C_M, in terms of the state variables, are obtained:

$$C_L = -(1/\rho\pi\Omega^2R^5)(\rho ac\Omega^2R^4/2)\{((B^4/4 + B^2\mu^2/4)\theta_o$$

$$- (B^3\mu/3)\theta_I + (B^3/3)\nu_o + (B^3\mu/6)\nu_{II} - (B^3\mu/6)\beta_I$$

$$- (B^4/4)(\dot{\beta}_o + \dot{\beta}_d\ (-1)^k))\sum_{k=1}^{b} \sin\psi_k + ((2B^3\mu/3)\theta_o$$

$$- (B^4/4 + 3B^2\mu^2/8)\theta_I + (B^2\mu/2)\nu_o + (B^4/4)\nu_{II} - (B^3\mu/3)(\dot{\beta}_o + \dot{\beta}_d\ (-1)^k)$$

$$- (B^4/4)(\dot{\beta}_{II} - \beta_I) - (B^2\mu^2/8)\beta_I)(1/2)\sum_{k=1}^{b}(1-\cos 2\psi_k)$$

$$+ ((B^4/4 + B^2\mu^2/8)\theta_{II} + (B^4/4)\nu_I - (B^4/4)(\dot{\beta}_I + \beta_{II})$$

$$- (B^3\mu/3)(\beta_o + \beta_d\,(-1)^k) + (B^2\mu^2/8)\beta_{II})(1/2)\sum_{k=1}^{b} \sin 2\psi_k$$

$$+ ((B^3\mu/3)\theta_{II} + (B^3\mu/6)\nu_I - (B^3\mu/6)(\dot{\beta}_I + \beta_{II})$$

$$- (B^2\mu^2/4)(\beta_o + \beta_d\,(-1)^k) - B^3\mu/6)(1/2)\sum_{k=1}^{b} (\cos\psi_k - \cos 3\psi_k)$$

$$+ ((-B^2\mu^2/4)\theta_o + (B^3\mu/3)\theta_I - (B^3\mu/6)\nu_{II} + (B^3\mu/6)(\dot{\beta}_{II} - \beta_I)$$

$$- (B^3\mu/6)\beta_I)(1/2)\sum_{k=1}^{b} (\sin 3\psi_k - \sin\psi_k) + ((B^2\mu^2/8)\theta_I$$

$$- (B^2\mu^2/8)\beta_I)(1/2)\sum_{k=1}^{b} (\cos 2\psi_k - \cos 4\psi_k) + ((-B^2\mu^2/8)\theta_{II}$$

$$+ (B^2\mu^2/8)\beta_{II})(1/2)\sum_{k=1}^{b} (\sin 4\psi_k - \sin 2\psi_k)$$

$$+ \kappa\,((\mu)(.886)(\sin 2t)(b)\beta_d + \sum_{k=1}^{b} (.2675)\mu^2\,(\cos 4\psi_k - 1)\beta_I$$

$$+ \sum_{k=1}^{b} (.2675)\mu^2 \sin 4\psi_k\,\beta_{II} + (.028)\mu\, b \cos 2t\,\dot{\beta}_d$$

$$- \sum_{k=1}^{b} (.028)(1 - \cos\psi 2_k)(\dot{\beta}_{II} - \beta_I))\}$$

(The signs of ν_o, ν_I and ν_{II} are now changed for positive down sign convention.)

$$= -(a\sigma/4)\{(2B^3\mu/3)\theta_o - (B^4/4 + 3B^2\mu^2/8)\theta_I$$

$$- (B^2\mu^2 \cos 4t/8)\theta_I - (B^2\mu^2 \sin 4t/8)\theta_{II} - (B^2\mu/2)\nu_o$$

$$- (B^3\mu/3)\dot{\beta}_o - (B^4/4)(\dot{\beta}_{II} - \beta_I) - (B^4/4)\nu_{II} - (B^2\mu^2/8)\beta_I$$

$$+ (B^2\mu^2 \cos 4t/8)\beta_I + (B^2\mu^2 \sin 4t/8)\beta_{II}$$

$$- (B^3\mu \cos 2t/3)\dot{\beta}_d + (B^3\mu \sin 2t/3)\beta_d$$

$$+ \kappa ((.886)(\mu \sin 2t)\beta_d + (.2675)\mu^2 (\cos 4t -)\beta_I$$

$$+ (.2675)\mu^2 \sin 4t\ \beta_{II} + (.028)\mu \cos 2t\ \dot{\beta}_d$$

$$- (.028)(\dot{\beta}_{II} - \beta_I))\} \qquad (139)$$

Similarly

$$C_M = -(1/\rho\pi\Omega^2R^5)(\rho ac\Omega^2R^4/2)\{(B^4/4 + B^2\mu^2/4)\theta_o$$

$$- (B^3\mu/3)\theta_I + (B^3/3)\nu_o + (B^3\mu/6)\nu_{II} - (B^3\mu/6)\beta_I$$

$$- (B^4/4)(\dot{\beta}_o + \dot{\beta}_d (-1)^k))\left(\sum_{k=1}^{b} \cos \psi_k\right) + ((2B^3\mu/3)\theta_o$$

$$- (B^4/4 + 3B^2\mu^2/8)\theta_I + (B^2\mu/2)\nu_o + (B^4/4)\nu_{II} - (B^3\mu/3)(\dot{\beta}_o + \dot{\beta}_d (-1)^k)$$

$$- (B^4/4)(\dot{\beta}_{II} - \beta_I) - (B^2\mu^2/8)\beta_I)(1/2)$$

$$\left(\sum_{k=1}^{b} \sin 2\psi_k\right) + \left((B^4/4 + B^2\mu^2/8)\theta_{II} + (B^4/4)\nu_I \right.$$

$$- (B^4/4)(\dot{\beta}_I + \beta_{II}) - (B^3\mu/3)(\beta_o + \beta_d (-1)^k) + (B^2\mu^2/8)\beta_{II})$$

$$(1/2)\left(\sum_{k=1}^{b} (1 + \cos 2\psi_k)\right) + ((B^3\mu/3)\theta_{II} + (B^3\mu/6)\nu_I$$

$$- (B^3\mu/6)(\dot{\beta}_I + \beta_{II}) - (B^2\mu^2/4)(\beta_o + \beta_d (-1)^k) - B^3\mu/6)$$

$$(1/2)\left(\sum_{k=1}^{b} (\sin \psi_k + \sin 3\psi_k)\right) + (-(B^2\mu^2/4)\theta_o + (B^3\mu/3)\theta_I$$

$$- (B^3\mu/6)\nu_{II} + (B^3\mu/6)(\dot{\beta}_{II} - \beta_I) - (B^3\mu/6)\beta_I)(1/2)$$

$$\left(\sum_{k=1}^{b} (\cos 3\psi_k + \cos \psi_k)\right) + ((B^2\mu^2/8)\theta_I - (B^2\mu^2/8)\beta_I)$$

$$(1/2)\left(\sum_{k=1}^{b} (\sin 2\psi_k + \sin 4\psi_k)\right) + (-(B^2\mu^2/8)\theta_{II} + (B^2\mu^2/8)\beta_{II})$$

$$(1/2)\left(\sum_{k=1}^{b} (\cos 2\psi_k + \cos 4\psi_k)\right) - \kappa\left(\sum_{k=1}^{b} -(.886)\mu(1 + \cos 2\ \psi_k)\beta_o\right.$$

$$+ \sum_{k=1}^{b} -(.886)\,\mu(1 + \cos 2\psi_k)(-1)^k\ \beta_d +$$

$$\sum_{k=1}^{b} -(.886)(\mu/2)(3 \cos \psi_k + \cos 3\ \psi_k)\beta_I - \sum_{k=1}^{b} (1.070)(\mu^2/2)(\sin 2\psi_k$$

$$+ \sin 4\psi_k/2)\beta_1 - \sum_{k=1}^{b} (.886)(\mu/2)(\sin 3\psi_k + \sin \psi_k)\beta_{II}$$

$$- \sum_{k=1}^{b} (1.070)(\mu^2/4)(1 - \cos 4\psi_k)\beta_{II} + \sum_{k=1}^{b} (.028)\mu \sin 2\psi_k (-1)^k \dot{\beta}_d$$

$$- \sum_{k=1}^{b} (.028)(\cos 2\psi_k + 1)(\dot{\beta}_I + \dot{\beta}_{II}))\}$$

The signs of ν_o, ν_I and ν_{II} are changed for positive down sign convention.

$$= -(a\sigma/4)\ \{(B^2\mu^2/8)\sin 4t\ \theta_I + (B^4/4) + B^2\mu^2/8)\theta_{II}$$

$$- (B^2\mu^2/8)\cos 4t\ \theta_{II} - (B^4/4)(\dot{\beta}_I + \beta_{II} + \nu_I) - (B^3\mu/3)\beta_o$$

$$- (B^2\mu^2/8)\sin 4t\ \beta_I + (B^3\mu/3)\sin 2t\ \dot{\beta}_d + (B^3\mu/3)$$

$$\cos 2t\ \beta_d - (B^2\mu^2/8)\beta_{II} + (B^2\mu^2/8)\cos 4t\ \beta_{II}$$

$$+ \kappa\ (-(.\ 5)\mu\beta_o + (.886)\mu \cos 2t\ \beta_d - (.2675)\mu^2$$

$$\sin 4t\ \beta_I - (.2675)\mu^2\ (1 - \cos 4t)\beta_{II} - (.028)\mu$$

$$\sin 2t\ \dot{\beta}_d - (.028)(\dot{\beta}_I + \beta_{II})\ )\} \qquad (140)$$

8.3 MULTIBLADE REPRESENTATION OF THE PERTURBATION FLAPPING EQUATIONS, INCLUDING REVERSE FLOW

$$\ddot{\beta}_o + (\gamma/2)(CO + CC4 + CN4)\dot{\beta}_o + (\omega_1^2 + (\gamma/2)PS4 \sin 4t)\beta_o$$

$$+ (\gamma/2)(-(1/2)CS1 + (CS3/2)\cos 4t - (CS5/2)\cos 4t$$

$$+ (PC7/2)\cos 8t + PC\ 1/2 + (PC3/2)\cos 4t$$

$$+ (PC5/2)\cos 4t)\beta_{\perp} + (\gamma/2)((CS3/2)\sin 4t + (CS5/2)\sin 4t)\dot{\beta}_I$$

$$+ (\gamma/2)((CS3/2)\sin 4t + (CS5/2)\sin 4t + (PC3/2)\sin 4t$$

$$- (PC5/2)\sin 4t + (PC7/2)\sin 8t)\beta_{II} + (\gamma/2)(CS1/2 - (CS3/2)\cos 4t$$

$$+ (CS5/2)\cos 4t)\ \dot{\beta}_{II} + (\gamma/2)(-PS2 \sin 2t - PS6 \sin 6t)\beta_d$$

$$- (\gamma/2)(CC2 \cos 2t + CC6 \cos 6t)\dot{\beta}_d$$

$$+ (\gamma/2)(DO + CC4 \cos 4t)\nu_o + (\gamma/2)(ES4 \sin 4t)\nu_I \qquad (141)$$

$$+ (\gamma/2)(FO + FC4 \cos 4t)\nu_{II}$$

$$= (\gamma/2)(YO + YC4 \cos 4t)\theta_I + (\gamma/2)(ZS4 \sin 4t)\theta_{II}$$

$$\ddot{\beta}_I + 2\ \dot{\beta}_{II} - \beta_I + (\gamma/2)(CS3 \sin 4t + CS5 \sin 4t)\dot{\beta}_o$$

$$+ (\gamma/2)(CO + CC2/2 + (CC2/2)\cos 4t + CC4 \cos 4t$$

$$+ (CC6/2)\cos 4t + (CC6/2)\cos 8t)(\dot{\beta}_I + \beta_{II}) + (\gamma/2)((CC2/2)\sin 4t$$

$$- (CC6/2)\sin 4t + (CC6/2)\sin 8t)(\dot{\beta}_{II} - \beta_I) + (\gamma/2)(PC1 +$$

$$PC3 \cos 4t + PC5 \cos 4t + PC7 \cos 8t)\beta_o + \omega_1^2 \beta_I$$

$$+ (\gamma/2)((PS2/2)\sin 4t + PS4 \sin 4t + (PS6/2)\sin 4t$$

$$+ (PS6/2)\sin 8t)\beta_I + (\gamma/2)(PS2/2 - (PS2/2)\cos 4t$$

$$+ (PS6/2)\cos 4t - (PS6/2)\cos 8t)\beta_{II} - (\gamma/2)(CS1 \sin 2t$$

$$+ CS3 \sin 2t + CS5 \sin 6t)\dot{\beta}_d - (\gamma/2)(PC1 \cos 2t$$

$$+ PC3 \cos 2t + PC5 \cos 6t + PC7 \cos 6t)\beta_d$$

$$+ (\gamma/2)(DS3 \sin 4t + DS5 \sin 4t)\nu_o + (\gamma/2)(EC1 +$$

$$EC3 \cos 4t + EC5 \cos 4t)\nu_I + (\gamma/2)(FS3 \sin 4t + FS5 \sin 4t)\nu_{II}$$

$$= (\gamma/2)(YS3 \sin 4t + YS5 \sin 4t)\theta_I + (\gamma/2)(ZC1 +$$

$$ZC3 \cos 4t + ZC5 \cos 4t)\theta_{II} \qquad (142)$$

$$\ddot{\beta}_{II} - 2\dot{\beta}_I - \beta_{II} + (\gamma/2)(CS1 - CS3 \cos 4t + CS5 \cos 4t)\dot{\beta}_0$$

$$+ (\gamma/2)((CC2/2)\sin 4t - (CC6/2)\sin 4t + (CC6/2)\sin 4t$$

$$+ (CC6/2)\sin 8t)(\dot{\beta}_I + \beta_{II}) + (\gamma/2)(CO - CC2/2 - (CC2/2)\cos 4t$$

$$+ CC4 \cos 4t - (CC6/2)\cos 4t - (CC6/2)\cos 8t)(\dot{\beta}_{II} - \beta_I)$$

$$+ (\gamma/2)(PC3 \sin 4t - PC5 \sin 4t + (PC7)\sin 8t)\beta_o$$

$$+ (\gamma/2)(PS2/2 - (PS2/2)\cos 4t + (PS6/2)\cos 4t - (PS6/2)$$

$$\cos 8t)\beta_I + \omega_1^2 \beta_{II} + (\gamma/2)(-(PS2/2)\sin 4t + PS4 \sin 4t$$

$$- (PS6/2)\sin 4t - (PS6/2)\sin 8t)\beta_{II} + (\gamma/2)(CS1 \cos 2t$$

$$- CS3 \cos 2t + CS5 \cos 6t)\dot{\beta}_d - (\gamma/2)(PC1\sin 2t - PC3 \sin 2t$$

$$+ PC5 \sin 6t - PC7 \sin 6t)\beta_d + (\gamma/2)$$

$$(DS1 - DS3 \cos 4t + DS5 \cos 4t)\nu_o + (\gamma/2)(EC3 \sin 4t$$

$$- EC5 \sin 4t)\nu_I + (\gamma/2)(FS1 - FS3 \cos 4t + FS5 \cos 4t)\nu_{II}$$

$$= (\gamma/2)(YS1 - YS3 \cos 4t + YS5 \cos 4t)\theta_I + (\gamma/2)(ZC3 \sin 4t$$

$$- ZC5 \sin 4t)\theta_{II} \qquad (143)$$

$$\ddot{\beta}_d - (\gamma/2)(CC2 \cos 2t + CC6 \cos 6t)\dot{\beta}_o - (\gamma/2)((CS1/2)$$

$$\sin 2t + (CS3/2)\sin 2t + (CS5/2)\sin 6t)(\dot{\beta}_I + \beta_{II})$$

$$+ (\gamma/2)((CS1/2)\cos 2t - (CS3/2)\cos 2t + (CS5/2)\cos 6t)$$

$$(\dot{\beta}_{II} - \dot{\beta}_{I}) - (\gamma/2)(PS2 \sin 2t + PS6 \sin 6t)\beta_o$$

$$- (\gamma/2)((PC1/2)\cos 2t + (PC3/2)\cos 2t + (PC5/2)\cos 6t$$

$$+ (PC7/2)\cos 6t)\beta_I - (\gamma/2)((PC1/2)\sin 2t - (PC3/2)\sin 2t$$

$$+ (PC5/2)\sin 6t - (PC7/2)\sin 6t)\beta_{II} + (\gamma/2)(CO + CC4 \cos 4t)$$

$$\dot{\beta}_d + \omega_1^2 \beta_d + (\gamma/2)PS4 \sin 4t\ \beta_d - (\gamma/2)(DC2 \cos 2t$$

$$+ DC6 \cos 6t)\nu_o - (\gamma/2)(ES2 \sin 2t + ES6 \sin 6t)\nu_I$$

$$- (\gamma/2)(FC2 \cos 2t + FC6 \cos 6t)\nu_{II}$$

$$= - (\gamma/2)(YC2 \cos 2t)\theta_I - (\gamma/2)(ZS2 \sin 2t + ZS6 \sin 6t)\theta_{II} \qquad (144)$$

The inflow model is same as that obtained without reverse flow (equation 68) except the thrust and the moment coefficients C_T, C_L and C_M are:

$$C_T = (2\ a\sigma/b)\{(-DTO - DTC4 \cos 4t)\nu_o + (-ETS4 \sin 4t)$$

$$\nu_I + (-FTO - FTC4 \cos 4t)\nu_{II} + (PTS4 \sin 4t + PTS8$$

$$\sin 8t)\beta_o + (CTO + CTC4 \cos 4t)\dot{\beta}_o + (-PTS2 \sin 2t$$

$$- \text{PTS6 sin } 6t)\beta_d + (-\text{CTC2 cos } 2t - \text{CTC6 cos } 6t)\dot{\beta}_d$$

$$+ (1/2)(\text{PTC3 cos } 4t + \text{PTC1} + \text{CTS1} - \text{CTS3 cos } 4t)\beta_I$$

$$+ (1/2)(\text{CTS3 sin } 4t)\dot{\beta}_I + (1/2)(\text{PTC3 sin } 4t +$$

$$\text{CTS3 sin } 4t)\beta_{II} + (1/2)(-\text{CTS1} + \text{CTS3 cos } 4t)\dot{\beta}_{II}$$

$$+ (\text{YTO} + \text{YTC4 cos } 4t)\theta_I + (\text{ZTS4 sin } 4t)\theta_{II}\} \qquad (145)$$

$$C_L = - (a\sigma/2b)\{-(2.\text{DS1} + (-2\ \text{DS3} + 2\ \text{DS5})\cos\ 4t)\nu_o$$

$$- (2\ \text{EC3} - 2\ \text{EC5})\sin\ 4t\ \nu_I - (2\ \text{FS1} + (-2\ \text{FS3}$$

$$+ 2\ \text{FS5})\cos\ 4t)\nu_{II} - ((2\ \text{PC3} - 2\ \text{PC5})\sin\ 4t$$

$$+ 2\ \text{PC7 sin } 8t)\beta_o - ((-2\ \text{PC1} + 2\ \text{PC3})\sin\ 2t +$$

$$2\ \text{PC7 sin } 6t)\beta_d + (-\text{PS2} + 2\ \text{C0} - \text{CC2} + (\text{PS2} - \text{PS6}$$

$$+ 2\ \text{CC4} - \text{CC2} - \text{CC6})\cos\ 4t + (\text{PS6} - \text{CC6})\cos\ 8t)\beta_I$$

$$+ ((-2\ \text{PS4} + \text{PS2} + \text{PS6} - \text{CC2} + \text{CC6})\sin\ 4t +$$

$$(\text{PS6} - \text{CC6})\sin\ 8t)\beta_{II} - (2\ \text{CS1} + (-2\ \text{CS3} + 2\ \text{CS5})$$

$$\cos 4t)\dot{\beta}_o - ((2\ CS1 - 2\ CS3)\cos 2t + 2\ CS5 \cos 6t)\dot{\beta}_d$$

$$+ ((-CC\ 2 + CC6)\sin 4t - CC6 \sin 8t)\dot{\beta}_I + ((-2\ C0$$

$$+ CC2) + (-2\ CC4 + CC2 + CC6)\cos 4t + CC6 \cos 8t)\dot{\beta}_{II}$$

$$+ (2\ YS1 + (-2\ YS3 + 2\ YS5)\cos 4t)\theta_I + (2\ ZC3 - 2\ ZC5)$$

$$\sin 4t\ \theta_{II}\} \qquad (146)$$

$$C_M = -(a\sigma/2b)\{-(2\ DS3 + 2\ DS5)\sin 4t\ \nu_o$$

$$- (2\ EC1 + (2\ EC3 + 2\ EC5)\cos 4t)\nu_I - (2\ FS3 +$$

$$2\ FS5)\sin 4t\ \nu_{II} + (-2\ PC1 + (-2\ PC3 - 2\ PC5)\cos 4t$$

$$- 2\ PC7 \cos 8t)\beta_o + ((2\ PC1 + 2\ PC3)\cos 2t +$$

$$(2\ PC5 + 2\ PC7)\cos 6t)\beta_d + ((-2\ PS4 - PS2 - PS6$$

$$+ CC2 - CC6)\sin 4t + (-PS6 + CC6)\sin 8t)\beta_I$$

$$+ ((-PS2 - 2\ CO - CC2) + (PS2 - PS6 - 2\ CC4 - CC2$$

$$- CC6)\cos 4t + (PS6 - CC6)\cos 8t)\beta_{II} + (-2\ CS3 - 2\ CS5)$$

$$\sin 4t\ \dot{\beta}_o + ((2\ CS1 + 2\ CS3)\sin 2t + 2\ CS5 \sin 6t)\dot{\beta}_d$$

$$+ ((-2\ C0 - CC2) + (-2\ CC4 - CC2 - CC6)\cos 4t - CC6 \cos 8t)\dot{\beta}_I$$

$$+ ((-CC2 + CC6)\sin 4t - CC6 \sin 8t)\dot{\beta}_{II}$$

$$+ (2\ YS3 + 2\ YS5)\sin 4t\ \theta_I + (2\ ZC1 + (2\ ZC3 + 2\ ZC5)\cos 4t)\theta_{II}\} \quad (147)$$

8.4 TABLE OF COEFFICIENTS FOR THE FLAPPING EQUATIONS GIVEN IN 8.3

$$K_T(\psi) = PTC1 \cos\psi + PTC3 \cos 3\psi + PTS2 \sin 2\psi + PTS4 \sin 4\psi + PTS6 \sin 6\psi + PTS8 \sin 8\psi \quad (148)$$

μ	PTC1	PTC3	PTS2	PTS4	PTS6	PTS8
.5	-.2509	.0157	-.1	-.0059	-.0009	0
.6	-.3094	.0271	-.1379	-.0103	-.0016	-.0005
.7	-.3723	.043	-.1794	-.0164	-.0026	-.0009
.8	-.4404	.0642	-.2234	-.0245	-.0039	-.0013
.9	-.5146	.0913	-.269	-.035	-.0056	-.0019
1.0	-.5955	.1252	-.3151	-.048	-.0077	-.002

$$C_T(\psi) = CT0 + CTC2 \cos 2\psi + CTC4 \cos 4\psi + CTC6 \cos 6\psi + CTS1 \sin\psi + CTS3 \sin 3\psi + CTS5 \sin 5\psi \quad (149)$$

μ	CT0	CTC2	CTC4	CTC6	CTS1	CTS3	CTS5
.5	-.3131	.0106	-.0015	-.0002	-.2195	-.005	.0001
.6	-.3195	.0183	-.0026	-.0003	-.2551	-.0088	.0001
.7	-.3285	.0291	-.0042	-.0005	-.2863	-.014	.0001
.8	-.3404	.0435	-.0062	-.0007	-.3122	-.021	.0002
.9	-.3557	.0619	-.0089	-.001	-.3321	-.03	.0002
1.0	-.3748	.0848	-.0121	-.0014	-.3454	-.0413	.0002

$$M_{\theta_{Y_T}}(\psi) = YT0 + YTC2 \cos 2\psi + YTC4 \cos 4\psi + YTS1 \sin \psi + YTS3 \sin 3\psi + YTS5 \sin 5\psi + YTS7 \sin 7\psi \quad (150)$$

μ	YT0	YTC2	YTC4	YTS1	YTS3	YTS5	YTS7
.5	-.2506	.2562	-.0054	-.4575	.0489	.0015	.0002
.6	-.3089	.3184	-.0092	-.5169	.0667	.0024	.0003
.7	-.3718	.3867	-.0146	-.5827	.086	.0038	.0004
.8	-.4399	.4619	-.0217	-.6535	.106	.0056	.0006
.9	-.514	.545	-.0308	-.728	.1262	.0079	.0008
1.0	-.5948	.6373	-.0421	-.8048	.1461	.0108	.001

$$M_{\theta_{II_T}}(\psi) = ZTC1 \cos \psi + ZTC3 \cos 3\psi + ZTC5 \cos 5\psi + ZTS2 \sin 2\psi + ZTS4 \sin 4\psi + ZTS6 \sin 6\psi \quad (151)$$

μ	ZTC1	ZTC3	ZTC5	ZTS2	ZTS4	ZTS6
.5	.3578	-.0516	-.0017	.2455	-.0056	-.0002
.6	.3793	-.0717	-.0028	.3	-.009	-.0002
.7	.4036	-.094	-.0046	.3576	-.0148	-.0003
.8	.4304	-.1182	-.0068	.4188	-.0219	-.0003
.9	.4593	-.1436	-.0097	.4838	-.031	-.0003
1.0	.49	-.17	-.0133	.5534	-.042	-.0003

$$M_{v_{o_T}}(\psi) = DT0 + DTC2 \cos 2\psi + DTC4 \cos 4\psi + DTS1 \sin \psi + DTS3 \sin 3\psi + DTS5 \sin 5\psi + DTS7 \sin 7\psi \quad (152)$$

μ	DT0	DTC2	DTC2	DTS1	DTS3	DTS5	DTS7
.5	.5329	-.0625	0	.3787	.0209	.0028	.0009
.6	.5604	-.09	0	.429	.0302	.0041	.0013
.7	.5928	-.1226	0	.4708	.0412	.0056	.0018
.8	.6303	-.1601	0	.5042	.0539	.0074	.0023
.9	.6727	-.2026	0	.529	.0683	.0094	.003
1.0	.7201	-.25	0	.545	.0843	.0118	.0037

$$M_{v_{I_T}}(\psi) = ETC1 \cos \psi + ETC3 \cos 3\psi + ETC5 \cos 5\psi + ETC7 \cos 7\psi + ETS2 \sin 2\psi + ETS4 \sin 4\psi + ETS6 \sin 6\psi \quad (153)$$

μ	ETC1	ETC3	ETC5	ETCT	ETS2	ETS4	ETS6
.5	.3079	-.0046	.0008	0	.1123	.0024	0
.6	.3105	-.0079	.0014	0	.1320	.0043	0
.7	.3141	-.0126	.0023	0	.1503	.0069	-.0001
.8	.3188	-.0187	.0034	.0004	.1668	.0104	-.0002
.9	.325	-.0266	.0049	.0006	.1813	.0149	-.0002
1.0	.3326	-.0365	.0067	.0008	.1935	.0205	-.0002

$$M_{\nu_{II_T}}(\psi) = FT0 + FTC1 \cos\psi + FTC2 \cos 2\psi + FTC4 \cos 4\psi + FTS1 \sin\psi + FTS3 \sin 3\psi + FTS5 \sin 5\psi + FTS7 \sin 7\psi \quad (154)$$

μ	FT0	FTC1	FTC2	FTC4	FTS1	FTS3	FTS5	FTS7
.5	.0551	.0013	-.0344	-.0208	.4171	-.0488	.0053	.0004
.6	.0785	.0012	-.0579	-.0208	.4171	-.0488	.0053	.0004
.7	.102	.0012	-.0814	-.0208	.4171	-.0488	.0053	.0004
.8	.1255	.0011	-.105	-.0208	.4171	-.0488	.0053	.0004
.9	.1490	.0010	-.1285	-.0208	.4171	-.0488	.0053	.0004
1.0	.1726	.001	-.1521	-.0207	.4171	-.0487	.0052	.0005

$$K(\psi) = PC1 \cos \psi + PC3 \cos 3\psi + PC5 \cos 5\psi + PC7 \cos 7\psi + PS2 \sin 2\psi + PS4 \sin 4\psi + PS6 \sin 6\psi \quad (155)$$

μ	PC1	PC3	PC5	PC7	PS2	PS4	PS6
.5	.154	-.0023	.0004	.00004	.0562	.0012	-.00005
.6	.1863	-.0048	.0008	.00010	.0792	.0026	0
.7	.2198	-.0088	.0016	.00019	.1052	.0048	0
.8	.2551	-.015	.0027	.00033	.1334	.0083	0
.9	.2925	-.024	.0044	$\simeq 0$	.1631	.0134	0
1.0	.3326	-.0365	.0067		.1935	.0205	0

$$C(\psi) = C0 + CC2 \cos 2\psi + CC4 \cos 4\psi + CC6 \cos 6\psi + CS1 \sin \psi + CS3 \sin 3\psi + CS5 \sin 5\psi \quad (156)$$

μ	C0	CC2	CC4	CC6	CS1	CS3	CS5
.5	.2233	-.0026	.0006	$\simeq 0$	.1485	.0014	-.0002
.6	.2254	-.0054	.0013	0	.1751	.003	-.0004
.7	.2288	-.01	.0025	0	.1993	.0057	-.0007
.8	.2341	-.017	.0043	0	.22	.0097	-.0012
.9	.2418	-.0273	.0068	0	.2366	.0157	-.0019
1.0	.2526	-.0416	.0103	0	.2476	.024	-.0028

$$M_{\theta_0}(\psi) = X0 + XC2 \cos 2\psi + XC4 \cos 4\psi + XS1 \sin\psi + XS3 \sin 3\psi \quad (157)$$

μ	X0	XC2	XC4	XS1	XS3
.5	.2781	-.0562	-.0006	.3076	-.0018
.6	.3019	-.0793	-.0013	.3722	-.0034
.7	.3289	-.1053	-.0024	.4393	-.0061
.8	.3589	-.1336	-.0042	.5097	-.0103
.9	.3912	-.1633	-.0067	.5844	-.0164
1.0	.4251	-.1937	-.01	.6647	-.0248

$$M_{\theta_I}(\psi) = Y0 + YC2 \cos 2\psi + YC4 \cos 4\psi + YS1 \sin \psi + YS3 \sin 3\psi + YS5 \sin 5\psi \quad (158)$$

μ	Y0	YC2	YC4	YS1	YS3	YS5
.5	-.1537	.1547	-.0008	-.3061	.028	.0004
.6	-.186	.1879	-.0019	-.3414	.029	.0008
.7	-.2195	.2228	-.0034	-.3815	.0517	.0013
.8	-.2547	.26	-.0057	-.4255	.0649	.0022
.9	-.292	.3004	-.0091	-.4726	.0785	.0035
1.0	-.3321	.3447	-.0137	-.5217	.0919	.0053

$$M_{\theta_{II}}(\psi) = ZC1 \cos \psi + ZC3 \cos 3\psi + ZC5 \cos 5\psi + ZS2 \sin 2\psi + ZS4 \sin 4\psi + ZS6 \sin 6\psi \quad (159)$$

μ	ZC1	ZC3	ZC5	ZS2	ZS4	ZS6
.5	.2501	-.0285	-.0003	.153	-.0009	0.0
.6	.2624	-.0404	-.0007	.1845	-.0017	0.0
.7	.2765	-.054	-.0012	.2167	-.0029	.0002
.8	.2923	-.069	-.0021	.25	-.0048	.0004
.9	.3097	-.085	-.0034	.2842	-.0075	.0007
1.0	.3284	-.1022	-.0051	.3202	-.0112	.0012

$$M_{\nu_o}(\psi) = D0 + DC2 \cos 2\psi + DC4 \cos 4\psi + DC6 \cos 6\psi + DS1 \sin \psi + DS2 \sin 3\psi + DS5 \sin 5\psi \quad (160)$$

μ	D0	DC2	DC4	DC6	DS1	DS3	DS5
.5	.313	-.0106	.0015	0	.2195	.005	-.0001
.6	.3195	-.0183	.0026	.0003	.2551	.0088	-.0001
.7	.3285	-.0291	.0042	.0005	.2863	.014	-.0002
.8	.3404	-.0435	.0062	.0007	.3122	.021	-.0002
.9	.3557	-.0619	.0089	.001	.3321	.03	-.0002
1.0	.3748	-.0848	.0121	.0014	.3454	.0413	-.0002

$$M_{\nu_I}(\psi) = EC1 \cos \psi + EC3 \cos 3\psi + EC5 \cos 5\psi + ES2 \sin 2\psi + ES4 \sin 4\psi + ES6 \sin 6\psi \quad (161)$$

μ	EC1	EC3	EC5	ES2	ES4	ES6
.5	.2221	-.001	.0003	.075	.0005	-.0001
.6	.2228	-.0021	.0007	.089	.0013	-.0003
.7	.2239	-.0038	.0012	.1025	.0024	-.0004
.8	.2257	-.0065	.0021	.115	.0042	-.00071
.9	.2283	-.0103	.0034	.1262	.0069	-.0011
1.0	.2318	-.0157	.0052	.1359	.0106	-.0016

$$M_{\nu_{II}}(\psi) = F0 + FC2 \cos 2\psi + FC4 \cos 4\psi + FC6 \cos 6\psi + FS1 \sin \psi + FS3 \sin 3\psi + FS5 \sin 5\psi \quad (162)$$

μ	F0	FC2	FC4	FC6	FS1	FS3	FS5
.5	.0742	-.0736	-.0008	.0001	.2245	-.0018	.0002
.6	.0875	-.0861	-.0017	.0002	.2280	-.0036	.0006
.7	.0996	-.0968	-.0032	.0003	.2337	-.0064	.0011
.8	.11	-.1052	-.0054	.0005	.2425	-.0109	.002
.9	.1182	-.1105	-.0088	.0008	.2554	-.0173	.0033
1.0	.1237	-.1119	-.0133	.0012	.2732	-.0262	.0051

9. BIBLIOGRAPHY

1. Stepner, D. E. and Mehra, R. K., "Maximum Likelihood Identification and Optimal Input Design for Identifying Aircraft Stability and Control Derivatives", NASA CR 2200, March 1973.

2. Iliff, K. W. and Taylor, L. W., "Determination of Stability Derivatives from Flight Data Using a Newton-Raphson Minimization Technique", NASA TN D-6579, March 1972.

3. Molusis, J. A., "Rotorcraft Derivative Identification from Analytical Models and Flight Test Data", AGARD Flight Mechanics Panel Specialists Meeting, NASA Langley, November 1974.

4. Gould, D. G. and Hindson, W. S., "Estimates of the Stability Derivatives of Helicopter and V/STOL Aircraft from Flight Data", DME/NAE Quarterly Bulletin No. 1974 (4), Ottawa, January 1975.

5. Hohenemser, K. H. and Prelewicz, D. A., "Computer Experiments on Periodic Systems Identification Using Rotor Blade Transient Flapping-Torsion Responses at High Advance Ratio", Rotorcraft Dynamics, NASA SP-352, February 1974.

6. Kuczynski, W. A. and Sissingh, G. J., "Characteristics of Hingeless Rotors with Hub Moment Feedback Controls including Experimental Rotor Frequency Response", Volumes I and II of the Final Report, Phase 2, Contract NAS 2-5419, January 1972.

7. Hohenemser, K. H. and Crews, S. T., "Unsteady Wake Effects on Progressing/Regressing Forced Rotor Flapping Modes", AIAA 2nd Atmospheric Flight Mechanics Conference, Palo Alto, California, September 11-13, 1972.

8. Curtis, H. C. Jr., and Shupe, N. K., "A Stability and Control Theory for Hingeless Rotors", Proceedings of the 27th Annual National Forum of the American Helicopter Society, Preprint No. 541, May 1971.

9. Ormiston, R. A. and Peters, D. A., "Hingeless Rotor Response with Non-Uniform Inflow and Elastic Blade Bending", Journal of Aircraft, Vol. 9, No. 10, October 1972, pp. 730-736.

10. Hohenemser, K. H. and Yin, S. K., "Concepts for a Theoretical and Experimental Study of Lifting Rotor Random Loads and Vibrations", Phase VI-A Report under Contract NAS 2-4151, June 1972, NASA CR-114480.

11. Peters, D. A., "Hingeless Rotor Frequency Response with Unsteady Inflow", Proceedings Specialists Meeting on Rotorcraft Dynamics, AHS/NASA Ames, Moffett Field, California, February 1974, NASA-SP-352.

12. Crews, S. T., "Unsteady Hovering Rotor Wake Parameters Identified from Dynamic Model Tests", D. Sc. Thesis, Sever Institute of Technology, Washington University, May 1977.

13. Curtis, H. C. Jr., "Complex Coordinates in Near Hovering Rotor Dynamics", Journal of Aircraft, Vol. 10,No. 5, May 1973, pp. 289-296.

14. Ormiston, R. A., "Application of Simplified Inflow Models to Rotorcraft Dynamic Analysis", Journal of American Helicopter Society, Volume 21, No. 3, July 1976, pp. 34-37.

15. Sissingh, G. J., "Dynamics of Rotors Operating at High Advance Ratios", Journal American Helicopter Society, Vol. 13, No. 3, July 1968, pp. 56-63.

16. Denery, D. G., "Identification of System Parameters from Input-Output Data with Application to Air Vehicles", NASA TN D-6468, August 1971.

17. Giese, C. and McGhee, R. B., "Estimation of Non-Linear System States and Parameters by Regression Methods", JACC, 1965, pp. 46-53.

18. Van Trees, A. L., "Detection, Estimation and Modulation Theory", Wiley, New York, 1968.

19. Mood, A. M. and Graybill, F. A., "Introduction to the Theory of Statistics", McGraw Hill Book Company, Inc., 1950.

20. Rediess, H. A., "An Overview of Parameter Estimation Techniques and Applications in Aircraft Flight Testing", NASA TN D-7647, April 1974, pp. 1-18.

21. Bryson, A. E. and Ho, Y. C., "Applied Optimal Control", Ginn & Co., 1969.

22. Hohenemser, K. H. and Yin, S. K., "Computer Experiments in Preparation of System Identification from Transient Rotor Model Tests", Part II of First Yearly Report under Contract NAS2-7613, June 1974.

23. Rauch, H. E., Tung, F. and Striebel, C. T., "Maximum Likelihood Estimates of Linear Dynamic Systems", AIAA Journal, Vol. 3, No. 8, August 1965, pp. 1445-1450.

24. Lebacqz, J. V., "Application of a Kalman Filter Identification Technique to Flight Data from the X-22A Variable Stability V/STOL Aircraft", NASA TN D-7647, April 1974, pp. 149-174.

25. Banerjee, D. and Hohenemser, K. H., "Optimum Data Utilization for Parameter Identification with Application to Lifting Rotors", Journal of Aircraft, Volume 13, Number 12, December 1976, pp. 1014-1016.

26. Bryant, W. H. and Hodge, W. F., "Effect of Flight Instrumentation Errors on the Estimation of Aircraft Stability and Control Derivatives", NASA TN D-7647, April 1974, pp. 261-280.

27. Molusis, J. A., "Helicopter Derivative Identification from Analytical Models and Flight Test Data", NASA TN D-7647, April 1974, pp. 175-186.

28. Taylor, L. W., "A New Criterion for Modeling Systems", NASA TN D-7647, April 1974, pp. 291-313.

29. Hohenemser, K. H., Banerjee, D. and Yin, S. K., "Method Studies on System Identification from Transient Rotor Tests", Part I of Second Yearly Report under Contract NAS2-7613, June 1975 NASA CR-137965.

30. Hohenemser, K. H. and Yin, S. K., "On the Question of Adequate Hingeless Rotor Modeling in Flight Dynamics", Presented at the 29th Annual National Forum of the American Helicopter Society, Washington, D.C., May 1973, Preprint 732.

31. Hohenemser, K. H. and Crews, S. T., "Model Tests on Unsteady Rotor Wake Effects", Journal of Aircraft, Vol. 10, No. 1, January 1973, pp. 58-60.

32. Chen, R. T. N., Eulrich, B. J. and Lebacqz, J. V., "Development of Advanced Techniques for the Identification of V/STOL Aircraft Stability and Control Parameters", Cornell Aeronautical Laboratory, Report No. BM-2820-F-1, August 1971.

33. Molusis, J. A., "Helicopter Stability Derivative Extraction from Flight Data Using the Bayesian Approach to Estimation", Journal of the American Helicopter Society, Vol. 18, No. 2, April 1973, pp. 12-23.

34. Hohenemser, K. H., Banerjee, D. and Yin, S. K., "Rotor Dynamic State and Parameter Identification from Simulated Forward Flight Transients", Part I of Third Yearly Report under Contract NAS2-7613, June 1976 NASA CR-137963.

35. Peters, D. A. and Hohenemser, K. H., "Application of Floquet Transition Matrix to Problems of Lifting Rotor Stability", Journal of the American Helicopter Society, April 1971.

36. Chen, R. T. N., "Input Design for Aircraft Parameter Identification Using Time-Optimal Control Formulation", Presented at AGARD Flight Mechanics Specialist's Meeting, NASA-Langley, November 1974.

37. Eykhoff, P., "System Identification", John Wiley & Sons, 1974.

38. Jazwinski, A. H., "Stochastic Processes and Filtering Theory", Academic Press, 1970.

39. Sage, A. P. and Melsa, J. L., "System Identification", Academic Press, 1971.

40. Kendall, M. G., "The Advanced Theory of Statistics", Volume II, Hafner Publishing Company, New York, 1951.